



**HAL**  
open science

## Ice-Ocean Exchange Processes in the Jovian and Saturnian Satellites

Krista Soderlund, Klára Kalousová, Jacob Buffo, Christopher Glein, Jason Goodman, Giuseppe Mitri, G. Wesley Patterson, Frank Postberg, Marc Rovira-Navarro, Tina Rückriemen, et al.

► **To cite this version:**

Krista Soderlund, Klára Kalousová, Jacob Buffo, Christopher Glein, Jason Goodman, et al.. Ice-Ocean Exchange Processes in the Jovian and Saturnian Satellites. *Space Science Reviews*, 2020, 216 (5), 10.1007/s11214-020-00706-6 . hal-03006542

**HAL Id: hal-03006542**

**<https://hal.science/hal-03006542>**

Submitted on 7 Feb 2024

**HAL** is a multi-disciplinary open access archive for the deposit and dissemination of scientific research documents, whether they are published or not. The documents may come from teaching and research institutions in France or abroad, or from public or private research centers.

L'archive ouverte pluridisciplinaire **HAL**, est destinée au dépôt et à la diffusion de documents scientifiques de niveau recherche, publiés ou non, émanant des établissements d'enseignement et de recherche français ou étrangers, des laboratoires publics ou privés.

1 **Ice-ocean exchange processes in outer solar system**  
2 **satellites**

3 **Krista M. Soderlund · Klára Kalousová ·**  
4 **Jacob J. Buffo · Christopher R. Glein ·**  
5 **Jason C. Goodman · Giuseppe Mitri ·**  
6 **G. Wesley Patterson · Frank Postberg ·**  
7 **Marc Rovira-Navarro · Tina Rückriemen ·**  
8 **Joachim Saur · Britney E. Schmidt ·**  
9 **Christophe Sotin · Tilman Spohn ·**  
10 **Gabriel Tobie · Tim Van Hoolst · Steven**  
11 **D. Vance · L.L.A. (Bert) Vermeersen**

12 Received: date / Accepted: date

---

K.M. Soderlund  
Institute for Geophysics  
Jackson School of Geosciences  
The University of Texas at Austin  
J.J. Pickle Research Campus, Bldg. 196  
10100 Burnet Road (R2200)  
Austin, TX 78758-4445  
Tel.: +1 218-349-3006  
Fax: +1 512-471-8844  
E-mail: krista@ig.utexas.edu

K. Kalousová  
Charles University, Faculty of Mathematics and Physics, Department of Geophysics, Prague,  
Czech Republic

J. J. Buffo  
Georgia Institute of Technology, Atlanta, GA, USA

C.R. Glein  
SouthWest Research Institute, San Antonio, MA, USA

J.C. Goodman  
Wheaton College, Norton, MA, USA

G. Mitri  
International Research School of Planetary Sciences, Università' d'Annunzio, Pescara, Italy  
Dipartimento di Ingegneria e Geologia, Università' d'Annunzio, Pescara, Italy

G.W. Patterson  
Johns Hopkins University Applied Physics Laboratory, Laurel, MD, USA

F. Postberg  
Freie Universität Berlin, Germany

---

M. Rovira-Navarro  
Technische Universiteit Delft, Delft, The Netherlands  
NIOZ Royal Netherlands Institute for Sea Research, Yerseke, The Netherlands

T. Rückriemen  
TU Berlin, Berlin, Germany  
DLR Institute of Planetary Research, Berlin, Germany

J. Saur  
University of Cologne, Cologne, Germany

B.E. Schmidt  
Georgia Institute of Technology, Atlanta, GA, USA

C. Sotin  
Jet Propulsion Laboratory-California Institute of Technology, Pasadena, USA

T. Spohn  
International Space Science Institute, Bern, Switzerland  
DLR Institute of Planetary Research, Berlin, Germany

G. Tobie  
Laboratoire de Planétologie et Géodynamique, UMR-CNRS 6112, Université de Nantes,  
Nantes, France

T. Van Hoolst  
Royal Observatory of Belgium, Brussels, Belgium  
Institute of Astronomy, KU Leuven, Leuven, Belgium

S.D. Vance  
Jet Propulsion Laboratory-California Institute of Technology, Pasadena, USA

L.L.A. Vermeersen  
Technische Universiteit Delft, Delft, The Netherlands  
NIOZ Royal Netherlands Institute for Sea Research, Yerseke, The Netherlands

**Abstract** A growing number of satellites in the outer solar system likely have global oceans beneath their outer icy shells. While the presence of liquid water makes these ocean worlds compelling astrobiological targets, the exchange of heat and materials from the deep interior to the surface also plays a critical role in promoting habitable environments. In this chapter, we combine geophysical, geochemical, and geological observations of the Jovian satellites Europa, Ganymede, and Callisto as well as the Saturnian satellites Enceladus and Titan to summarize our current state of understanding of their interiors and surface exchange processes. Potential mechanisms for driving exchange processes upward from the ocean floor and downward from the satellite surface are then reviewed, which are primarily based on numerical models of ice shell and ocean dynamics and complemented by terrestrial analog studies. Future missions to explore these exo-oceans will further revolutionize our understanding of ice-ocean exchange processes and their implications for the habitability of these worlds.

**Keywords** Ice-Ocean Exchange · Europa · Ganymede · Callisto · Enceladus · Titan

In this chapter, we review ice-ocean exchange processes in outer solar system satellites that are the best candidates to host subsurface oceans: the icy Galilean satellites Europa, Ganymede, and Callisto and the Saturnian satellites Enceladus and Titan. Section 1 summarizes our current state of knowledge of the interiors of these moons, Section 2 describes surface exchange processes, Section 3 describes ice shell dynamics and exchange processes, Section 4 describes ocean dynamics and exchange processes, Section 5 describes terrestrial analogs, and Section 6 concludes with implications for habitability and future exploration.

## 1 Interiors of Icy Ocean Worlds

Most of what we know about the interiors of known icy ocean worlds comes from the *Galileo* (1989-2003) and *Cassini-Huygens* (1997-2017) missions. As reviewed by Hussmann et al (2015) among others, the interiors of icy satellites are explored through the following data: radius and mass, gravity field, magnetic field, rotational state and shape/topography, surface temperatures and heat flow, composition of surface and atmosphere, activity at the surface, and knowledge of its formation and evolution including surface geology and tectonics, orbital dynamics, and chemical environment during accretion. Complementary to these observational data are laboratory and numerical data on the material properties of water/ice, rock, and metal, as well as their equations of state (e.g., Choukroun and Grasset, 2010; Vance and Brown, 2013; McDougall and Barker, 2011; Lemmon et al, 2007; Connolly, 2009; Balog et al, 2003). In this section, we first review the differentiation states and ocean existence, followed by more detailed descriptions of interior structures of the most prominent ocean worlds among the outer solar system satellites.

### 1.1 Differentiation and Ocean Existence

Mass and radius allow calculation of the mean density and an assessment of whether a satellite is rich in rock/iron or in ice. The gravity data, in particu-

lar the  $J_2$  and  $C_{22}$  components (e.g., Anderson et al, 1996, 1998b,a, 2001), can be used to derive the moment of inertia factor (MoI) if the satellite can be assumed to be in hydrostatic equilibrium. Only for Titan have both gravitational coefficients been determined and this ratio of nearly 10/3 is compatible with hydrostatic equilibrium at  $2\sigma$  (Durante et al, 2019). Together with mass and radius, the MoI allows construction of simple, albeit non-unique, interior structure models that indicate whether or not a satellite has differentiated. The MoI factor of a homogeneous density sphere is 0.4, and a smaller value indicates an increase of density with depth, hence possible differentiation. Ice on the surface together with a low enough value of the moment of inertia factor allows speculation about a water/ice layer on top of a rock layer. Table 1 collects data on the mass, radii, and MoI of major icy satellites of the solar system.

**Table 1** Mass, radii, and moment of inertia of major icy satellites of the solar system. Data: Hussmann et al (2015) for Europa, Ganymede, and Callisto; Iess et al (2014), Roatsch et al (2009), and Jacobson et al (2006) for Enceladus; and Durante et al (2019) for Titan.

	Europa	Ganymede	Callisto	Enceladus	Titan
Mass ( $10^{22}$ kg)	4.8	14.8	10.8	0.01	13.5
Radius (km)	1565	2631	2410	252	2575
Mean density (kg)	2989	1942	1835	1609	1881
MoI	0.346	0.312	0.355	0.335	0.341

The bulk densities of Ganymede, Callisto, Enceladus, and Titan suggest that their interiors contain 40 to 60% of ice/water, while Europa is a predominantly rocky body with a bulk ice/water mass fraction of only 6-9% (Hussmann et al, 2015). The level of differentiation of the interiors, however, likely differs between the satellites. Europa and Ganymede are thought to be fully differentiated into a central metallic core, a silicate mantle, and outer water ice-liquid shell (e.g., Anderson et al, 1996, 1998b). Enceladus is differentiated with a water ice-liquid outer shell and central rocky core that may be porous given the satellite’s low mass and mean density, which prohibits a substantial metallic contribution (e.g., Iess et al, 2014; Roberts, 2015; Āadek et al, 2016; Beuthe et al, 2016). In contrast, Callisto and Titan are only partially differentiated with an  $H_2O$  layer overlying a core of ice mixed with rocks and metal up to significant depth, maybe up to the center (e.g., Anderson et al, 1998b; Sohl et al, 2003; Iess et al, 2010; Castillo-Rogez and Lunine, 2010; Tobie et al, 2005; Gao and Stevenson, 2013; Baland et al, 2014). A model of slow and incomplete differentiation of Callisto has been discussed by Nagel et al (2004), while Barr and Canup (2010) suggest partial differentiation of Titan due to undifferentiated accretion and core formation due to impacts that allowed only some of Titan’s rock to form a core.

It is widely agreed that these icy satellites have an outer ice I layer that is, in most cases, underlain by an ocean. The strongest observational evidence for the icy Galilean satellites was the detection of magnetic induction signals counteracting the time-variable magnetic field of Jupiter in the satellites’ rest frames (Khurana et al, 1998; Neubauer, 1998; Zimmer et al, 2000; Kivelson et al, 2002). These signals are best explained by the presence of a electrically conducting fluid (i.e. a salty ocean) beneath the surface of the satellite. Strong geologic evidence for a global ocean also exists for Europa (e.g., Pappalardo et al, 1999), and observations

of oscillations in auroral ovals by the *Hubble Space Telescope* have confirmed that Ganymede has a global subsurface ocean (Saur et al, 2015). In contrast, the case for Callisto is less clear since induction within the satellite’s ionosphere may also explain the observed magnetic fields (Hartkorn and Saur, 2017).

For satellites of Saturn, the same approach is not feasible since Saturn’s magnetic field is not inclined with respect to the rotation axis, in contrast to Jupiter (dipole tilt of 9 degrees), and therefore the satellites do not sense a systematic time-periodic field in their rest frame. Instead, the existence of subsurface oceans and characterisation of their properties have relied on a variety of other methods. *Cassini* measurements of water vapour (e.g., Porco et al, 2006; Dougherty et al, 2006) and salty grains from geysers on Enceladus (e.g., Postberg et al, 2009) indicated the existence of water reservoirs beneath the surface, and the global character of the distribution of water as a subsurface ocean was demonstrated by gravity data (McKinnon, 2015) and libration measurements (Thomas et al, 2016). Evidence for a subsurface ocean on Titan is based on the tidal Love number estimation from time-varying gravity field (Iess et al, 2012), detection of an electric perturbation by Huygens during its descent through Titan’s atmosphere that was interpreted as a Schumann resonance (Béghin et al, 2012), and precise measurements of the spin pole orientation (e.g., Baland et al, 2014).

The bottom of the water layer may border to a rocky layer as in the case of Europa and Enceladus or to a high pressure ice layer as is likely the case for Ganymede, Callisto, and Titan. It is also possible that the underlying ice layer is mixed with rock as may be the case for Callisto and Titan if these are incompletely differentiated. High-pressure ice layers are not feasible on Europa and Enceladus due to their small size. More detailed discussions on the the high-pressure ice layer can be found in Journaux et al (2019) (this issue).

The feasibility of subsurface oceans from energy balances of the satellites has been concluded by, for example, Spohn and Schubert (2003), Hussmann et al (2006), and others (compare section 3 below). Maintaining an ocean until the present day requires energy sources and/or the depression of the ice melting point due to the inclusion of other components such as salts or ammonia. Possible energy sources are internal heating coming from radioactive decay in the rocky part of the satellite (e.g., Spohn and Schubert, 2003); dissipation of tidal energy in the rocky interior (e.g., Choblet et al, 2017a), the ocean (e.g., Tyler, 2009; Wilson and Kerswell, 2018), and/or the outer ice shell (e.g., Hussmann et al, 2006); and ohmic dissipation in the ocean (Gissinger and Petitdemange, 2019). Tidal heating is likely important for Europa and Enceladus, but less so for Titan, Ganymede, and Callisto. This is because of Europa’s proximity to Jupiter and the Laplace resonance and because Enceladus likely has a porous core that maintains strong tidal friction; both satellites also have the smallest pressure gradient shifting the water ice triple point to greater depth. Ohmic dissipation is expected to be relatively weak, but can be enhanced locally (Gissinger and Petitdemange, 2019, see Section 4.3). Another crucial factor in sustaining an ocean is heat transport in the ice I layer. Spohn and Schubert (2003) (see also references cited in section 3 below) investigated various scenarios assuming a purely conductive and a convective ice I layer. They find that for pure water ice, convection might lead to complete freezing of the oceans, although the results depend on uncertain parameter values for the viscosity of the ice I layer and the scaling of convective vigor. A present-day global ocean for Enceladus has proven hard to explain based on thermal evolution mod-

143 els, which predict heat production rates given by present orbital conditions below  
 144 the expected global heat flow (Roberts and Nimmo, 2008; Tobie et al, 2008). The  
 145 discrepancies between estimates of surface heat flow and tidal heating rates could  
 146 potentially be explained if Enceladus formed relatively recently, if tidal heating  
 147 and cooling were highly variable rate (episodic or periodic), or if the effective  
 148 rate of dissipation within Saturn is larger than the conventional value (Nimmo  
 149 et al, 2018).

## 150 1.2 Internal Structure

151 With this general picture in mind, we will now review more detailed structures for  
 152 each of the satellites. Interior models that represent possible internal structures of  
 153 Jovian and Saturnian icy ocean worlds are shown in Figure 1.

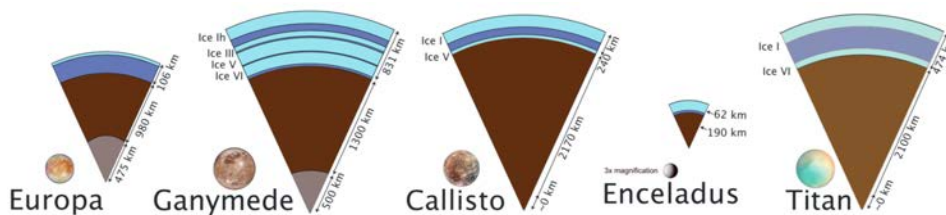


**Fig. 1** Spherically symmetric internal structure models that are consistent with geophysical constraints and use state-of-the-art equations of state and thermodynamic properties from Vance et al (2018a). *Cassini* radio science and imaging measurements provide further details for the structures of Enceladus (Čadež et al, 2019; Hemingway and Mittal, 2019) and Titan (Corlies et al, 2017; Durante et al, 2019), revealing that their ice shells are not uniform in thickness, likely owing to thermal or compositional heterogeneities.

### 154 1.2.1 Europa

155 Gravity data in combination with the mass and radius constraints permit con-  
 156 struction of density profiles with radius. These profiles typically take the form of  
 157 three-layer interior models an outer ice-liquid water layer, a rocky mantle, and a  
 158 central metallic core for Europa. Hydrostatic equilibrium is also assumed because  
 159 independent measurements of  $C_{22}$  and  $J_2$  are lacking (e.g., Schubert et al, 2004).  
 160 For a three-layer model, the core and mantle radii can be determined if the density  
 161 of each layer is assumed, leading to uncertainties in their values. In addition, solid  
 162 ice and liquid water layers cannot be distinguished due to the small density con-  
 163 trast between them. These models suggest that Europa has a outer  $H_2O$  layer that  
 164 ranges from 80 km to 170 km (Anderson et al, 1998b; Sohl et al, 2002). Geologic  
 165 and geodynamic arguments predict ice shell thicknesses that range from  $\sim 3$  km  
 166 to  $>30$  km based on mechanical, thermal, cratering, and other methods (Billings  
 167 and Kattenhorn, 2005, see their Table 1 for a summary). The core radius depends  
 168 on its assumed composition as well as the water layer thickness, ranging from 700  
 169 km for a Fe-FeS eutectic core composition and 100 km thick water layer to 200 km  
 170 for a pure Fe core composition and 170 km thick water layer (Sohl et al, 2002).

171 Mantle densities are consistent with an olivine-dominated mineralogy, becoming  
172 increasingly forsterite rich with decreasing water layer thickness (Sohl et al, 2002).

173 Magnetic field measurements add additional constraints on the interior struc-  
174 ture and composition because their observational characterisation can, in principle,  
175 constrain the electrical conductivity, depth beneath the surface, and thickness of  
176 the ocean (e.g., Zimmer et al, 2000; Khurana et al, 2002; Seufert et al, 2011).  
177 Since the *Galileo* mission only observed induction from the main signal caused by  
178 Jupiter’s synodic period seen in the satellite’s rest frame, it was not possible to  
179 estimate these parameters individually. Schilling et al (2007) found magnetic field  
180 data are best explained by electrical conductivity values of  $\gtrsim 0.5$  S/m with ocean  
181 thicknesses of  $\lesssim 100$  km.

182 The composition—dissolved organic and inorganic speciation, salinity, and  
183 pH—of Europa’s ocean is poorly constrained. Most models and aqueous leach-  
184 ing experiments suggest that magnesium sulfate ( $\text{MgSO}_4$ ) is the dominant salt,  
185 in contrast to sodium chloride ( $\text{NaCl}$ ) as in Earth’s ocean (Fanale et al, 2001;  
186 Kargel et al, 2000; Zolotov and Shock, 2001; McKinnon and Zolensky, 2003), al-  
187 though the concentration varies strongly between models and spans nearly five  
188 orders of magnitude across the literature. Recent spectroscopic observations from  
189 Earth (Fischer et al, 2015; Trumbo et al, 2019), which trade the higher spatial  
190 resolution of *Galileo* near-infrared imaging for better spectral resolution—reveal  
191 chlorides associated with active features. Recent interpretations of *Galileo* Near  
192 Infrared Mapping Spectrometer (NIMS) data in the light of new laboratory spec-  
193 tra find that perchlorates—oxidized Cl ostensibly from the internal ocean—can  
194 also match absorption features of surface materials (Hanley et al, 2014). The red-  
195 dish tint of Europa’s non-icy materials surface materials has been attributed to  
196 radiation-induced flaws in crystalline sodium (e.g., Hand and Carlson, 2015). These  
197 many lines of evidence for endogenous chlorine do not rule out a sulfate dominated  
198 ocean. As noted by Zolotov and Kargel (2009), a highly oxidized ocean dominated  
199 by  $\text{Mg}^{2+}$  and  $\text{SO}_4^{2-}$  also has substantial  $\text{Na}^+$  and  $\text{Cl}^-$ . Equilibrium freezing of  
200 such an ocean yields a fractionated eutectic composition of mainly  $\text{NaCl}$  that is  
201 nearly identical to the result of applying the same method to seawater (Vance  
202 et al, 2019). Further complicating the interpretation of Europa’s ocean compo-  
203 sition based on the composition of its surface, the speciation of surface salts is  
204 influenced by radiation and by the speed at which freezing (or refreezing) oc-  
205 curs (Vu et al, 2016). Thus, it is best to remain agnostic about Europa’s ocean  
206 composition until firmer constraints on interior structure, ice thickness, surface  
207 composition, and potentially plume composition, can be obtained with NASA’s  
208 *Europa Clipper* mission.

### 209 1.2.2 *Ganymede*

210 Models for Ganymede’s internal structure, again constrained by mass and gravity  
211 data under the assumption of hydrostatic equilibrium, suggest an outer ice-liquid  
212 water layer between 600 to 900 km thick, with significant high-pressure ice phases;  
213 an intermediate mantle with thicknesses up to 1000 km and density consistent with  
214 an olivine-dominated, mostly dehydrated composition; and a central metallic core  
215 whose radius may extend from about 500 km to more than 1000 km depending  
216 on core composition (Anderson et al, 1996; Deschamps and Sotin, 2001; Kuskov

217 and Kronrod, 2001; Sohl et al, 2002; Vance et al, 2014, 2018a). Multiple pressure-  
 218 induced phase transitions are expected within Ganymede’s outer water layer, and  
 219 the outermost ice I shell is expected to be less than  $\sim 150$  km thick (Vance et al,  
 220 2014, 2018a).

221 Measurements of the induced magnetic field by *Galileo* and auroral oval oscil-  
 222 lations observed by the *Hubble Space Telescope* indicate that the ocean electrical  
 223 conductivity is at least 0.09 S/m, which corresponds to a minimum salt concen-  
 224 tration of 0.9 gram  $\text{MgSO}_4$  per kilogram of ocean water, for an ocean between 150  
 225 to 250 km depths (Saur et al, 2015). As for Europa, a bias toward a magnesium  
 226 sulfate ocean composition for Ganymede is based firstly on models for the aqueous  
 227 alteration of CI chondrites (Kargel, 1991)—subsequently shown to be erroneous  
 228 (McKinnon and Zolensky, 2003)—that provided a good match to *Galileo* NIMS  
 229 spectra that fit well to  $\text{MgSO}_4$ . The ocean’s oxidation state, and thus the domi-  
 230 nant ionic composition, remain to be confirmed by further measurements, notably  
 231 by the European Space Agency’s *JU*piter *IC*y moon *EX*plorer (JUICE) mission  
 232 Grasset et al (2013). The intrinsic magnetic field of Ganymede further implies the  
 233 formation of an iron-rich core that may itself be layered with a solid inner and  
 234 fluid outer core (e.g., Rückriemen et al, 2018).

### 235 1.2.3 Callisto

236 The interior structure of Callisto is the least constrained of the Galilean satellites.  
 237 Here, the interpretations are less clear because the satellite may not be in hydro-  
 238 static equilibrium (Gao and Stevenson, 2013) and the induced magnetic field signal  
 239 may be due to the ionosphere rather than a subsurface ocean (Hartkorn and Saur,  
 240 2017). The MoI-factor assuming hydrostatic equilibrium (Anderson et al, 2001)  
 241 prohibits a metallic core, requires low mantle densities that are consistent with a  
 242 saturated pyrolite composition, and corresponds to water layers that are  $\lesssim 250$   
 243 km thick (Vance et al, 2018a). Conversely, a significantly lower MoI estimate that  
 244 does not assume hydrostatic equilibrium (Gao and Stevenson, 2013) requires a  
 245 central iron core and mantle densities that are consistent with an anhydrous pyro-  
 246 lite composition (Vance et al, 2018a). If an ocean is present, Zimmer et al (2000)  
 247 found that the magnetic field data are best explained by electrical conductivity  
 248 values of  $\gtrsim 0.02$  S/m with ocean thicknesses of  $\lesssim 300$  km. Because Callisto formed  
 249 farthest from Jupiter of the Galilean satellites, any ocean that is present may be  
 250 nearly frozen, making it an appealing target for studying the end stage dynamics  
 251 of a large ocean world.

### 252 1.2.4 Enceladus

253 Recent observational data from the *Cassini-Huygens* mission has shed new light  
 254 on the interiors of Saturnian satellites. At Enceladus, measurements of the gravity  
 255 field, the shape and rotational state, and direct sampling of plume material all pro-  
 256 vide constraints on internal structure and composition. Early shape and gravity  
 257 measurements, in combination with geyser activity near the south pole, indicated  
 258 the presence of a subsurface water reservoir (e.g., Porco et al, 2006; Dougherty  
 259 et al, 2006; Thomas et al, 2007; Collins and Goodman, 2007; Iess et al, 2014). A  
 260 global ocean was determined decisively by detection of a significant physical libra-  
 261 tion (Thomas et al, 2016). The libration amplitude is about four times larger than

262 expected for a solid Enceladus due to the decoupling of the rotational behaviour  
263 of the shell with respect to the deeper solid interior and indicates that the ocean is  
264 about 20 km beneath the surface on average and that the mean ocean thickness is  
265 between 21 and 67 km (Thomas et al, 2016; Van Hoolst et al, 2016). Independent  
266 confirmation of these results was obtained by gravity (Iess et al, 2014) and topog-  
267 raphy (Nimmo et al, 2011; Tajeddine et al, 2017) data that predict, assuming  
268 isostasy at the long wavelengths observed in the gravity field, a core radius of  $\sim 190$   
269 km, an ocean thickness of  $\sim 40$  km, and a shell thickness of  $\sim 20$  km, on average  
270 (Beuthe et al, 2016; Ćadek et al, 2016). Large variations in ice shell thickness  
271 exist, with mean equatorial, north polar, and south polar thicknesses of approx-  
272 imately 30 km, 15 km, and 5 km, respectively. (McKinnon, 2015; Thomas et al,  
273 2016; Beuthe et al, 2016; Ćadek et al, 2016, 2019; Hemingway and Mittal, 2019).  
274 A thinner ice shell at the south pole of Enceladus favors the exchange between the  
275 rocky interior, where hydrothermal processes are likely present (Hsu et al, 2015),  
276 and the surface (see Section 2.4).

277 Out of all the water oceans that inevitably exist in the universe, Enceladus'  
278 is the one that we know about second best (Glein et al, 2018; Postberg et al,  
279 2018a). Measurements of the composition of grains and gases erupted out of Ence-  
280 ladus in the form of a plume show that the satellite's ocean contains four classes  
281 of materials. The first class is salts (Postberg et al, 2009, 2011) that are domi-  
282 nated by sodium chloride (NaCl), and sodium bicarbonate (NaHCO<sub>3</sub>) or carbon-  
283 ate (Na<sub>2</sub>CO<sub>3</sub>). Potassium salts also appear to be present, but are  $\sim 10^2$  times less  
284 abundant than their sodium counterparts (Postberg et al, 2009). Second, *in situ*  
285 observations of dust in the inner Saturn system (Hsu et al, 2015) indicate that  
286 some plume grains from Enceladus contain embedded nanometer-sized particles  
287 of nearly pure silica (SiO<sub>2</sub>). Third, the major plume volatiles are H<sub>2</sub>O, H<sub>2</sub>, NH<sub>3</sub>,  
288 CO<sub>2</sub>, and CH<sub>4</sub> (Waite et al, 2017). The presence of minor and trace species, includ-  
289 ing volatile organic compounds (VOCs), is also implied by the mass spectrometry  
290 data from *Cassini*, although identifying and quantifying individual minor and trace  
291 species is challenging because the insufficiently resolved mass spectra allow multi-  
292 ple degenerate solutions to the composition (Magee and Waite, 2017). Two effects  
293 that may lead to more uncertainty in the volatile composition are chemical reac-  
294 tions induced by grain impacts onto instrument surfaces (Waite et al, 2009), and  
295 adsorption of VOCs onto ice grains in the plume (Bouquet et al, 2019). These ef-  
296 fects can be partially mitigated by focusing on the most weakly adsorbing volatiles  
297 (e.g., hydrocarbons) during the slowest flybys. The fourth class of materials in the  
298 plume are macromolecular organic compounds (Postberg et al, 2018b). The data  
299 from *Cassini* suggest that these materials have high molecular masses ( $>200$  u),  
300 and are carbon-rich (low H/C ratios) owing to an abundance of unsaturated car-  
301 bon atoms in unfused benzene rings. These features result in hydrophobic phase  
302 separation from water. The data also suggest the presence of further chemical  
303 complexity in the form of oxygen- and nitrogen-bearing functional groups in the  
304 observed organic matter.

### 305 1.2.5 Titan

306 Multiple lines of evidence from the *Cassini-Huygens* mission also constrain Titan's  
307 interior. The observation of a Schumann-like resonance by the *Huygens* probe is

308 not compatible with an entirely solid satellite and can be explained by a conduct-  
309 ing ocean 55 to 80 km below the surface, which acts as a reflecting boundary for  
310 Extremely Low Frequency (ELF) waves (Béghin et al, 2012). Gravity and topog-  
311 raphy also indicate an ocean that is, on average, about 100 km beneath the surface  
312 (Nimmo and Bills, 2010). Measurements of the time-varying gravity field of Titan  
313 determining the tidal Love number ( $k_2 = 0.616 \pm 0.067$ ) (Durante et al, 2019) also  
314 imply an ice shell thickness between 50-100 km (e.g., Mitri et al, 2014), which is  
315 consistent with thermal modeling results (Tobie et al, 2006; Mitri et al, 2010).

316 The gravitational constraints provide not only unambiguous evidence of a sub-  
317 surface ocean close to the surface, but also indicate that Titan’s subsurface ocean  
318 is likely much denser than pure water. The ocean appears to have a high bulk den-  
319 sity, exceeding  $1100 \text{ kg/m}^3$ , based on the large value of the measured tidal Love  
320 number (Iess et al, 2012; Baland et al, 2014; Lefevre et al, 2014; Mitri et al, 2014;  
321 Vance et al, 2018a; Durante et al, 2019). Magnesium and ammonium sulfates have  
322 been proposed on the basis of chemical and physical models (Fortes et al, 2007)  
323 and in the context of experiments investigating the chemistry of these compounds  
324 (Hogenboom, 1995; Hogenboom et al, 1997; Vance and Goodman, 2013). The high  
325 density constraint could be met with 10 wt%  $\text{MgSO}_4$  (Vance et al, 2018a). A re-  
326 ducing ocean dominated instead by chlorides can obtain similar large densities,  
327 but equation of state data in the relevant pressure range are not yet available to  
328 demonstrate this. A saline ocean is not expressly required by the current uncer-  
329 tainty in the Love number, though, which permits densities as low as  $1100 \text{ kg/m}^3$ ,  
330 consistent with the pure water or even 3 wt% ammonia ( $\text{NH}_3$ ) cases as described  
331 by Vance et al (2018a). The high Love number could alternatively be explained  
332 by a significant viscous behavior of the interior below the ocean (Durante et al,  
333 2019) or by a resonantly excited internal gravity mode, which would require the  
334 ocean to be stably stratified (Luan, 2019).

335 A dense, salty ocean and thin ice require a high heat flux, exceeding 800 GW  
336 ( $10 \text{ mW/m}^2$ ) (Vance et al, 2018a). Such a high heat flux would be consistent  
337 with recent geological activation of Titan, perhaps concurrent with the formation  
338 of Saturn’s rings (Ćuk et al, 2016). A dense ocean and thin ice only worsen the  
339 problem of accounting for the low density ( $2600 \text{ kg/m}^3$ ) of Titan’s rocky interior.  
340 It thus seems likely that Titan is weakly differentiated, highly porous, or both.  
341 Alternatively, a differentiated Titan with a small metallic core ( $R < 400 \text{ km}$ )  
342 would be permitted by the gravitational constraints if the low density layer under  
343 the ocean can be explained (Vance et al, 2018a). The presence of some dissolved  
344 electrolytes in Titan’s ocean solutes is consistent with the model used for the ELF  
345 waves, and with a potential low temperature at the top ocean compatible with a  
346 likely rigid ice shell (Vance et al, 2018a). An intriguing possibility is that the low  
347 density of Titan’s interior can be explained by the presence of organic materials.  
348 Geochemical modeling can reproduce the ratios of  $^{36}\text{Ar}/\text{N}_2$  and  $^{15}\text{N}/^{14}\text{N}$  as mea-  
349 sured by *Huygens* in Titan’s atmosphere, if the building blocks of Titan contained  
350 abundant organic materials that were subsequently heated and outgassed from  
351 the deep interior (Miller et al, 2019). This idea is challenging to model because it  
352 requires thermodynamic descriptions of organic-rich mineral assemblages that are  
353 rare or non-existent in Earth’s geology.

## 2 Surface Exchange Processes

Potential surface expressions of ice-ocean material exchange occur vary widely in morphology and age across the satellites. The mechanisms of exchange can be broadly categorized into those caused by impact processes, tectonic processes, cryovolcanic/outgassing processes, and plume processes; a unique morphology characterized by *in situ* surface disruption suggestive of lithospheric thinning, termed chaos, is observed on Europa and will be discussed separately. Europa exhibits global resurfacing with a surface age between 30 and 90 million years (Bierhaus et al, 2009), while Enceladus' surface exhibits both ancient terrains and ongoing geologic activity (e.g., Patterson et al, 2018). Titan's surface is also geologically active, with its thick atmosphere and hydrocarbons seas playing a significant role that will not be discussed in detail here (see Jaumann et al (2009) for a review). Conversely, Ganymede and Callisto show older and more limited signs of surface exchange (Schenk et al, 2004).

### 2.1 Impact Processes

Multi-ringed structures observed on the icy worlds Callisto, Ganymede, and Europa range in size from the  $\sim 2000$  km diameter Valhalla basin ring system on Callisto (Kinnon and Melosh, 1980; Moore et al, 2004; Schenk et al, 2004) to the  $\sim 300$  km diameter Tyre multi-ringed structure on Europa (Schenk et al, 2004; Schenk and Turtle, 2009). They all share morphological characteristics that suggest impact into a relatively thin brittle lithosphere underlain by a ductile or liquid subsurface (Kinnon and Melosh, 1980; Melosh, 1989). The scale of multi-ring basins on Callisto and Ganymede suggests the possibility of direct exchange between the ice shell and ocean of the satellites. However, the depth to the ice-ocean interface at the time of formation for these basins is not known, leaving open the possibility that their ice shells were not breached during the formation of these features. An abrupt transition from complex crater morphologies to multi-ring morphologies observed on Europa indicates a similarly abrupt transition from ice to water may occur at depths of 10 to a few 10s of km (Schenk et al, 2004) and suggests impacts that formed multi-ring structures could have sampled the satellite's subsurface ocean. However, a lack of radial faulting associated with the formation of multi-ring structures on Europa argues that they may not have breached its ice shell (Turtle, 1998; Kadel et al, 2000). While clear evidence for direct ice-ocean material exchange is not present in association with this process, the potential for convection within the ice shells of Callisto, Ganymede, and Europa (Shoemaker et al, 1982; Schubert et al, 2004; Barr and Showman, 2009) indicates that indirect ice-ocean exchange could still occur.

Palimpsests are impact features that appear to be unique to Callisto and Ganymede. They are generally circular to slightly elliptical albedo features that leave a barely discernable topographic imprint and are characterized by faint concentric lineations and, often, a central smooth region (Schenk et al, 2004; Patterson et al, 2010). Their diameters are measured in 100s of km and, similar to the older multi-ring basins, their formation has been attributed to impact into a relatively thin brittle lithosphere (Shoemaker et al, 1982). As with multi-ring basins, it is possible that direct ice-ocean exchange could have occurred when these features

399 formed, but not clearly so. However, as with the multi-ring basins and structures,  
400 indirect exchange of material is also a possibility.

401 Several numerical studies using hydrocodes have been performed to investigate  
402 under which conditions melt may be generated upon impact and impact cratering  
403 may excavate oceanic water to the surface (e.g., Artemieva and Lunine, 2003;  
404 Kraus et al, 2011; Senft and Stewart, 2011). For thin ice shells ( $\leq 10$ km), a pro-  
405 jectile of a few kilometers in diameter is sufficient to break the entire shell and  
406 expose water to the surface (e.g., Turtle and Pierazzo, 2001; Lunine et al, 2010).  
407 For thicker ice shells, exposure of oceanic water is still possible if the projectile  
408 size is about half the ice shell thickness (e.g., Artemieva and Lunine, 2005; Lunine  
409 et al, 2010). Large impacts such as the one that formed the Menrva crater on  
410 Titan, for example, should have brought large volume of water to the surface and  
411 temporarily changed the climate of Titan by potentially rising the surface tem-  
412 perature by 80 K (Zahnle et al, 2014). Monteux et al (2016) also showed that an  
413 impactor of 25 km in radius at moderate velocity ( $\sim 2$  km s $^{-1}$ ) was able to totally  
414 disrupt the ice shell and excavate huge volume of oceanic water to the surface.  
415 Even if such large impact events remain rare during the moon history, they have  
416 the potential to induce resurfacing from regional to global scale, for sufficiently  
417 large impacts.

## 418 2.2 Tectonic Processes

419 Ridges on Europa come in a variety of morphological forms, are observed on length  
420 scales of up to 1000s of kilometers, and can range from linear to cycloidal to  
421 anastomosing in planform (Prockter and Patterson, 2009). Double ridges are by  
422 far the most common ridge type on Europa and are observed over most of the  
423 satellite's visible surface history (Figueredo and Greeley, 2000, 2004). Numerous  
424 models have been suggested for the formation of ridges on Europa, all of which  
425 appeal to the exploitation of a pre-existing fracture in Europa's ice shell. The  
426 most widely accepted model of ridge formation suggests that cyclical strike-slip  
427 motion on a pre-existing fracture will dissipate heat and cause the warmer, now  
428 more buoyant, ice flanking the fracture to uplift and form a double ridge (Nimmo  
429 and Gaidos, 2002; Han and Showman, 2008; Kalousova et al, 2016). This process  
430 could also create melt that would migrate down the fracture and, provided the  
431 fracture penetrates the brittle lithosphere, could provide a direct or indirect path  
432 of bringing surface material to Europa's subsurface ocean. The path taken would  
433 depend on the thickness and rheology of the shell. Other models of ridge formation  
434 suggest they could be pathways for fissure eruptions (Kadel et al, 1998), dike  
435 intrusions (Turtle et al, 1998), linear diapirism (Head et al, 1999), or melt squeezed  
436 to the surface via cyclical tidal (Greenberg et al, 1998). More recently, subsurface  
437 sills feeding cryoclastic eruptions has been proposed (Dombard et al, 2013; Craft  
438 et al, 2016). In contrast with the shear heating model, these models imply that  
439 ocean material would be brought to the surface or near surface.

440 Some double ridges and ridge complexes (another morphological feature class)  
441 on Europa are flanked by deposits that are relatively low albedo and extend for  
442 up to 10 km on either side of the feature they are associated with (Lucchitta  
443 and Soderblom, 1982; Belton et al, 1996). The dark material is likely a relatively  
444 thin surficial deposit that drapes over the preexisting terrain (Geissler et al, 1998;

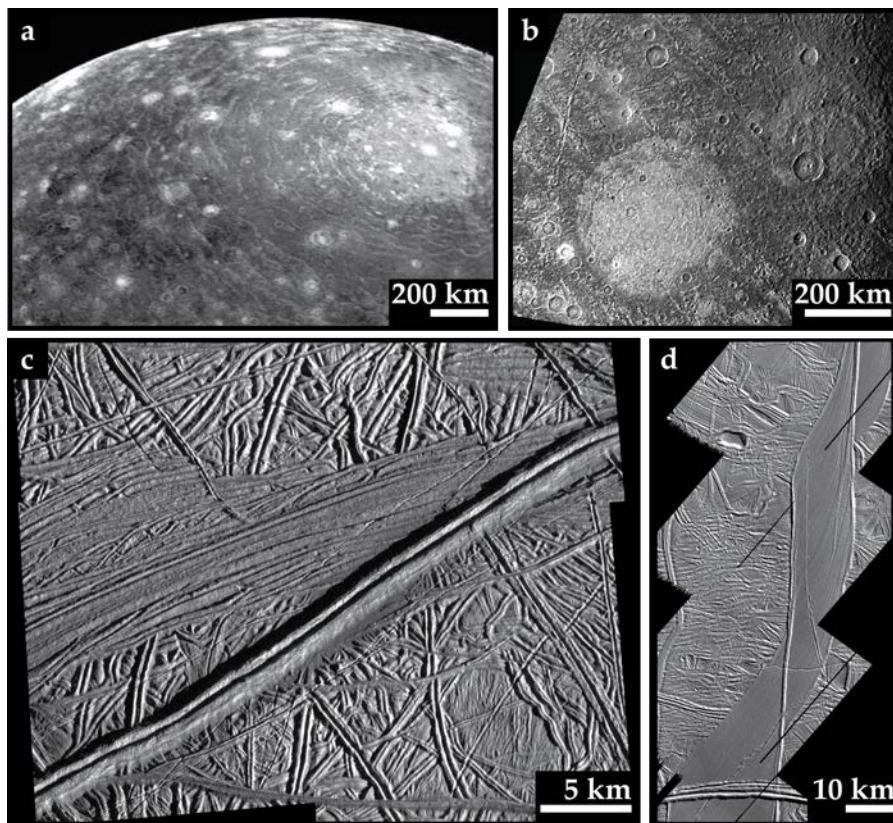


**Fig. 2** Impact and tectonic features of icy ocean worlds. (a) The prominent impact basin Valhalla on Callisto. The circular region is 300 km in diameter and basin rings extend 1500 km from the basin center. (b) The 340 km diameter palimpsest Memphis Facula on Ganymede. (c) An archetype double ridge on Europa, Androgeous Linea. (d) A dilational band, Astypalaea Linea, on Europa.

445 Fagents et al, 2000). These deposits may be continuous along the flanks of a ridge,  
 446 or spaced in discrete subcircular regions along the margins of a ridge (Prockter  
 447 and Patterson, 2009). Observations by the *Galileo* NIMS instrument suggest that  
 448 low albedo deposits associated with tectonic features on Europa are composed  
 449 of sulfates (McCord et al, 2002) or  $MgCl_2$  (Brown and Hand, 2013; Ligier et al,  
 450 2016) that are converted into magnesium sulfates through radiolytic processes.  
 451 The proposed compositions of low albedo deposits suggest that they were initially  
 452 emplaced by an endogenic process and have subsequently been affected by exposure  
 453 to the local radiation environment.

454 Ridges on Enceladus also come in a variety of forms (Patterson et al, 2018)  
 455 but the most relevant of them for discussing ice-ocean exchange are the ‘tiger  
 456 stripes’ of the South Polar Terrain (SPT). The SPT is a pervasively fractured,  
 457 geologically young, and low-lying region bound by a quasi-polygonal circumpolar  
 458 system of scarps that are intermittently broken by Y-shaped structures (Porco  
 459 et al, 2006; Helfenstein, 2014). Within this terrain are the ridges Damascus Sulcus,  
 460 Baghdad Sulcus, Cairo Sulcus, and Alexandria Sulcus, collectively referred to as

461 tiger stripes. These features are associated with anomalously high heat flows and  
462 are geologically active, as evidenced by eruptive jets (see Section 2.4) of water  
463 and other constituents (e.g., Porco et al, 2006; Hansen et al, 2008) that are likely  
464 sourced directly from Enceladus' subsurface ocean (Spencer et al, 2018).

465 Bands on Europa are another class of tectonic feature whose formation could  
466 facilitate ice-ocean material exchange. This feature can be subdivided into three  
467 morphological classes: dilational bands, bright bands, subsumption bands. Dila-  
468 tional bands, also referred to as pull-apart bands, are the more commonly observed  
469 feature type (Figueredo and Greeley, 2000, 2004). These bands have margins that  
470 can be easily reconstructed (Schenk and McKinnon, 1989; Pappalardo and Sulli-  
471 van, 1996; Sullivan et al, 1998), indicating that their interiors consist of subsurface  
472 material that has been emplaced at the surface of Europa (e.g., Howell and Pap-  
473 palardo, 2018). Dilational band formation represents a significant process by which  
474 Europa's crust has been resurfaced (Schenk and McKinnon, 1989; Pappalardo and  
475 Sullivan, 1996; Prockter et al, 2002). Two endmember models have been proposed  
476 for the formation of pull-apart bands. One is the tidal pumping model proposed  
477 by (Tufts et al, 2000). That model suggests that bands are part of a continuum  
478 process that begins with the formation of a fracture, progresses to a ridge, and  
479 ultimately ends in the formation of a dilational band. This mechanism proposes  
480 direct exchange of ocean material with the surface of Europa. The second model,  
481 by Prockter et al (2002), proposes that band formation is distinct from that of  
482 ridges and involves solid-state material rising to fill the separating margins of a  
483 preexisting fracture in a manner analogous to terrestrial mid-ocean ridges. This  
484 mechanism would imply indirect exchange of ocean material with the surface. Ana-  
485 log wax experiments have indicated that oblique opening and shearing commonly  
486 associated with the formation of dilational bands is best explained with the latter  
487 model of formation (Manga and Sinton, 2004). Bright bands are linear features  
488 that disrupt preexisting terrain and have internal textures reminiscent of dila-  
489 tional bands. However, unlike that feature type, bright bands are far less common  
490 and have margins that do not appear as if they can be reconstructed. Forma-  
491 tion mechanisms relying on dilational, contractional, and/or lateral deformation  
492 have all been proposed to explain the unique characteristics of this type of band  
493 (Prockter and Patterson, 2009). Depending on the formation mechanism used (or  
494 combination thereof), ice-ocean exchange is possible, but without additional data  
495 to test the proposed formation models, the potential importance of this feature  
496 type for material exchange is not as clear as it is with dilational bands. Recent  
497 work has introduced a new band feature class: subsumption bands (Kattenhorn  
498 and Prockter, 2014). This feature type has been observed within Falga Regio on  
499 Europa and is associated with the loss of surface material. It is not clear if material  
500 subducted in this manner would reach the ice-ocean interface, though.

501

### 502 2.3 Cryovolcanic and Outgassing Processes

503 The potential for cryovolcanic activity on Ganymede has changed significantly  
504 between analyses conducted using *Voyager* versus *Galileo* data. Based on *Voy-*  
505 *ager* images, dark material on Ganymede was interpreted to have been modified  
506 by cryovolcanic activity (Murchie and Head, 1989; Croft et al, 1994). This in-

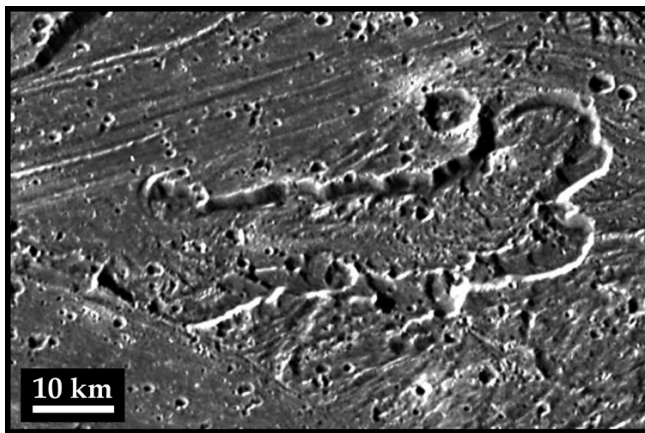


**Fig. 3** Oblique view of a depression found within Sippar Sulcus, Ganymede, and acquired during the G8 encounter at 179 m/pixel, where south is up. This feature has a surface texture that may be indicative of flow toward its open end, consistent with it being a source region for icy volcanic material. From (Patterson et al, 2010).

507 terpretation was supported by an apparent absence of small craters, embayment  
 508 relationships observed in association with large craters, and smooth areas asso-  
 509 ciated with tectonic and impact features (Casacchia and Strom, 1984; Murchie  
 510 et al, 1990; Schenk and Moore, 1995). Groove lanes that pervasively disrupt dark  
 511 material on Ganymede were interpreted to represent regions of resurfacing by cryo-  
 512 volcanic flows, which were subsequently tectonized in some areas to form grooves  
 513 (Golombek and Allison, 1981; Golombek, 1982; Shoemaker et al, 1982; Allison  
 514 and Clifford, 1987). However, higher-resolution *Galileo* image data imaging of  
 515 Ganymede revealed no unequivocal observation of lobate materials with an iden-  
 516 tifiable source vent or any other identifiable morphology related to cryovolcanism  
 517 associated with dark material (Prockter et al, 2000). Candidate cryovolcanic units  
 518 identified from *Voyager* data at lower resolution on the basis of embayment and  
 519 texture instead appeared to be the result of fluidized impact ejecta (Pappalardo  
 520 et al, 2004) and dark smooth materials in topographic lows appeared to have  
 521 accumulated by downslope movement of loose material, instead of by some cryo-  
 522 volcanic mechanism (Prockter et al, 1998). Higher-resolution *Galileo* image data of  
 523 groove lanes on Ganymede have also lacked clear morphological evidence for flow  
 524 fronts, source vents, embayment relationships, or any other evidence suggestive  
 525 of cryovolcanic emplacement. However, indirect evidence for volcanic resurfacing  
 526 has been identified in the form of small isolated caldera-like features (Lucchita,  
 527 1980; Schenk and Moore, 1995; Spaun et al, 2001) and smooth, topographically  
 528 low bright lanes (Schenk et al, 2001).

529 For Titan, the only ocean world with a dense atmosphere, evidence of out-  
 530 gassing comes from the presence of  $^{40}\text{Ar}$  in Titan's atmosphere (Niemann et al,  
 531 2005; Waite et al, 2005; Atreya et al, 2006) because  $^{40}\text{Ar}$  is produced by the decay  
 532 of  $^{40}\text{K}$  that is initially contained in the silicate fraction. The amount of  $^{40}\text{Ar}$  in  
 533 Titan's atmosphere was measured by the Gas Chromatograph Mass Spectrome-  
 534 ter (GCMS) onboard the *Huygens* probe in 2005 (Niemann et al, 2005) and by  
 535 the *Cassini* Ion and Neutral Mass Spectrometer (INMS) (Waite et al, 2005). The  
 536 value was revised to  $3.39 (\pm 0.12) \times 10^{-5}$  mole fraction by Niemann et al (2010).  
 537 Depending on the elementary composition of the silicate fraction, the outgassing  
 538 corresponds to 5 to 20% of the total amount of  $^{40}\text{Ar}$  produced by the decay of  
 539  $^{40}\text{K}$ . Another clue for the existence of exchange process comes from the presence

540 of methane in Titan’s atmosphere because methane is destroyed by photolysis.  
541 Current models (Wilson and Atreya, 2000; Bézard et al, 2014) suggest that the  
542 present amount of methane would disappear in less than 30 Myr, which is a short  
543 time relative to geological timescales. Therefore, methane has to be resupplied into  
544 the atmosphere, and endogenic (e.g., cryovolcanic) processes have been proposed  
545 as a possible process (Tobie et al, 2006). Potential cryovolcanic features on Titan  
546 are relatively young, not widely distributed across the surface, and include flow  
547 fields near Hotei Arcus, Tui Regio, and Ganesa Macula (see Jaumann et al (2009)  
548 for a review).

#### 549 2.4 Plume Processes

550 As described in Section 2.2, there are tectonic processes on Enceladus and Eu-  
551 ropa that can provide potential (in the case of Europa) or actual (in the case of  
552 Enceladus) conduits for ice-ocean exchange relating to plume activity.

553 For Enceladus, approximately 100 supersonic jets of gas and ice grains have  
554 been observed to erupt from the four SPT tiger stripes to form a large plume  
555 towering above the south pole (Spahn et al, 2006; Porco et al, 2006; Hansen et al,  
556 2008; Porco et al, 2014; Spitale et al, 2015). Observed plume intensities vary be-  
557 tween 100 kg/s and 1000 kg/s of water vapour, with an average of about 200 kg/s,  
558 escaping into the plume (Hansen et al, 2011, 2017). The vapour redeposits onto the  
559 vent’s ice walls or condenses to tiny ice grains (e.g., Ingersoll and Pankine, 2010;  
560 Schmidt et al, 2008; Yeoh et al, 2015), and a substantial part of the ice grains  
561 appear to be frozen ocean spray entrained in the flow that might directly sample  
562 the composition of the ocean (Postberg et al, 2009, 2011). Estimates for the gas to  
563 ice ratio in the plume vary greatly, although recent estimates suggest an average  
564 value of  $\sim 10$  (Kempf et al, 2018; Postberg et al, 2018a). While the ejection speeds  
565 for plume vapour are generally above Enceladus’ escape speed (Goldstein et al,  
566 2018), only a fraction of the ice grains escape the moon’s gravity to form Saturn’s  
567 E ring (Kempf et al, 2018) and a greater part falls back to form surface deposits  
568 (Scipioni et al, 2017; Southworth et al, 2019).

569 The jets and plume are temporally and spatially variable. Jets appear to turn  
570 on and off on typical time scales of years, indicating occasional opening / sealing of  
571 certain ice vents (Nimmo et al, 2014), and systematic variations observed across the  
572 fissures suggest trends in the composition of the plume material and/or variations  
573 in the plumbing connecting these reservoirs to the surface (Hedman et al, 2018).  
574 In contrast, plume activity is coupled most prominently to the moon’s orbital  
575 period, with brightness variations on the order of years as well (Hedman et al,  
576 2013; Nimmo et al, 2014; Ingersoll and Ewald, 2017); variations in the integrated  
577 emitted gas flux over time seem to be milder (Hansen et al, 2017; Teolis et al,  
578 2017).

579 The detection of silica nano particles (Hsu et al, 2015), salts, and large or-  
580 ganic molecules in the erupted ice grains (Postberg et al, 2009, 2011, 2018b) in  
581 combination with  $\text{MH}_4$  and  $\text{H}_2$  measured in the plume (Waite et al, 2017) sug-  
582 gests that material originating from the moon’s rocky core enters the plume. This  
583 indicates that the tiger stripe fractures penetrate the entire thickness of the ice  
584 shell, tapping into the global ocean underneath (Porco et al, 2006; Kite and Rubin,  
585 2016; Spencer et al, 2018). From buoyancy arguments, water should fill large parts

586 of these fractures and the level of neutral buoyancy should be situated at  $\sim 90\%$   
 587 of the distance from the ocean to the moon's surface, above which the fractures  
 588 would be vapor-filled. With an apparent ice shell thickness of not more than 5 km  
 589 (e.g., Čadek et al, 2019), it seems plausible that liquid water could be situated at  
 590 only a few hundred meters depth within the fractures with some variability ( $\sim 10$ s  
 591 of meters) due to flushing from tidal flexing of the crust (Kite and Rubin, 2016).  
 592 *Cassini* measurements constrain the outlet diameters to be  $< 10$  m (Goguen et al,  
 593 2013), and models suggest that the average width of cracks narrows to less than  
 594 a few 10s of centimeters above the water surface (Schmidt et al, 2008; Postberg  
 595 et al, 2011; Nakajima and Ingersoll, 2016) and is on the order of 1 m for the water  
 596 filled portion (Kite and Rubin, 2016; Spencer et al, 2018).

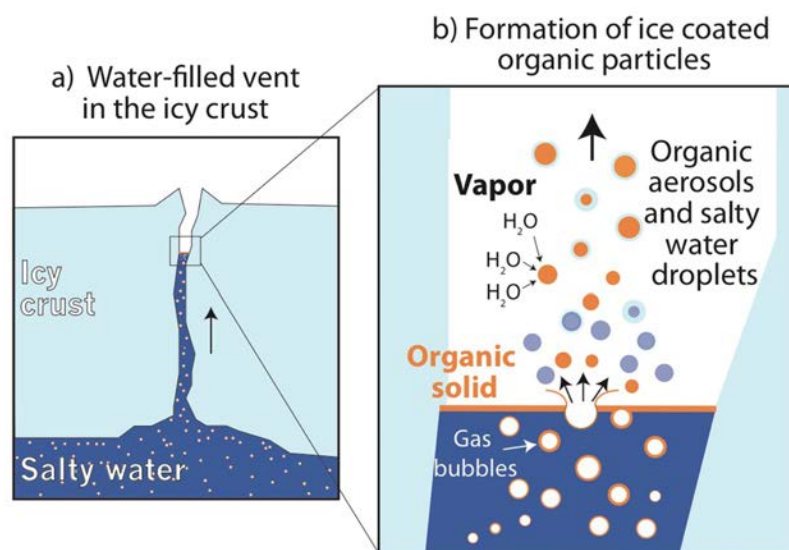


**Fig. 4** Schematic of the formation of ice grains from heterogeneous nucleation (not to scale). (a) Ascending gas bubbles in the ocean efficiently transport organic material into water-filled cracks in the south polar ice crust. (b) Organics ultimately concentrate in a thin organic layer on top of the water table inside the icy vents. When gas bubbles burst, they form aerosols made of insoluble organic material that later serve as efficient condensation cores for the production of an icy crust from water vapor, thereby forming organic-rich particles. Another effect of the bubble bursting is that larger, pure saltwater droplets form, which freeze and are later detected as salt-rich ice particles in the plume and the E ring. The figure implies the parallel formation of both organic and saltwater spray, but their formation could actually be separated in space (e.g., at different tiger stripe cracks) or time (e.g., dependent on the varying tidal stresses). From Postberg et al (2018b).

597 The mechanical and thermodynamic driver of the plume is evaporation of ocean  
 598 water from the water surface inside back-pressured ice vents (Spencer et al, 2018).  
 599 There, temperatures and pressures are close to the triple point of water, which  
 600 allows water to evaporate efficiently. Together with volatile gases emerging from  
 601 depth or exsolving from the ocean water, vapor is quickly accelerated to supersonic  
 602 speeds (Hansen et al, 2008) by the pressure gradient to nearby open space (Gold-  
 603 stein et al, 2018). During this ascend, the gases cool substantially and, depending

604 on their composition, will partially condense onto walls and into ice grains (Waite  
605 et al, 2017; Bouquet et al, 2019; Khawaja et al, 2019). Almost pure water ice grains  
606 and most of the likewise salt poor, but organic-bearing grains are thought to form  
607 in this way from supersaturated vapor inside (Schmidt et al, 2008; Postberg et al,  
608 2009) and at the outlets (Yeoh et al, 2015) of ice vents. The majority of ice grains  
609 in the plume are in a crystalline state (Dhingra et al, 2017), indicative of formation  
610 temperatures above 135 K.

611 The apparent heterogeneity of ice grain compositions strongly argues for differ-  
612 ent grain formation mechanisms (Fig. 4). Salty ice grains are thought to be frozen  
613 ocean spray generated when bubbles burst at the water surface inside the vertical  
614 cracks (Postberg et al, 2009, 2011). These bubbles might be formed from either  
615 mildly boiling water close to its triple point or upwelling volatile gases (e.g., CO<sub>2</sub>,  
616 CH<sub>4</sub>, or H<sub>2</sub>). Consequently, these grains seem to be samples of oceanic near-surface  
617 waters (Postberg et al, 2009). A similar mechanism has been proposed to form ice  
618 grains containing complex organic substances in high concentrations. In analogy  
619 to similar processes on Earth’s oceans (e.g., Wilson et al, 2015), this solid organic  
620 material might have accumulated as part of an organic film near the oceanic sur-  
621 face. Upon bubble bursting, these organics become aerosolized and then serve as  
622 condensation cores to form a water ice crust that is entrained in the vapor flow  
623 rising through Enceladus’ ice vents (Postberg et al, 2018b).

624 For Europa, the first tentative telescopic detection of a plume occurred dur-  
625 ing a *Hubble Space Telescope* observation in December 2012. Localized ultraviolet  
626 line emission of hydrogen and oxygen were attributed as dissociative products of  
627 H<sub>2</sub>O vapor (Roth et al, 2014). Using off-limb observations while absorbing back-  
628 ground light during Europa transits in front of Jupiter, Sparks et al (2016, 2017)  
629 twice found indications for a plume at identical positions by. However, both au-  
630 thors also report non-detections on several occasions, indicating either sporadic  
631 or at least highly variable activity. In a reanalysis of *Galileo* magnetometer data  
632 recorded below 400 km altitude during the space crafts closest Europa flyby, Jia  
633 et al (2018) reported anomalies consistent with plume activity close to the position  
634 of the Sparks et al (2016, 2017) observations. Each of the individual observations  
635 does not provide unequivocal proof of a plume. However, the sum of all obser-  
636 vations with three different techniques, argue strongly for some level of at least  
637 intermittent venting activity. The origin of these putative plumes, however, re-  
638 mains an open question. Although a similar interpretation has been invoked for  
639 Europa as Enceladus (Southworth et al, 2015), the absence of correlation with true  
640 anomaly (Sparks et al, 2017) and the much larger gravity on Europa challenge this  
641 interpretation.

## 642 2.5 Chaos Terrain

643 A terrain unique to Europa, and covering approximately a quarter of its surface,  
644 is termed Chaos. Chaotic terrain is formed by disruption of the preexisting sur-  
645 face into isolated plates, coupled with the development of lumpy matrix material  
646 between the plates. Models for the formation of chaotic terrain that have been pro-  
647 posed in the literature fall into 1 of 5 categories – melt-through, diapirism, brine  
648 mobilization, sill injection, or impact – and are reviewed in Collins and Nimmo  
649 (2009). The melt-through model for chaos formation was born from the visible sim-

650 ilarity of plates in chaotic terrain to terrestrial pack ice (Carr et al, 1998; Greeley  
651 et al, 1998). In this model, a heat source at the base of the icy shell facilitates melt-  
652 ing of the overlying ice, exposing the ocean below, and leading to the formation  
653 of plates equivalent to icebergs that float in a matrix of refrozen ocean material  
654 (Greenberg et al, 1999; Thomson and Delaney, 2001). The diapirism model for  
655 chaos formation proposes that the morphology of chaotic terrain and pits, spots,  
656 and domes (collectively termed lenticulae) represents the surface expression of ris-  
657 ing diapirs (Pappalardo et al, 1998; Rathbun et al, 1998; Figueredo et al, 2002;  
658 Mével and Mercier, 2007). Such diapirs would develop due to either thermal or  
659 compositional buoyancy within the ice shell (Barr and Showman, 2009). In an-  
660 other model of chaos formation, Head and Pappalardo (1999) and Collins et al  
661 (2000) suggest that the formation of matrix material arises from partial melting of  
662 non-water-ice, low-melting-point materials and the mobilization of resulting briny  
663 liquids within the ice shell. Another way to deliver liquid into the icy shell of  
664 Europa is to inject it directly from the ocean. In this formation model, sills of  
665 melt form within Europa’s icy shell from pressurized water injected from frac-  
666 tures that penetrate its base (Crawford and Stevenson, 1988; Collins et al, 2000;  
667 Manga and Wang, 2007). Here, ice-water interactions and freeze out of the liquid  
668 sill describe the unique morphological and topographic characteristics of chaos on  
669 Europa (Schmidt et al, 2011). Finally, morphological similarities between chaotic  
670 terrain on Europa and terrestrial explosion craters (Billings and Kattenhorn, 2003)  
671 have led to the suggestion of an impact origin for the formation of chaos (Cox et al,  
672 2008; Cox and Bauer, 2015). In this model, floating plates of the original ice sur-  
673 face are preserved in a slushy matrix, filling an irregular hole in the ice left by the  
674 explosion crater.

### 675 **3 Ice Shell Dynamics and Exchange Processes**

676 Exchange processes between the deep ocean and the surface can provide key in-  
677 formation about the chemistry and organic content of the ocean, including the  
678 chemical processes at work at the rocky core/ocean interface, as has been demon-  
679 strated for Enceladus. Similarly important is assessing the downward transfer from  
680 the surface to the ocean since surface material may provide compounds, such as  
681 oxidants, required to maintain the chemical disequilibrium between the ocean and  
682 possible hydrothermal fluids in the rocky core, a process that seems required for life  
683 (Hand et al, 2007). Exchange between the ocean and the surface involves transport  
684 through the icy shell.

#### 685 **3.1 Thermal State of the Ice Shell**

686 The thickness of the outer ice shell is the principal characteristic that influences po-  
687 tential exchanges between the interior and the surface (Chyba and Phillips, 2002).  
688 It is controlled by thermal equilibrium between the shell and the subsurface ocean,  
689 which depends on how the energy from internal heating (radiogenic and/or tidal)  
690 is transported through the ice shell – both conduction and subsolidus convection  
691 are suitable heat transport mechanisms (e.g., Spohn and Schubert, 2003; Mitri  
692 and Showman, 2005; Tobie et al, 2006). The temperature profile is quite different

693 between a conductive (colder) and a convective (warmer) shell. Moreover, various  
 694 studies have shown that the convective processes can be separated into different  
 695 regimes (e.g., Moresi and Solomatov, 1995). In the stagnant lid regime, a thick  
 696 conductive lid is present on top of the convective layer which effectively slows  
 697 down the heat transfer and possibly limits the exchange between the ocean and  
 698 the surface, while in the mobile lid regime, which represents plate tectonics, the  
 699 lid is thinner and more heat and/or material can be transferred (Fig. 5a).

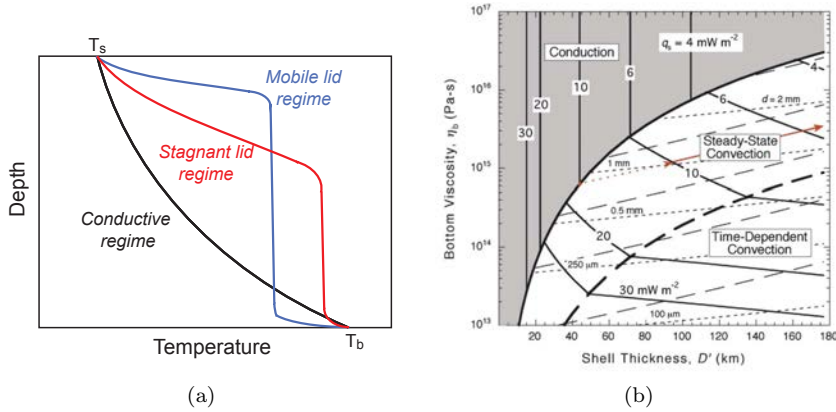


**Fig. 5** (a) Conductive (black) and convective thermal profiles in the stagnant (red) or mobile (blue) regime in the ice shell and (b) occurrence of convection (stationary or time-dependent) as a function of ice shell thickness and bottom viscosity in the stagnant lid regime (McKinnon, 2006).

700 Subsolidus convection is an efficient way to transport material between the deep  
 701 interior and the surface. On Earth, this process is coupled with plate tectonics that  
 702 leads to the major tectonic features such as mid-ocean ridges, subduction zones,  
 703 and transform faults. It also produces most of the volcanism. Terrestrial convection  
 704 is also characterized by the presence of hot plumes that form at a hot thermal  
 705 boundary layer or are triggered by the presence of partial melt (Ogawa, 2014).  
 706 Although it is controlled by the same physical processes, thermal convection in icy  
 707 shells differs significantly from terrestrial mantle convection for several reasons.  
 708 First, silicate mantles are heated from within by radiogenic decay while icy mantles  
 709 are mostly heated from below and, in some cases, from within by tidal heating.  
 710 Second, internal melting creates a negative buoyancy due to the high density of  
 711 liquid water relative to ice, while in silicate mantles, it favors the rise of hot  
 712 thermal upwellings. Third, in the case of an icy crust above an internal ocean,  
 713 the bottom interface is not fixed as for silicate mantles but evolves depending on  
 714 crystallization/melting processes.

715 Thermal evolution models have provided some constraints on the ice shell thick-  
 716 ness of ocean worlds in our solar system although more information is needed to ob-  
 717 tain accurate present-day estimates. According to models, the outer ice shells can  
 718 undergo large thickness variations during their evolution (Hussmann et al, 2002;  
 719 Sotin et al, 2009; Mitri et al, 2010) and potentially produce multiple transitions  
 720 between conductive and convective states (Mitri and Showman, 2005). The cou-

721 pling between the thermal and orbital evolution of Europa and Ganymede together  
722 with Io in the Laplace resonance could have produced multiple heat pulse events,  
723 potentially producing tectonic activity such as grooved terrains on Ganymede and  
724 internal melting in the crusts (Showman and Malhotra, 1997; Bland et al, 2009).  
725 For most satellites, except probably Enceladus (Choblet et al, 2017a), tidal heat-  
726 ing mainly occurs in the ice shell, where the visco-elastic timescale can be of the  
727 order of the orbital period of the tidal forcing (Tobie et al, 2003; Sotin et al,  
728 2009; Beuthe, 2013). Tidal heating in thin ice shells is larger at the poles than at  
729 equatorial regions by a factor of about four (Tobie et al, 2003; Beuthe, 2013) and  
730 also strongly depends on regional shell structure (e.g., the presence of faults) and  
731 thickness variations, since the tidal stress is approximately inversely proportional  
732 to the local shell thickness (Souček et al, 2016; Běhounková et al, 2017; Beuthe,  
733 2018; Souček et al, 2019).

734 Although the question of thickness and thermal state of the ice shells is not  
735 satisfactorily resolved, various models of solid state convection have been devel-  
736 oped. Consolmagno and Lewis (1978) initiated these studies, and more realistic  
737 models have subsequently been developed (e.g., Deschamps and Sotin, 2000; To-  
738 bie et al, 2003; Barr and Pappalardo, 2005; Mitri and Showman, 2005; Barr and  
739 McKinnon, 2007; Han and Showman, 2010; Běhounková et al, 2015; Weller et al,  
740 2019) once it was discovered that taking into account the variability of viscosity  
741 was key to a good description of heat transfer by convection (Davaille and Jaupart,  
742 1993; Moresi and Solomatov, 1995). The vigor of convection is measured through  
743 the non-dimensional Rayleigh number with the two main parameters being the  
744 ice shell thickness and the ice viscosity. Heat transfer by convection can become  
745 more efficient than by conduction as the layer thickens because the conductive  
746 heat flux is inversely proportional to the thickness of the layer. The critical value  
747 of the thickness at which convection starts has been investigated by a number of  
748 studies that included different complexities in the viscosity laws applicable to ice  
749 (e.g., Deschamps and Sotin, 2000; Mitri and Showman, 2005; Barr and McKinnon,  
750 2007) and showed that the likelihood of subsolidus convection in the icy shells of  
751 ocean worlds depends strongly on the deformation properties of ice.

752 The creep behavior of ice I has been studied in laboratory (e.g., Durham and  
753 Stern, 2001; Goldsby and Kohlstedt, 2001; De La Chapelle et al, 1999) and ob-  
754 served on terrestrial glaciers (e.g., Hudleston, 2015). Several mechanisms can occur  
755 to accommodate the deformation rate of ice: propagation of dislocations, diffusion,  
756 grain boundary sliding, and basal slip, each of them dominating in certain condi-  
757 tions. The deformation rate can be expressed as a combination of these different  
758 processes (Goldsby and Kohlstedt, 2001) and depends on pressure ( $P$ ), temper-  
759 ature ( $T$ ), shear stress ( $\tau$ ), and grain size ( $d$ ), which also depends on the  $P$ - $T$ - $\tau$   
760 conditions. Although each process has been well characterized, the grain size is  
761 poorly constrained for icy moons (Barr and McKinnon, 2007). Yet its knowledge  
762 is crucial to determine the icy shells' thermal state since the smaller the grain  
763 size, the lower the value of viscosity and thus the thinner the layer at the onset  
764 of convection. Barr and McKinnon (2007) suggest that the minimum thickness for  
765 convection to initiate in large ocean worlds such as Ganymede would be between 35  
766 and 66 km for grain sizes of 3 to 8 mm, respectively. In a study applied to Callisto,  
767 McKinnon (2006) proposes maps showing the conditions for convection to exist  
768 as a function of the viscosity at the ice/ocean interface and the thickness of the  
769 ice layer (Fig. 5b). Although the domain for convection seems large and suggests

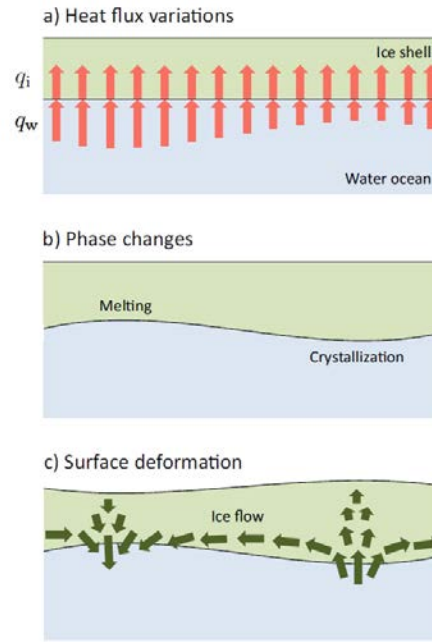


**Fig. 6** Sketch of the processes occurring at the ice/water interface and their consequences for the ice shell evolution (Kvorka et al, 2018). (a) The normal component of heat flux is not generally continuous at a phase interface. Melting occurs in regions where heat flux from the ocean is larger than heat flux in the ice shell. The opposite situation leads to crystallization. (b) In regions of melting, the ice shell loses mass and its thickness decreases. Crystallization is accompanied by ice mass gain and ice shell thickening. Both processes tend to restore the heat flux balance at the boundary. (c) Undulations of the ice/water interface generate pressure gradients that induce flows in the ice shell. These flows deform the upper boundary of the shell. Depressions develop above the regions of melting, while the surface tends to rise above the regions of crystallizations.

770 that convection would be dominant for thicknesses larger than 20 km, note that  
 771 the value of the corresponding grain size is less than 1 mm, which is more than  
 772 on order of magnitude smaller than the values predicted in Barr and McKinnon  
 773 (2007). Note also that the grain size evolution model predicts an increase in grain  
 774 size after convection starts, leading to increased viscosity and less vigorous convec-  
 775 tion. Finally, the presence of impurities would affect the grain size of ice as it has  
 776 been observed and modeled in cold ice sheets on the Earth (Durand et al, 2006).  
 777 Convection processes in the icy crust may have been intermittent on Ganymede,  
 778 Titan (Tobie et al, 2005, 2006), Europa (Hussmann et al, 2002), and Enceladus  
 779 (Barr, 2008), and a definite answer has to await measurements by future missions.

### 780 3.2 Global Dynamics of the Ice Shell

781 Long-wavelength topography and gravity can be used to constrain the lateral vari-  
 782 ations in shell thickness. Its amplitude and pattern provide insights on the thermal  
 783 state and global dynamics of the ice shell as well as on the coupling with the un-  
 784 derlying ocean (e.g., Nimmo et al, 2011). In combination with heat production  
 785 within the ice shell, strong heat flux anomalies coming from the seafloor and heat  
 786 flux patterns due to oceanic circulation can lead to a modulation of the ice/ocean  
 787 interface. The 3D structure of the ice shell and its global dynamics thus result from  
 788 a balance between the heat transfer through the ice shell, melting/crystallization  
 789 processes at the base and within the ice shell, and lateral ice flow (Čadek et al,  
 790 2017; Kvorka et al, 2018)(Fig. 6).

791 From the inversion of the topography and gravity data collected by *Cassini*,  
 792 maps of ice shell thickness have been inferred by several studies on Titan (Lefevre

793 et al, 2014; Mitri et al, 2014; Kvorka et al, 2018) and Enceladus (Čadek et al,  
 794 2016, 2019; Beuthe et al, 2016; Hemingway and Mittal, 2019). On Titan, the long-  
 795 wavelength topography is associated with small gravity anomalies indicating a  
 796 high degree of compensation (e.g., Durante et al, 2019). The observed topography,  
 797 characterized by relatively small amplitudes (about 1 km peak to peak) and an  
 798 anomalous equatorial bulge (the poles are about 300 m lower than the equator)  
 799 can be explained either by a deflection of the ocean/ice interface (Nimmo and  
 800 Bills, 2010; Hemingway et al, 2013; Lefevre et al, 2014) or by density variations  
 801 in the upper crust, likely due to heavy hydrocarbon clathrates (Choukroun and  
 802 Sotin, 2012). Assuming that surface topography is due to ice/ocean interface de-  
 803 flection, the inferred deflection amplitude ( $\pm 5$  km) indicates a very slow ice flow  
 804 at the base of the ice shell. It also implies a conductive and highly viscous ice  
 805 shell above a relatively cold ocean ( $T < 250$  K) (Lefevre et al, 2014; Kvorka et al,  
 806 2018). By modeling the shape evolution of Titan’s ice shell including diffusive heat  
 807 transfer through the ice shell, heterogeneous tidal heating in the ice shell, heat flux  
 808 anomalies from the ocean and basal ice flow, Kvorka et al (2018) show that the  
 809 observed topography is not consistent with tidal heating pattern in the ice shell  
 810 and rather indicates heat flux anomalies in the ocean (Fig. 7a). The anomalous  
 811 topographic bulge would be consistent with lateral variations of ocean heat flux  
 812 on the order of 0.1-1 mW/m<sup>2</sup>, characterized by upwelling of warm water in polar  
 813 regions and downwelling of cold water at low latitudes (Kvorka et al, 2018). The  
 814 origin of this oceanic flow is unclear. It may be a natural flow for the present-day  
 815 ocean configuration or it may result from heat flux forcing from the base of the  
 816 ocean (Soderlund, 2019).

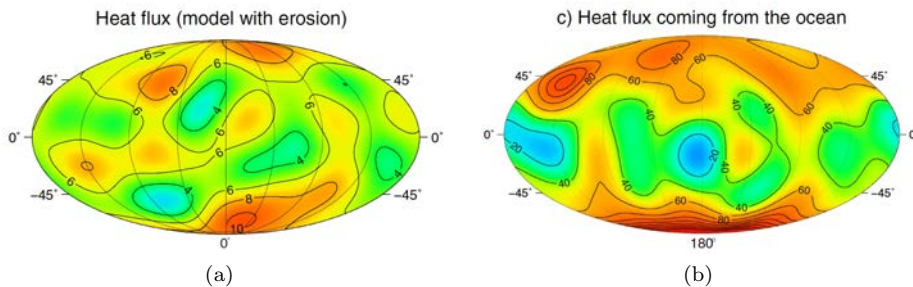


**Fig. 7** Heat flux anomalies from the ocean derived from the ice shell thickness variations, assuming a conductive ice shell, on (a) Titan for a model including surface mass redistribution by erosion (Kvorka et al, 2018) and (b) Enceladus (Čadek et al, 2019).

817 Using a similar approach, Čadek et al (2019) estimated the heat flux anomalies  
 818 at the bottom of Enceladus’ ice shell in order to explain the observed topography  
 819 (Tajeddine et al, 2017) and gravity (Iess et al, 2014). Compared to Titan, the ice  
 820 shell thickness variations are much larger, ranging from 5 km at the south pole to  
 821 35 km at the equator that are associated with heat flux anomalies about ten times  
 822 larger than on Titan (Fig. 7b). By modelling the ice flow driven by variations in  
 823 hydrostatic pressure on the ice/water interface, Čadek et al (2019) demonstrated  
 824 that Enceladus’ ice shell is in a steady state, with melting located in polar regions  
 825 and crystallization occurring in the equatorial region. The observed pattern is

826 consistent with the heat flux pattern predicted by tidally-heated water flow in the  
 827 porous core of Enceladus (Choblet et al, 2017a), likely modulated by oceanic flow  
 828 (Soderlund, 2019).

829 The global shape data of Europa retrieved from *Galileo* limb profiles indicate  
 830 that, if variations exist, they should be relatively small, thus implying an efficient  
 831 ice flow at the base of the shell (Nimmo et al, 2007) or redistribution of topogra-  
 832 phy through pressure-induced melting and freezing (Soderlund et al, 2014). The  
 833 absence of significant ice shell thickness variations does not imply that there is  
 834 no significant heat flow anomaly at the base of the ice shell. As shown by Čadek  
 835 et al (2017), any ice/ocean deflection relaxes much faster in Europa’s conditions  
 836 than in Enceladus’ case because of its larger size. For the same ice shell thickness  
 837 and viscosity structure, the relaxation rate is 100 times faster on Europa than  
 838 on Enceladus, requiring a large heat flux anomaly to build up significant long-  
 839 wavelength topography. Ashkenazy et al (2018) modeled the global meridional ice  
 840 flow in Europa’s ice shell due to pressure gradients associated to equator-to-pole  
 841 ice thickness variations. They show that the thickness variations barely exceed a  
 842 few kilometers and are limited by ice flow and oceanic heat transport.

### 843 3.3 Melt Transport

844 While the observations of plumes at Enceladus and Europa support the possibility  
 845 of liquids present within their ice shells, the physical processes leading to near-  
 846 surface melting and liquids accumulation within the crust or their emplacement  
 847 on the surface are still subject to discussion. Generation of liquids within the  
 848 icy crust requires a heat source, such as tidal heating, and/or the presence of a  
 849 secondary phase depressing the melting point. Two geodynamical contexts have  
 850 been proposed for generation of melts by enhanced tidal heating inside the ice shell:  
 851 either in hot upwelling plumes as a result of thermally-reduced viscosity (e.g., Sotin  
 852 et al, 2002; Tobie et al, 2003; Běhouňková et al, 2010) or along the faults due to  
 853 tidally-activated strike-slip motions (e.g., Gaidos and Nimmo, 2000; Nimmo and  
 854 Gaidos, 2002). Alternative sources of liquids would be a direct connection from  
 855 the subsurface ocean through water-filled cracks (Fig. 8a, Section 2.4) and impact  
 856 cratering (Fig. 8b, Section 2.1).

857 Contrary to the analogous setting on the Earth (silicate solids being denser  
 858 than their melts), the negative buoyancy of water with respect to ice I is often seen  
 859 as an obstacle to maintaining englacial water (Tobie et al, 2003; Kalousová et al,  
 860 2016). However, several possibilities have been proposed to overcome the negative  
 861 buoyancy of water (e.g., Fagents, 2003; Hammond et al, 2018): (i) volatiles such  
 862 as CO<sub>2</sub>, CO, or SO<sub>2</sub> may be exsolved in water thus significantly increasing the  
 863 fluid buoyancy, (ii) non-ice substances may be present in water or ice which will  
 864 modify the density contrast between the two phases - either by decreasing the fluid  
 865 density (e.g., NH<sub>3</sub>, CH<sub>4</sub>, N<sub>2</sub>) or by increasing the ice density (silicate particles,  
 866 clathrates), (iii) compaction and associated low permeability of ice that allows an  
 867 accumulation of melts within the shell, and (iv) partial freezing of a discrete liquid  
 868 reservoir will lead to its overpressurization, which may further promote cracking  
 869 and lead to water ascent.

870 Over long timescales, oceanic materials – either in the form of melt pockets or  
 871 solid phase (salts, clathrate) – can be advected from the ice/ocean interface to the

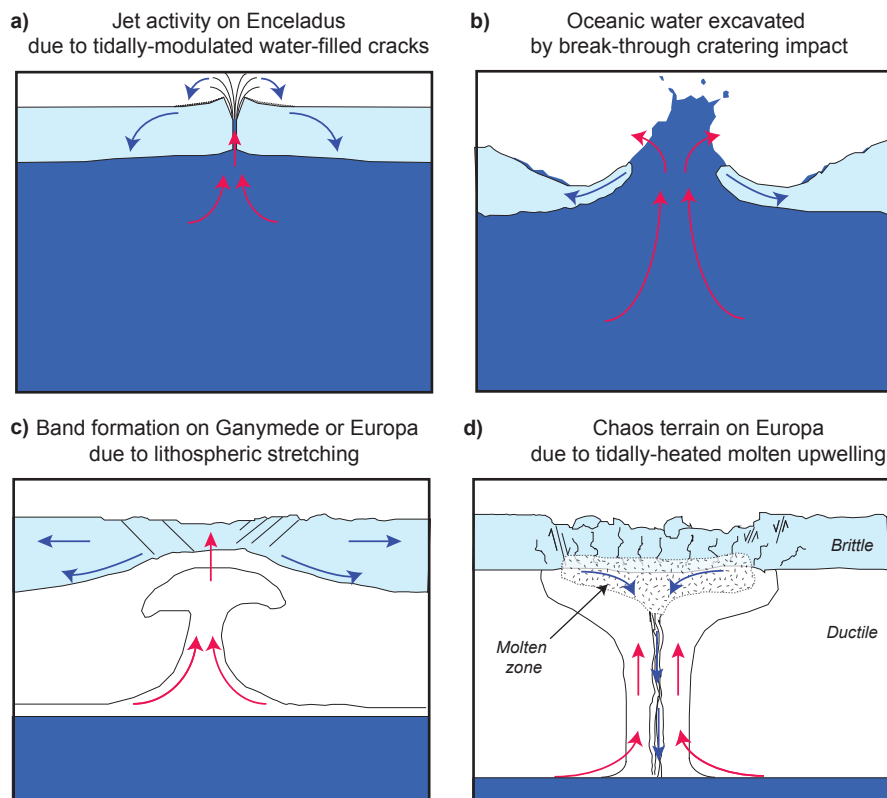


**Fig. 8** Four possible mechanisms leading to exchange between the subsurface ocean and the surface, which are mostly controlled by the ice shell thickness and the force acting on it : a) oceanic water injection and associated jet activity requiring relatively thin shells ( $\lesssim 5$  km) and strong tidal forces (after Postberg et al, 2018b); b) oceanic water excavation due to break-through cratering impact requiring ice shell thickness and impactor radius to be of comparable size (after Lunine et al, 2010); c) indirect transport of oceanic materials by upwelling ices from the ocean/ice interface to shallow depths, associated with band formation and lithospheric stretching, occurring in 10-20 km thick shells under the action of significant tectonic stress (after Howell and Pappalardo, 2018); d) ice melting at shallow depths by tidally-heated thermal plumes and potential percolation of meltwater to the ocean, occurring for relatively thick ice shells ( $\gtrsim 25$  km) subjected to significant tidal forcing (after Sotin et al, 2002).

872 surface by thermal convection. The conductive lid separating the convective part  
 873 from the surface (Fig. 5a) acts as a barrier for chemical exchanges. Rupture of the  
 874 conductive lid, either by large-scale tectonic stresses and melt-induced collapse  
 875 (Fig. 8c-d), is required to allow the exposure of materials brought by convective  
 876 upwellings. Rupture of the lid provides also a mean to recycle surface materials  
 877 to the subsurface and potentially to advect them to the ocean (Kattenhorn and  
 878 Prockter, 2014; Johnson et al, 2017; Klaser et al, 2019). In numerical simulations  
 879 of thermal convection in icy shells, melting of water and its transport is often  
 880 completely neglected (e.g., Han and Showman, 2005, 2010) or highly simplified

881 (Běhounková et al, 2012). Some authors, however, have included water generation  
882 and considered its dynamic effect on the ice flow (Tobie et al, 2003; Kalousová  
883 et al, 2016). In these studies, the water content (porosity) is computed but the  
884 ice is considered to be effectively impermeable to the interstitial water transport  
885 (percolation) and water is thus simply advected by the flowing ice. These authors  
886 found that the occurrence of a few percents of water leads to fast (with respect  
887 to convection time scales) destabilization of the partially molten region, thus not  
888 supporting the long term stability of liquid water bodies. Let us note however,  
889 that only pure ice was considered and that the addition of salts may promote  
890 the melting process while the addition of volatiles may improve the buoyancy of  
891 the liquid. Alternatively, the water transport by interstitial percolation has been  
892 modeled by using a two-phase mixture formalism by Kalousová et al (2014) for  
893 Europa and Hammond et al (2018) for Triton. The drawback of these studies is that  
894 they only consider a one-dimensional geometry and thus neglect water advection  
895 by flowing ice (cf. above). The only simulations that took into account both water  
896 transport mechanisms, i.e. advection by ice and interstitial percolation, have been  
897 performed for the high-pressure ice layers of Ganymede (Kalousová et al, 2018;  
898 Kalousová and Sotin, 2018) and Titan (Kalousová and Sotin, 2019). More details  
899 can be found in Journaux et al (2019) (this issue). On the basis of the effect of  
900 melt on the dynamics and structure of the high-pressure ice layer, one can predict  
901 that a temperate layer (i.e. with temperature following the melting curve) would  
902 be present at the icy crust/ocean interface but details on its characteristics must  
903 await dedicated work.

904 Models have also been constructed to assess the possibility of cryolava ascent  
905 on the surface of icy satellites. Manga and Wang (2007) found that overpressure  
906 generated by freezing a few kilometers of ice is not sufficient for liquid water to  
907 erupt on the surface of Europa, while it may be sufficient on smaller satellites such  
908 as Enceladus. However, Quick and Marsh (2016) and Quick et al (2017) found  
909 that cryolava may reach Europa's surface at temperatures as high as 250 K and  
910 undergo rapid cooling to form cryovolcanic domes. Even if the liquids do not reach  
911 the surface, they may be placed in the shallow subsurface where processes such as  
912 impact cratering can transport the deposited material on the surface.

913 The presence of near-surface liquid reservoirs was proposed to explain some  
914 ocean world surface morphologies in comparison with Earth-like processes. Michaut  
915 and Manga (2014) and Manga and Michaut (2017) investigated thermo-mechanical  
916 constraints on the emplacement and evolution of liquid water sills and proposed  
917 that Europa's pits, domes, and small chaos morphology could result from the evo-  
918 lution of these sills located at depths of 1 to 5 kilometers. Moreover, they suggest  
919 that the pits should be located above bodies of liquid water, which is in agreement  
920 with Schmidt et al (2011) who proposed that Europa's chaos terrains form above  
921 liquid water lenses  $\sim 3$  kilometers below the surface. Walker and Schmidt (2015)  
922 investigated the effects of a subsurface liquid water body on the flexural response  
923 of an ice shell and the resulting topography. Their results reproduce the observed  
924 geology of Europa's chaos terrains as well as Enceladus' SPT, suggesting that they  
925 both formed by the ice collapse above a liquid water body. Similarly, sills and dikes  
926 have also been implicated for the formation of ridges on Europa (Dombard et al,  
927 2013; Johnston and Montési, 2014; Craft et al, 2016).

## 928 4 Ocean Dynamics and Exchange Processes

929 Oceans are an essential component of the ice-ocean exchange process as the inter-  
930 mediary layer between the outer ice shell and the underlying mantle/high pressure  
931 ice layer. Moreover, because the oceans are nearly inviscid and strong currents  
932 are expected, heat and materials are transported relatively quickly across them.  
933 Fluid motions within icy satellite oceans are driven by convection due to thermo-  
934 compositional density gradients, mechanical forcings (e.g., tides, libration, and  
935 orbital precession), and magnetic forcing due to electromagnetic pumping. The  
936 resulting flows will promote mixing within the bulk ocean, which will influence  
937 the distribution of thermo-compositional gradients, especially along the seafloor  
938 and ice-ocean interface, and potentially have important implications for the ice  
939 shell and habitability.

### 940 4.1 Convection

#### 941 4.1.1 Hydrothermal Plumes

942 The earliest efforts to understand ocean dynamics within icy worlds focused on  
943 local circulation driven by hydrothermal plumes upwelling from the rocky interior  
944 (Thomson and Delaney, 2001; Goodman et al, 2004). The goal of these efforts was  
945 to explore connections between localized seafloor heating and geological features  
946 on the surface of Europa’s ice crust. Initial work in this area (Thomson and De-  
947 laney, 2001) argued that Coriolis forces would constrain the outward spread of  
948 the turbulent buoyant plume, creating a narrow “chimney” of warm fluid which  
949 could potentially deliver hydrothermal heat to a narrow patch of ice despite the  
950 depth of the ocean, and speculated that they could form the 5-20 km diameter  
951 lenticulae (Greenberg et al, 1999) or pits, domes, and spots (Pappalardo et al,  
952 1998) commonly seen on Europa’s surface. They further noted that these forces  
953 would create anticyclonic (counter-clockwise in the northern hemisphere) currents  
954 at the ice-water interface, which were consistent with the apparent motion of ice  
955 rafts in the large Conamara Chaos (Spaun et al, 1998).

956 Later work based on theoretical scaling laws for point-source plumes (Fernando  
957 et al, 1998), supplemented with laboratory tank experiments (Goodman et al,  
958 2004) and numerical simulations (Goodman and Lenferink, 2012), demonstrated  
959 that while the plumes would have a narrow aspect ratio, they would still be at least  
960 20-50 km in diameter, far wider than the common sizes of pits, domes, and spots,  
961 suggesting that these features were more likely created by internal ice dynamics.  
962 However, the plume size was found to be compatible with the largest chaos regions  
963 on Europa. Temperature anomalies were found to be very small (mK) and flow  
964 velocities very weak (mm/s), making it unlikely that hydrothermal plumes would  
965 have any direct mechanical effect on the overlying ice layer. Mantle heat transport  
966 calculations by Lowell and DuBose (2005) also support the lack of melt-through  
967 events by hydrothermal plumes.

968 More recent work by Farber and Goodman (2014) included a better treatment  
969 of planetary rotation in these plumes and studied their implications for astrobi-  
970 ology. In Earth’s oceans, the horizontal component of the planetary rotation axis  
971 (perpendicular to gravity) can be ignored, but this approximation is not valid for

972 convection in deep icy world oceans. As a result, hydrothermal plumes should rise  
973 parallel to the planetary rotation axis (i.e. diagonally), rather than vertically. This  
974 would cause a plume’s projection onto the ice surface to be an ellipse with the long  
975 axis oriented toward the pole. Hydrothermal plumes are also astrobiologically sig-  
976 nificant, both in providing a route for metabolically significant molecules to move  
977 from seafloor to surface, and for delivering potential biosignatures to the ice. Far-  
978 ber and Goodman (2014) also showed that tracer particles require thousands of  
979 years to move from top to bottom of Europa’s ocean.

980 One important caveat remains, however. Local convective plumes will rise  
981 through a background ocean whose properties are determined by the ocean com-  
982 position and global circulation. Compositional modification of these results is dis-  
983 cussed below, and global convective flows are discussed in Section 4.1.2.

984 The extent to which hydrothermal plumes will buoyantly rise depends on the  
985 ocean composition. In a freshwater ocean, buoyancy of the plumes depends on its  
986 temperature relative to the surrounding ocean water; since the warmer plumes are  
987 less dense, they are expected to reach the ice-ocean interface. However, the thermal  
988 expansion coefficient of water is negative between 0 and 3.98 °C (at 1 bar) such that  
989 the maximum fluid density is reached below at a temperature above the freezing  
990 point. As a result, the ocean would have a stable “stratosphere” beneath the ice-  
991 ocean interface that would prohibit further rising of the plume (Melosh et al,  
992 2004). Increased pressure and ocean salinity move the temperature of maximum  
993 density towards the freezing temperature, reducing this effect. These temperatures  
994 coincide at pressures exceeding 27 MPa and salinities exceeding ~3 wt% for both  
995 seawater and magnesium sulfate compositions (Feistel and Hagen, 1995; Melosh  
996 et al, 2004; Vance and Brown, 2005). Further, considering a saline ocean, if the salt  
997 content is larger near the seafloor due to interactions with the underlying mantle  
998 or precipitates, its entrainment into the plumes would increase their density and  
999 cause them to reach the point of neutral density before reaching the ice-ocean  
1000 interface (Vance and Brown, 2005). However, Travis et al (2012) argue that this  
1001 initial salinity gradient would eventually become homogenized such that thermal  
1002 buoyancy would regain dominance.

#### 1003 4.1.2 Global Circulations

1004 Heat flow from the seafloor combined with heat loss through the overlying ice  
1005 shell is expected to drive thermal convection globally in the oceans, modulated by  
1006 compositional buoyancy associated with salinity gradients that may enhance the  
1007 vigor of convection (positive gradient) or have a stabilizing effect (negative gradi-  
1008 ent). The resulting fluid flows are governed by the Navier-Stokes equations where  
1009 the most prominent forces are inertia, Coriolis, pressure gradient, and buoyancy,  
1010 in combination with the ocean geometry and boundary conditions (see Taubner  
1011 et al (2019), this issue). The hydrothermal plume studies above generally assume  
1012 the ocean to be geostrophic, meaning a balance between the Coriolis and pres-  
1013 sure gradient forces that effectively organizes the convective flows into quasi-two-  
1014 dimensional structures that are aligned with the rotation axis, frequently called  
1015 Taylor columns (Fig. 9a). On a global scale, non-linear stresses associated with  
1016 these columns will drive an eastward jet at low latitudes with multiple, alternat-  
1017 ing jets towards the poles, reminiscent of the jets in Jupiter’s atmosphere (Fig. 9b;

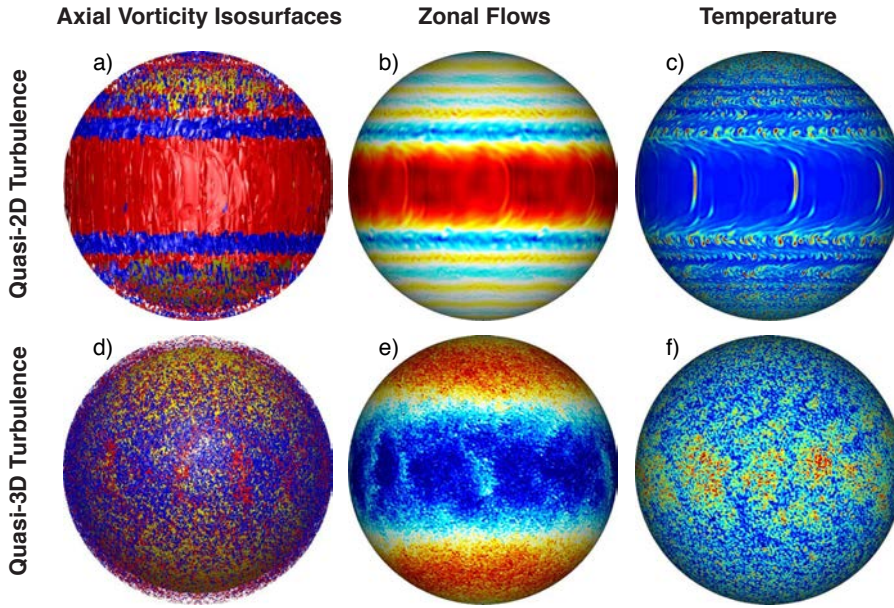


**Fig. 9** Flow structures, zonal flows, and temperature fields in convection models at a snapshot in time. Top row: Simulation with quasi-2D turbulence. Bottom row: Simulation with quasi-3D turbulence. Left column: axial vorticity isosurfaces,  $\omega_z = (\nabla \times \mathbf{u}) \cdot \hat{\mathbf{Z}}$ . Red (blue) indicates cyclonic (anticyclonic) circulations aligned with the vertical  $\hat{\mathbf{Z}}$  direction; the yellow sphere represents the seafloor. Middle column: zonal flows along the outer boundary; red (blue) indicates eastward (westward) flow. Right column: superadiabatic temperature fields below the outer boundary; red (blue) indicates warm (cool) fluid. Adapted from Soderlund et al (2014).

1018 e.g., Heimpel et al, 2015; Soderlund et al, 2014). The ocean is warmest at high lat-  
 1019 itudes due to the efficiency of vertical convection columns there (Fig. 9c; Aurnou  
 1020 et al, 2008).

1021 As convection becomes more vigorous, however, the Taylor columns break down  
 1022 and fluid flows become three-dimensionalized. Here, mixing of absolute angular  
 1023 momentum will instead drive a westward equatorial jet and eastward jets at high  
 1024 latitudes (Fig. 9d; e.g., Aurnou et al, 2007; Gastine et al, 2013). A large-scale  
 1025 meridional overturning circulation also develops with upwelling flow near the equa-  
 1026 tor and downwelling flow at higher latitudes in each hemisphere (Fig. 9e; Soderlund  
 1027 et al, 2013). This circulation brings warm ocean water preferentially toward the  
 1028 ice-ocean interface at low latitudes ((Fig. 9f; Soderlund et al, 2014).

1029 The transition between these convective regimes is an active area of research  
 1030 subject to considerable debate (e.g., Gastine et al, 2016; Cheng et al, 2018). Al-  
 1031 though the oceans are traditionally assumed to be strongly organized by rotation,  
 1032 Soderlund et al (2014) postulated that Europa’s ocean is characterized by quasi-3D  
 1033 turbulence by estimating the convective regime following several potential scaling  
 1034 laws. These arguments are updated and extended to the oceans of Enceladus, Ti-  
 1035 tan, and Ganymede in Soderlund (2019), who predicts thermal convection in the  
 1036 oceans of Europa, Ganymede, and Titan to all behave similarly (Fig. 9, bottom  
 1037 row). Rotation is predicted to play a more significant role for Enceladus. Consid-  
 1038 ering the satellites collectively, peak zonal flow speeds are predicted to reach at

1039 least 10s of cm/s (up to meters per second) and mean (i.e. averaged over both  
1040 time and all longitudes) radial flows span the mm/s to cm/s range (Soderlund,  
1041 2019).

1042 Complementary to the formation of individual chaos features through hy-  
1043 drothermal plumes, global convection models have focused the distribution of  
1044 chaos terrains across Europa. Soderlund et al (2014) hypothesized that the low  
1045 latitude enhancement of ocean heating promotes the formation of these terrains  
1046 through increased melting of the ice shell and subsequent accretion of relatively  
1047 pure marine ice. Considering the other satellites, heat flux anomalies from the  
1048 ocean derived recently for Enceladus (Čadek et al, 2019) and Titan (Kvorka et al,  
1049 2018) provide useful constraints for models of these oceans (see Fig. 7). The mod-  
1050 els of Soderlund (2019) are consistent with these heat flow patterns only if salinity  
1051 effects are taken into account. However, the distribution of heating from the un-  
1052 derlying mantle/high pressure ice layer may be spatially heterogeneous (Travis  
1053 et al, 2012; Choblet et al, 2017a,b; Kalousová et al, 2018) and these effects have  
1054 not yet been taken into account.

1055 Ocean composition and its thermodynamic properties may have a significant  
1056 impact on global circulations due to the presence of a stable stratosphere if the  
1057 thermal expansion coefficient is negative (Melosh et al, 2004) or if salinity gra-  
1058 dients are maintained across the ocean. If salinity increases towards the seafloor,  
1059 the thermal and compositional gradients oppose each other and double-diffusive  
1060 convection may be expected (Vance and Brown, 2005; Bouffard et al, 2017) with  
1061 layering that can evolve into a ‘staircase’ configuration with well-mixed layers  
1062 that are characterized by steps in salinity and temperature (e.g., Schmitt, 1994).  
1063 Conversely, if salinity increases toward the ice-ocean interface, both thermal and  
1064 compositional gradients are unstable, leading to more vigorous convection. Melting  
1065 and freezing along the ice-ocean interface will also lead to regions that are locally  
1066 enhanced with fresher (i.e. stably stratified) and saltier (i.e. unstably stratified)  
1067 water, respectively, that may drive additional circulations (Jansen, 2016; Ashke-  
1068 nazy et al, 2018; Zhu et al, 2017). Moreover, if heterogeneous melting/freezing  
1069 leads to large-scale topographic variations along the ice-ocean interface, they may  
1070 also impact the characteristics of convection and promote mechanically driven  
1071 flows (see Section 4.2).

## 1072 4.2 Mechanical Forcings

1073 The icy satellites are tidally locked, meaning that their rotational periods equal  
1074 their orbital periods. This results in the moons having triaxial ellipsoid shapes with  
1075 their longer axes pointing towards the planet. If the moons’ orbits were perfectly  
1076 circular and their rotational axis aligned with their orbital axis, there would not  
1077 be any mechanical forcing. However, their orbits are eccentric and their rotational  
1078 axes are tilted with respect to their orbital axes, resulting in time-changing tidal  
1079 bulges, librations, and precessions (Fig. 10) that can drive ocean currents.

1080 A common approach for studying ocean tides is to use the Laplace Tidal Equa-  
1081 tions (LTE) that control the barotropic ocean response (Hendershott, 1981). The  
1082 LTE assume a shallow ocean of constant density, and radial (vertical) ocean cur-  
1083 rents are considered to be negligible with respect to horizontal currents such that  
1084 the problem becomes 2D. The resulting equations, which allow for surface gravity

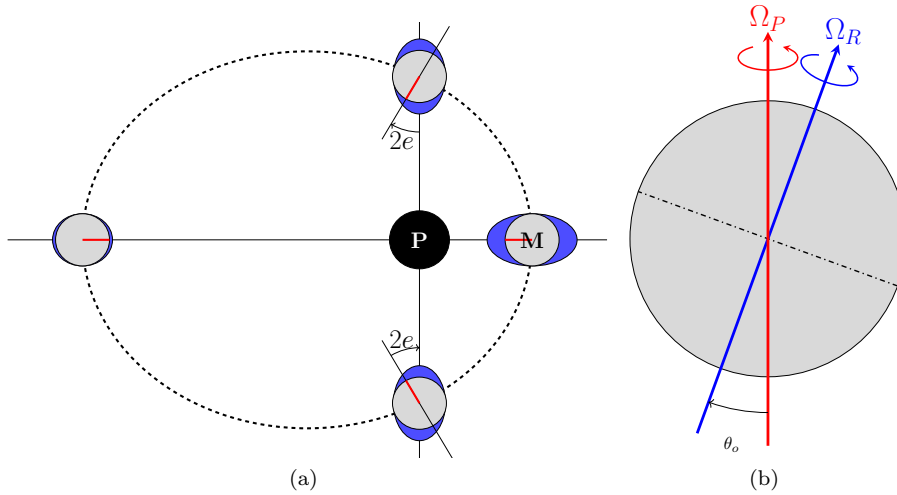


**Fig. 10** (a) A moon’s eccentric orbit, where the equilibrium tidal bulge is indicated in blue and the  $0^\circ$  meridian is marked with a red line. Note the change of the tidal bulge amplitude and the longitudinal libration of the subplanet point. (b) A moon’s rotation axes, where the moon rotates around its rotational axis with angular velocity  $\Omega_R$  and precesses with angular velocity  $\Omega_P$ , separated by the moon’s obliquity  $\theta_o$ .

1085 waves and planetary Rossby waves (e.g., Longuet-Higgins, 1968), have been used  
 1086 to study the response of an ice-free ocean of constant thickness (e.g., Tyler, 2008,  
 1087 2009; Chen et al, 2014; Hay and Matsuyama, 2017). The ocean response highly  
 1088 depends on the surface gravity wave speed. For thick oceans, the surface gravity  
 1089 wave speed is high, the ocean quickly adjusts to the perturbing tidal potential, and  
 1090 its response is mainly given by the equilibrium tide; this is the case of tides raised  
 1091 by a satellite’s eccentricity (Fig. 11a). However, a high surface gravity wave speed  
 1092 does not hamper the propagation of tangentially non-divergent Rossby waves as  
 1093 they do not involve up and down motions (Fig. 11b).

1094 Obliquity of the satellite can excite planetary Rossby waves of sufficient am-  
 1095 plitude to maintain a liquid ocean in Europa (Tyler, 2014), but is insufficient to  
 1096 prevent Enceladus’ ocean from freezing (e.g., Chen and Nimmo, 2011; Matsuyama,  
 1097 2014). For thin oceans, gravity wave resonances can also occur. Nevertheless, char-  
 1098 acteristic ocean thicknesses for which these resonances occur are far from those  
 1099 inferred from observations; as an example, the thickest ocean for which a resonance  
 1100 occurs in Enceladus is around 350 m. If an ocean eventually begins to freeze out,  
 1101 it will necessarily go through resonant states where enhanced heat production pre-  
 1102 vents further freezing. Recently, Beuthe (2016); Matsuyama et al (2018); Hay and  
 1103 Matsuyama (2019) considered the effect of the overlying ice layer and showed that  
 1104 obliquity-forced dissipation is enhanced but the eccentricity tide is significantly  
 1105 dampened in satellites with high effective rigidity (Enceladus) and enhanced in  
 1106 satellites with low effective rigidity (Ganymede, Europa, Titan).

1107 The LTE hold as long as the ratio of the characteristic vertical and horizontal  
 1108 length scales is small (Miles, 1974). However, this may not be sufficiently accurate  
 1109 for icy satellite oceans. Using the ocean thickness and body’s radius as a measure  
 1110 of vertical and horizontal length scales, higher ratios are obtained for Europa and

1111 Enceladus than for Earth ( $\sim 0.06$  and  $\sim 0.15$  versus  $\sim 0.001$ ), suggesting that  $3D$   
1112 effects are relevant in the icy moons. Without the shallow water approximation,  
1113 internal inertial waves can be excited. These waves have properties markedly differ-  
1114 ent from shallow water waves. Upon reflection, an internal wave packet can change  
1115 its wavelength. Depending on the ocean geometry, this can lead to the focusing of  
1116 energy along internal shear layers (e.g., Rieutord et al, 2011; Maas, 2005).

1117 Recently, Rovira-Navarro et al (2019) used the linearized Navier-Stokes equa-  
1118 tions to study the three dimensional response of an unstratified ocean of constant  
1119 thickness to tidal forcing. They observed patterns of periodic inertial waves that  
1120 take energy from the global tidal forcing and focus it along internal viscous shear  
1121 layers that propagate in the ocean (see Fig. 11c). These shear layers fluid flows can  
1122 have an amplitude of a few cm/s, but the dissipation due to inertial waves in an  
1123 ocean of constant thickness is not sufficient to prevent an European or Enceladan  
1124 ocean from freezing. Requier et al (2019) extended this work to study the excita-  
1125 tion of inertial waves by Enceladus' libration and concluded that this mechanism  
1126 generates more dissipation than tidal forcing.

1127 Rovira-Navarro et al (2019); Requier et al (2019) ignored the advection terms in  
1128 the Navier-Stokes equations which otherwise can result in flow instabilities and the  
1129 development of turbulence. Flow instabilities in spherical and ellipsoidal containers  
1130 have been widely studied (e.g., Malkus, 1994; Kerswell and Malkus, 1998; Rieu-  
1131 tord, 2004). In a librating sphere, the viscous boundary layer at the solid-liquid  
1132 interface can become unstable and break down to small scale turbulence. Wilson  
1133 and Kerswell (2018) estimated the amount of tidal dissipation due to boundary  
1134 layer instabilities and suggested that it should be potent enough to explain Ence-  
1135 ladus' heat flux. If the container is ellipsoidal, the interaction of inertial waves  
1136 with the mean-flow excited by libration, precession, or tides can lead to the well-  
1137 known elliptical instability, which also results in a turbulent flow regime similar  
1138 to that shown in Fig. 11d (e.g., Kerswell, 2002; Le Bars et al, 2015). Experimen-  
1139 tal and numerical work shows that Enceladus and Europa are likely unstable to  
1140 libration-driven elliptic instability, while Titan, Ganymede and Callisto are prob-  
1141 ably not (Grannan et al, 2014, 2017; Lemasquerier et al, 2017). So far, ocean  
1142 currents excited by mechanical forcing and convection (Section 4.1.2) have been  
1143 studied separately. The interaction of mechanically driven and convective currents  
1144 requires further attention.

1145 The previous discussion assumes the ocean to be unstratified and contained  
1146 within ellipsoidal or spherical shells devoid of topographical features. On Earth,  
1147 stratification and ocean topography play a crucial role in shaping the ocean's  
1148 response to tides by controlling the barotropic ocean response and the conversion  
1149 of the barotropic tide to the (internal) baroclinic tide (Munk, 1997; Egbert and  
1150 Ray, 2000). In icy ocean worlds, we expect the ocean floor and the basal ice shell  
1151 topography to deviate from the idealized shapes explored so far in mechanically  
1152 driven flow studies. For instance, Enceladus' ice shell thickness varies from  $\sim 5$  km  
1153 at the south pole to  $\sim 30$  km at the equator (Section 1.2). Additionally, under  
1154 certain circumstances a subsurface ocean might be stratified (Section 4.1.2). The  
1155 study of mechanically-excited flows for complex ocean geometries and stratified  
1156 subsurface oceans is an exciting topic for future research.

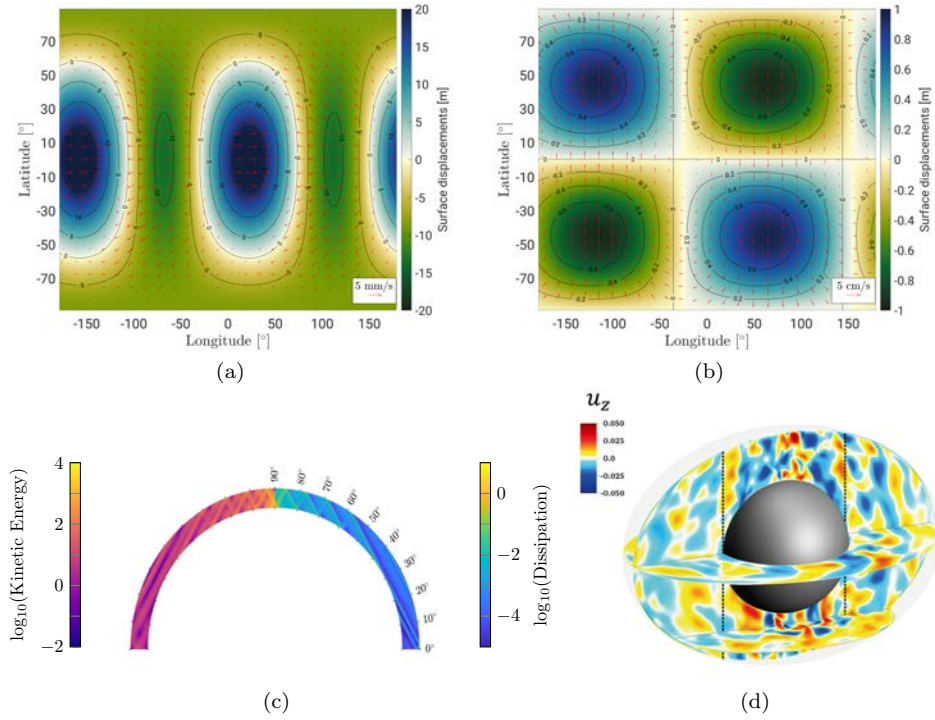


**Fig. 11** Characteristic flow fields for mechanical forcings. Flow field and surface displacements excited in Europa by the (a) eccentricity and (b) obliquity tide. The ocean is assumed to be 80 km and covered by a 20 km thick ice shell. Overlaid are contours corresponding to the equilibrium tide. The flow pattern propagates towards the east and west for the eccentricity and obliquity tides, respectively. Credit: M. Rovira-Navarro. (c) Internal waves excited by the eccentricity tide in an ice-free 30 (185) km thick Enceladus (European) ocean; the left and right quadrants respectively show the amplitude of kinetic energy and viscous dissipation. A logarithmic non-dimensional scale is used for both quantities with the maximum kinetic and viscous energy corresponding to 4.7 (0.65)  $\text{J}/\text{m}^3$  and 0.50 (0.026)  $\mu\text{W}/\text{m}^3$  for Enceladus (Europa), respectively (Rovira-Navarro et al, 2019). (d) Turbulent flow regime attained due to the libration-driven elliptical instability, where the vertical component of the non-dimensional velocity ( $u_z$ ) is shown. For more details, see Lemasquerier et al (2017).

### 1157 4.3 Magnetic Forcing

1158 Jupiter's magnetic field is offset by  $\sim 10^\circ$  with respect to the orbital plane of  
 1159 the Galilean satellites. As a result, the satellites experience a time-varying mag-  
 1160 netic field that induces electrical currents in the ocean. If the phases of the Jo-  
 1161 vian magnetic field and the oceanic induced magnetic field are not aligned, their  
 1162 offset could generate a Lorentz force that drives a retrograde jet and weaker up-  
 1163 welling/downwelling motions at low latitudes (Gissinger and Petitdemange, 2019).  
 1164 Mean flow speeds of the equatorial jet are expected to reach a few cm/s in Europa's  
 1165 ocean, reducing to a few mm/s for Ganymede and  $< 1$  mm/s for Callisto where  
 1166 the Jovian magnetic field is weaker. This process is not expected to be significant  
 1167 for the Saturnian satellites due to the planet's nearly axisymmetric magnetic field.  
 1168 Magnetic pumping leads to Ohmic dissipation within the oceans of  $\lesssim 10^8$  W (at

1169 Europa), which is several orders of magnitude weaker than both radiogenic and  
1170 tidal heating. However, the dissipation may still be significant if it is spatially  
1171 concentrated at high latitudes in a thin layer below the ice-ocean interface due to  
1172 the skin effect (Gissinger and Petitdemange, 2019). Moreover, because the zonal  
1173 jet is characterized only by retrograde flow, it may contribute to the reorientation  
1174 of Europa’s ice shell (i.e. non-synchronous rotation) and the associated formation  
1175 of lineaments (e.g., Helfenstein and Parmentier, 1985).

## 1176 5 Terrestrial Analogs

1177 While a great amount of the work on ocean worlds has focused on geologic pro-  
1178 cesses analogous to those seen within the solid Earth, studies of ice and ocean  
1179 processes on Earth are equally important for understanding physical and biologi-  
1180 cal processes on these moons. Here, we will show how analogs for the freezing and  
1181 geochemical properties of planetary ice shells can draw from knowledge of sea ice  
1182 and marine ice on Earth (e.g., Buffo, 2019) as well as models of Snowball Earth  
1183 (e.g., Ashkenazy et al, 2018).

### 1184 5.1 Terrestrial Ice-Ocean Interfaces

1185 The outer shells of icy satellites likely formed through top-down freeze-out of their  
1186 oceans. On Earth, the majority of thick ice (ice sheets/shelves) is meteoric, form-  
1187 ing via the compaction of snow. However, sea ice and marine ice on Earth form  
1188 directly from the ocean and thus are analogous to what is expected on ocean bear-  
1189 ing satellites. While forming under different environmental pressures, the thermal  
1190 gradient is the main controller of ice chemistry in both sea ice and marine ice (e.g.,  
1191 Buffo et al, 2018; Buffo, 2019). Analogously, it is likely that the ice-ocean inter-  
1192 faces of ice shells will be in either a high or low thermal gradient state, depending  
1193 on shell thickness and age, where the high thermal gradient regime is similar to  
1194 that observed in sea ice and the low thermal gradient by marine ice formed at the  
1195 base of ice shelves.

1196 Representative of the high thermal gradient regime, sea ice is easy to observe,  
1197 both in the field and with remote sensing, and thus much is known about its struc-  
1198 ture and formation. The majority of sea ice is composed of granular and columnar  
1199 ice (Dempsey and Langhorne, 2012; Dempsey et al, 2010) driven by turbulent  
1200 and quiescent ice-ocean interface conditions, respectively. However, in ice-shelf-  
1201 adjacent sea ice in Antarctica, another process occurs that may be relevant to icy  
1202 satellites: platelet ice accretion. Through a process known as the ice pump (e.g.,  
1203 Lewis and Perkin, 1986), deep ice is melted at high pressures, creating a plume  
1204 of fresher water that rises buoyantly along the shelf and out below the sea ice. As  
1205 the plume rises, depressurization causes the water to become supercooled (having  
1206 temperatures below its *in situ* freezing point) and ice crystals called platelets form  
1207 in the water column, rise up to the ice surface, and form a layer of poorly organized  
1208 and highly porous ice. Under ice shelves, this layer can grow to immense thick-  
1209 nesses (>100 m) and becomes marine ice (Fricker et al, 2001; Craven et al, 2005,  
1210 2009; Galton-Fenzi et al, 2012). Under sea ice, this platelet layer can be incorpo-  
1211 rated into the growing sea ice or remain unconsolidated. At the base of actively

1212 forming first year sea ice with low current velocities, transient brine drainage into  
1213 supercooled water can additionally form brinicles (icicles that form around brine  
1214 drainage channels), but these become inactive once the sea ice growth slows or  
1215 platelet accretion takes over.

1216 Two lessons can be gained from sea ice and applied to icy satellites. First,  
1217 thermal gradients are critical to the structure and composition of the ice. The  
1218 thermal gradient within forming columnar sea ice is  $\sim 10$  K/m, for which the  
1219 salinity is  $\sim 4$ -5 ppt (freezing from 34 ppt ocean), and it exhibits a critical porosity  
1220 of 4-5% beyond which no brine drainage is observed (e.g., Dempsey et al, 2010;  
1221 Golden et al, 2007). High thermal gradient conditions are only relevant for very  
1222 shallow ice ( $< 1$  km) on icy satellites, or if ocean water is injected rapidly from  
1223 depth into the upper regions of their ice shells (Buffo, 2019). In areas where rapid  
1224 ice growth does occur, there could be important gradients in rheological properties  
1225 that might make these regions more probable to fracture or re-melt (Buffo, 2019).  
1226 Second, ice accretion forced by melting of deep draft ice affects the thickness  
1227 and properties of distant ice, which is key to consider as an interface process for  
1228 other ice-ocean worlds. The thickness of the platelet ice layer is determined not  
1229 by ice formation rate through surface cooling, but by the conditions of the ocean  
1230 – very thick in large supercooling plumes to non-existent where the ocean is not  
1231 supercooled. This layer can be efficiently modeled as an upward sedimented layer  
1232 of platelets whose crystal size is controlled by the degree of supercooling and the  
1233 layer thickness by the lifetime of the plume (Buffo et al, 2018).

1234 Representative of the low thermal gradient regime, marine ice is found in areas  
1235 where supercooled water drives ice accretion onto the base of ice shelves (10s of  
1236 meters to kilometers thick meteoric ice). This regime is characterized by very low  
1237 thermal gradients,  $\ll 1$  K/m. The thickest marine ice observed on Earth is  $\sim 500$  m  
1238 thick, comprising about half the thickness of the Amery ice shelf at its midpoint  
1239 (Fricker et al, 2001). Borehole observations showed a many tens of meters thick  
1240 unconsolidated platelet layer forming at the bottom of the marine ice (Craven  
1241 et al, 2005). The marine ice in Amery demonstrates nearly complete brine rejection  
1242 with salinities of 0.03-0.56 ppt (Craven et al, 2009), suggesting compaction driven  
1243 desalination. Observations of accreting columnar marine ice at the bottom of the  
1244 Ross Ice Shelf can be reproduced using sea ice models and lower thermal gradients:  
1245 5% critical porosity at 0.08 K/m yields a theoretical salinity of 1.7 ppt, while 1.95  
1246 ppt is estimated using constitutive equation based model results (Buffo, 2019),  
1247 which agrees well with field observations of 2.32 ppt (Zotikov et al, 1980).

1248 The thermal gradient expected for most ice shells is squarely within the low-  
1249 thermal gradient regime (e.g., 0.02 K/m for Europa (McKinnon, 1999)). Once an  
1250 ice shell reaches its diffusive limit ( $< 1$  km thick ice), the bulk salinity is unlikely  
1251 to appreciably change, meaning that while the ice still contains some salt through  
1252 accretion, the properties at the ice ocean interface do not change significantly with  
1253 regards to the rate or properties of ice accreted (Buffo et al, 2019), in the absence  
1254 of platelet ice accretion. This diffusive limit marks how much ocean material the  
1255 ice could deliver to the upper shell through convection or diapirism. These values  
1256 are robust if the critical porosity is the physical limit past which brines are trapped  
1257 within the ice, which is the observed limit in sea ice (Golden et al, 1998, 2007)  
1258 and brine layers in ice shelves (Kovacs and Gow, 1975) and matches observations  
1259 of sub-ice shelf columnar ice (Buffo, 2019).

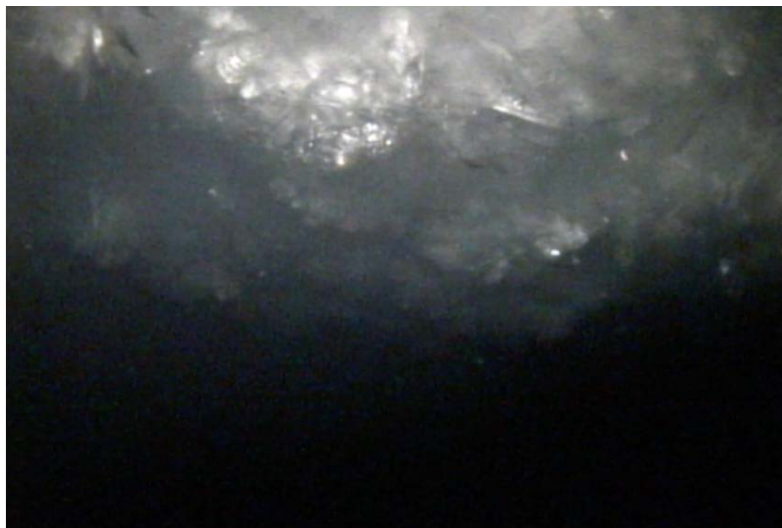


**Fig. 12** Platelet ice accreting under the McMurdo Ice shelf, imaged from Icefin (Credit: B. E. Schmidt/Icefin/RISEUP). These ice crystals form in supercooled water below the shelf and accrete onto the ice shelf base. In some places, these compact to become marine ice, which may also be a process relevant to planetary ice-ocean interface processes.

1260 Preliminary work by Buffo (2019) suggests that multiphase, hydraulically con-  
1261 nected layers at the base of planetary ice shells are likely a stable, and thus  
1262 common, phenomenon. Furthermore, the environmental pressures these layers are  
1263 subject to (i.e., gravity, thermal gradient, ocean composition) likely dictate their  
1264 thicknesses and structural properties. As the exchange boundary for energy and  
1265 mass between the underlying ocean and ice shell, the structure and dynamics of  
1266 these regions will substantially impact the thermochemical evolution of planetary  
1267 cryospheres. Additionally, in the analogous terrestrial environments (sea ice and  
1268 marine ice), the porous nature of the ice-ocean interface provides a gradient rich  
1269 substrate that supports a diverse biome.

## 1270 5.2 Snowball Earth

1271 At least two extreme glaciations occurred on Earth during the late Neoproterozoic  
1272 era (750-580 Ma) (Hoffman and Schrag, 2002). The Snowball Earth hypothesis  
1273 proposes that the oceans froze over entirely during these episodes, so that the  
1274 Earth was an icy ocean world. While debate continues over whether ice cover was  
1275 total or partial (Liu and Peltier, 2010), this episode may provide our best terrestrial  
1276 proxy for ice covered oceans on a global scale. As with icy worlds in the outer solar  
1277 system, a Snowball Earth ocean would be geothermally heated but isolated from  
1278 direct solar heating or wind forcing. However, differential solar heating would still  
1279 create variations in thickness which would drive global ice flow from pole to equator  
1280 (Goodman and Pierrehumbert, 2003). This flow would be balanced by melting and  
1281 freezing into the ocean, leading to variations in salinity which would drive ocean  
1282 circulation, would close the glaciological cycle through the ocean, creating an ocean

haline-driven circulation (Ashkenazy et al, 2013). All of these dynamics are similar to predictions for the ice-covered oceans of the outer solar system, particularly the coupled interaction of global ice flow and haline-driven ocean circulation (Collins and Goodman, 2007; Ashkenazy et al, 2018; Zhu et al, 2017). Interestingly, the unsolved question “Was the liquid ocean ever exposed at the surface?” is of key importance to both fields.

However, there are three key differences. First and most obviously, Earth’s oceans are relatively shallow and are interrupted by continents. Their depth lessens the importance of planetary rotation (especially its horizontal component; Farber and Goodman, 2014). The continents block global east-west flows of the type explored by Soderlund et al (2014). On the other hand, coastlines allow fluid parcels to change their vorticity, enabling strong north-south currents that would otherwise be limited by angular momentum constraints (Pedlosky, 1987).

A second difference between Snowball Earth and the icy worlds of the outer solar system is that Snowball Earth’s surface temperatures would have been far warmer, leading to a totally different pattern of ice flow dynamics. On Earth, modern-day and Snowball ice sheets flow via uniform strain, gradually spreading and thinning while maintaining constant flow velocity with depth (Weertman, 1957; Goodman and Pierrehumbert, 2003). However, this model does not work in the outer solar system: ice near the surface is too cold to flow at all. Instead, ice moves by vertical shear flow: warm ice near the base of the ice shell flows horizontally beneath a rigid upper shell (e.g., Collins and Goodman, 2007; Ashkenazy et al, 2018).

Third, Snowball Earth would have had much thinner ice than the icy ocean worlds. Models of the Snowball Earth ice thickness typically predict ice 200 - 1000 m thick (Goodman and Pierrehumbert, 2003), though local regions where clear ice allows solar penetration could be as thin as a few meters (Warren et al, 2002). In contrast, ice shell thicknesses in the outer solar system range from ~5 km at Enceladus’ SPT to hundreds of kilometers for large satellites (e.g., Vance et al, 2018a). Many of these moons are then likely to be experiencing solid-state convection, while heat flow through Snowball Earth’s ice shell probably occurred by conduction only. The thickness and weak thermal gradients within ice shells of ocean worlds also promotes the horizontal movement of ice via vertical shear rather than uniform strain, as discussed above.

Other important differences also abound, including greater uncertainties about solutes and seafloor heating distribution in the oceans of the outer solar system, but the similarities provide ample ground for collaboration between investigators in both fields.

## 6 Discussion and Perspectives

### 6.1 Habitability of Icy Ocean Worlds

The potential habitability of ocean worlds is an exciting prospect that has been commonly discussed for the past three decades, with increasing sophistication (e.g., Reynolds et al, 1983, 1987; Chyba, 2000; Chyba and Phillips, 2001; Hand et al, 2009; Barge and White, 2017; Russell et al, 2017; Schmidt, 2019), mirroring progress in astrobiology towards understanding the requirements to maintain

1328 a habitable planet. During this time, the direction of progress has been towards  
1329 systems science, which is important for ocean worlds given that while they share  
1330 many similarities with the Earth, conditions may be quite different. In particular,  
1331 capturing coupled interactions between the geophysical and geochemical evolu-  
1332 tion of planets is needed given that the Earth and its biosphere coevolved (e.g.,  
1333 Des Marais et al, 2008; Hays et al, 2015).

1334 Understanding the energy to support life in a given planetary system is the  
1335 central organizing principle of the study of habitability. For the ocean worlds, this  
1336 is a chance to understand not just what inventory of material they may have, but  
1337 which processes continually supply energy for life. Here, the state of the interior,  
1338 implied thermal and chemical evolution, and modern exogenic processes all couple  
1339 together. Since light transmission even through pure glacial ice ceases at  $< 10$  m  
1340 (Christner et al, 2014), photosynthesis is not a viable energetic pathway for the  
1341 ocean worlds. Thus, understanding potential pathways for chemosynthesis (Zolotov  
1342 and Shock, 2003, 2004; Russell et al, 2017; Barge and White, 2017) is critical for  
1343 understanding the habitability of icy ocean worlds.

1344 Europa's global ocean, coupled with a potentially reducing interior (e.g., Zolo-  
1345 tov and Shock, 2001; Lowell and DuBose, 2005; Vance et al, 2007, 2016) and  
1346 oxidized surface (e.g., McCord et al, 2002; Paranicas et al, 2009) may provide a  
1347 source of redox energy for a subsurface biosphere. Life on Earth may have begun in  
1348 relatively anoxic conditions potentially similar to conditions on Europa (Barge and  
1349 White, 2017; Russell et al, 2017). The surface of Europa is littered with spectrally  
1350 detected salts that include  $MgSO_4$ ,  $NaCl$ , and  $SO$  compounds as well as sulfur  
1351 implanted from the Io torus (see Carlson et al (2009) for review), and  $CO$  and  
1352  $CO_2$  have been observed on the other moons but are likely unstable on Europa's  
1353 surface (Hibbitts et al, 2000, 2003). Whether the ocean is highly reduced through  
1354 interactions between the ocean and the seafloor (e.g., Zolotov and Shock, 2001;  
1355 Vance and Goodman, 2009; Vance et al, 2014) or acidic due to downward trans-  
1356 mission of oxidants from the surface (Pasek and Greenberg, 2012) depends heavily  
1357 on surface geology and the exchange rate with the ocean. However, it is unclear  
1358 how much of the surface is actually drawn down into the interior and how efficient  
1359 surface-subsurface mixing could be. Determining what fraction of the surface is  
1360 recycled or reprocessed in place, and how, will be important to constrain with  
1361 *Europa Clipper*, alongside the elemental composition of surface materials. Overall,  
1362 conditions of Europa's formation and later bombardment, as well as its past and  
1363 potentially present activity, suggest the ingredients for life and present day energy  
1364 to support it may exist.

1365 For Enceladus, direct measurements of its ocean composition have been made  
1366 by the *Cassini* mission. The ocean likely contains compounds that suggest on-  
1367 going interaction between the seafloor and ocean, as well as potential fuel for  
1368 chemosynthetic life. Ocean-derived material erupting from Enceladus' south pole  
1369 contains both simple and complex organics, ice crystals, and salts (Waite et al,  
1370 2006, 2009, 2017; Postberg et al, 2011, 2018b), while Hsu et al (2015) demon-  
1371 strated the presence of silica nanoparticles that are interpreted as evidence for extensive  
1372 hydrothermalism and a well-mixed ocean. Waite et al (2017) demonstrated the  
1373 presence of molecular hydrogen that would be available energy for metabolism;  
1374 however, it bears questions as to whether hydrogen would be detected if the ocean  
1375 were inhabited since this material could be consumed by life. Nonetheless, Ence-  
1376 ladus' ocean geochemistry is the only measured to date and contains products

1377 known to support life on Earth, and therefore is habitable by current standards.  
1378 A mission that would return to Enceladus and search for higher chained organics  
1379 and organic complexity *in situ* within the plume could reveal strong indications  
1380 as to whether life is present on Enceladus (e.g., Lunine et al, 2018).

1381 For Ganymede and Titan, where high pressure ice phases become important,  
1382 the most pertinent question is whether any interaction can be maintained between  
1383 the silicate layer and the oceans. Though Ganymede's outer shell is presently  
1384 inactive at the surface, its deeper ice layers may overturn under basal heating  
1385 from the deeper interior (e.g., Kalousová et al, 2018). Vance et al (2014) showed  
1386 that the phase behavior of water-MgSO<sub>4</sub> salt mixtures under Ganymede conditions  
1387 can form multiple ocean layers separated by high pressure ice layers, potentially  
1388 with a deep reservoir of saline liquid above the silicate core that may argue for  
1389 the possibility of serpentinization. Similar conditions could be possible at Titan,  
1390 where clathrates may also play a role (Castillo-Rogez and Lunine, 2010) and the  
1391 ice shell may not be convecting (e.g., Nimmo and Bills, 2010). It is unclear whether  
1392 sources of oxidants could exist within ocean planets with outer ice shells in the  
1393 stagnant lid regime, like Ganymede and Titan. However, if mixing between these  
1394 reservoirs is possible, or if the decomposition of clathrates can deliver new sources  
1395 of energy, these moons could be habitable. Titan's surface habitability is a different  
1396 question all together; with liquid ethane and methane across the surface, Titan  
1397 could support exotic kinds of habitability, fueled by different chemical compounds,  
1398 including benzene (see Lunine et al (2019) for a review).

## 1399 6.2 *In Situ* Exploration of Terrestrial Habitats

1400 Ice on Earth is rich with life both within the ice and along its interfaces (e.g., Priscu  
1401 and Christner, 2004; Deming and Eicken, 2007). Analog habitats in Antarctica in-  
1402 clude perennially ice-covered lakes (e.g., Priscu et al, 1998; Murray et al, 2012) and  
1403 subglacial lakes such as Vostok and Whillians (Christner et al, 2014; Mikucki et al,  
1404 2016). Although communities are supported primarily by the silicate materials at  
1405 the bed, most of the communities are chemosynthetic, or rely on the oxidation and  
1406 reduction of species such as iron, sulfur, nitrogen and methane as metabolisms. In  
1407 the Arctic, subglacial volcanos in Iceland (e.g., Gaidos et al, 2004) and sulfur-rich  
1408 subglacial springs expressed at the surface of Borup Fjord (Gleeson et al, 2011,  
1409 2012) power similar communities.

1410 A growing amount of research is conducted via field studies with analog mis-  
1411 sion technologies, from *in situ* and remote sensing instrumentation to full vehicle  
1412 platforms. Drilling vehicles are being developed for future missions as well as deep  
1413 glacial access. In addition to ocean gliders (e.g., Lee and Rudnick, 2018) and open  
1414 ocean AUVs (e.g., Jenkins, 2010; Dutrieux et al, 2014) that have been devel-  
1415 oped for oceanographic operations on Earth, vehicles developed with ocean world  
1416 exploration beyond Earth in mind include BRUIE (Berisford et al, 2013), EN-  
1417 DURANCE (Gulati et al, 2010), ARTEMIS (Kimball et al, 2018), Nereid Under  
1418 Ice (German and Boetius, 2019), and Icefin (Meister et al, 2018) and have operated  
1419 under either lake ice, sea ice and/or ice shelves. These vehicles are returning data  
1420 about physical and oceanographic processes as well as communities under the ice,  
1421 including ice-ocean exchange.

## 1422 6.3 Future Exploration

1423 Future missions can investigate ice-ocean exchange in the outer solar system.  
1424 NASA’s planned *Europa Clipper* mission concept would conduct multiple science  
1425 investigations (Buffington et al, 2017). *In situ* sampling of Europa’s atmosphere  
1426 would look for compositional and isotopic signatures of ocean pH and water-rock  
1427 interactions. Remote sensing from the ultraviolet to mid-infrared would provide  
1428 global mapping of 95% of the surface to better than 50 m/pixel. Ice-penetrating  
1429 radar would sound through kilometers of ice to characterize ice shell structure and  
1430 search for the ice-ocean interface. Gravity science, magnetometer/plasma, and  
1431 altimetry investigations to constrain the thickness of the ocean and underlying  
1432 silicate layer, as well as the vigor of tidal heating, are also important for under-  
1433 standing the workings of the ice relative to the underlying materials (Pauer et al,  
1434 2010; Verma and Margot, 2018; Steinbrügge et al, 2018). A complementary suite  
1435 of instrument investigations are planned to fly on ESA’s *JUICE* spacecraft Grasset  
1436 et al (2013), which is set to orbit Ganymede in the early 2030’s.

1437 Landed geophysical investigations on Europa (Pappalardo et al, 2013; Hand  
1438 et al, 2017) could more precisely evaluate the satellite’s radial density structure,  
1439 rheological state and thermal state of its mantle, and extent of seafloor hydration  
1440 (Vance et al, 2018a,b). At the time of this writing, the *InSight* mission is con-  
1441 ducting a geophysical investigation of Mars, using seismometers and heat probes  
1442 to further characterize the radial structure, composition, and temperature of the  
1443 interior (Smrekar et al, 2018). The *DragonFly* concept, selected as NASA’s next  
1444 New Frontiers class mission, would include seismic and mass spectrometer inves-  
1445 tigation that could reveal the hydration state of silicates in Titan’s interior and  
1446 the degree of ice-ocean exchange (Turtle et al, 2017).

1447 **Acknowledgements** K.M.S. was supported by NASA Grant NNX14AR28G. K.K. was sup-  
1448 ported by the Czech Science Foundation through project No. 19-10809S and by Charles Uni-  
1449 versity Research Program No. UNCE/SCI/023. G.M. acknowledges support from the Italian  
1450 Space Agency (2018-25-HH.0). M.R.N. has been financially supported by the Space Research  
1451 User Support program of the Netherlands Organization for Scientific Research (NWO) under  
1452 contract number ALW-GO/16-19. T.R. was supported by the Helmholtz Association (project  
1453 VH-NG-1017). Work by JPL co-authors was partially supported by strategic research and  
1454 technology funds from the Jet Propulsion Laboratory, Caltech, and by the Icy Worlds and  
1455 Titan nodes of NASA’s Astrobiology Institute (13-13NAI7\_2-0024 and 17-NAI8-2-017). The  
1456 authors thank the European Space Agency (ESA) and the Belgian Federal Science Policy  
1457 Office (BELSPO) for their support in the framework of the PRODEX programme.

1458 **References**

- 1459 Allison ML, Clifford SM (1987) Ice-covered water volcanism on Ganymede. *J Geo-*  
1460 *phys Res Solid Earth* 92(B8):7865–7876, DOI 10.1029/JB092iB08p07865
- 1461 Anderson JD, Lau EL, Sjogren WL, Schubert G, Moore WB (1996) Gravitational  
1462 constraints on the internal structure of Ganymede. *Nature* 384(6609):541
- 1463 Anderson JD, Schubert G, Jacobson RA, Lau EL, Moore WB, Sjogren WL (1998a)  
1464 Distribution of rock, metals, and ices in Callisto. *Science* 280(5369):1573 – 1576,  
1465 URL <http://dx.doi.org/10.1126/Science.280.5369.1573>

- 1466 Anderson JD, Schubert G, Jacobson RA, Lau EL, Moore WB, Sjogren WL (1998b)  
1467 Europa's differentiated internal structure: Inferences from four galileo encoun-  
1468 ters. *Science* 281:2019–2022
- 1469 Anderson JD, Jacobson RA, McElrath TP, Moore WB, Schubert G, Thomas PC  
1470 (2001) Shape, mean radius, gravity field, and interior structure of Callisto. *Icarus*  
1471 153(1):157–161
- 1472 Artemieva N, Lunine J (2003) Cratering on Titan: impact melt, ejecta, and the fate  
1473 of surface organics. *Icarus* 164:471–480, DOI 10.1016/S0019-1035(03)00148-9
- 1474 Artemieva N, Lunine JI (2005) Impact cratering on Titan II. Global melt, escaping  
1475 ejecta, and aqueous alteration of surface organics. *Icarus* 175:522–533, DOI  
1476 10.1016/j.icarus.2004.12.005
- 1477 Ashkenazy Y, Gildor H, Losch M, Macdonald FA, Schrag DP, Tziperman  
1478 E (2013) Dynamics of a Snowball Earth ocean. *Nature* 495:90–93, URL  
1479 <https://doi.org/10.1038/nature11894>
- 1480 Ashkenazy Y, Sayag R, Tziperman E (2018) Dynamics of the global meridional  
1481 ice flow of Europa's icy shell. *Nature Astron* 2(1):43–49, DOI 10.1038/s41550-  
1482 017-0326-7, URL <https://doi.org/10.1038/s41550-017-0326-7>
- 1483 Atreya SK, Adams EY, Niemann HB, Demick-Montelara JE, Owen TC,  
1484 Fulchignoni M, Ferri F, Wilson EH (2006) Titan's methane cycle. *Planet Space*  
1485 *Sci* 54(12):1177 – 1187, DOI 10.1016/j.pss.2006.05.028
- 1486 Aurnou JM, Heimpel MH, Wicht J (2007) The effects of vigorous mixing in a  
1487 convective model of zonal flow on the Ice Giants. *Icarus* 190:110–126
- 1488 Aurnou JM, Heimpel MH, Allen L, King EM, Wicht J (2008) Convective heat  
1489 transfer and the pattern of thermal emission on the gas giants. *Geophys J Int*  
1490 173:793–801
- 1491 Baland RM, Tobie G, Lefevre A, Van Hoolst T (2014) Titan's internal structure  
1492 inferred from its gravity field, shape, and rotation state. *Icarus* 237:29–41
- 1493 Balog PS, Secco RA, Rubie DC, Frost DJ (2003) Equation of state of liquid Fe-10  
1494 wt% S: Implications for the metallic cores of planetary bodies. *J Geophys Res*  
1495 *Solid Earth* 108(B2)
- 1496 Barge LM, White LM (2017) Experimentally testing hydrothermal vent origin of  
1497 life on Enceladus and other icy/ocean worlds. *Astrobiology* 17(9):820–833
- 1498 Barr AC (2008) Mobile lid convection beneath Enceladus' south polar terrain. *J*  
1499 *Geophys Res Planets* 113(E7)
- 1500 Barr AC, Canup RM (2010) Origin of the Ganymede–Callisto dichotomy by im-  
1501 pacts during the late heavy bombardment. *Nature Geosci* 3(3):164
- 1502 Barr AC, McKinnon WB (2007) Convection in ice I shells and mantles  
1503 with self-consistent grain size. *J Geophys Res Planets* 112(E2), DOI  
1504 10.1029/2006JE002781
- 1505 Barr AC, Pappalardo RT (2005) Onset of convection in the icy Galilean  
1506 satellites: Influence of rheology. *J Geophys Res Planets* 110(E12), DOI  
1507 10.1029/2004JE002371
- 1508 Barr AC, Showman AP (2009) Heat Transfer in Europa's Icy Shell. In: Pappalardo  
1509 RT, McKinnon WB, Khurana KK (eds) *Europa*, University of Arizona Press,  
1510 Tucson, pp 405–430
- 1511 Béghin C, Randriamboarison O, Hamelin M, Karkoschka E, Sotin C, Whitten RC,  
1512 Berthelier JJ, Grard R, Simões F (2012) Analytic theory of Titan's Schumann  
1513 resonance: Constraints on ionospheric conductivity and buried water ocean.  
1514 *Icarus* 218(2):1028–1042

- 1515 Běhouňková M, Tobie G, Choblet G, Čadek O (2010) Coupling mantle convec-  
1516 tion and tidal dissipation: Applications to Enceladus and Earth-like planets. *J*  
1517 *Geophys Res Planets* 115(E14):E09011, DOI 10.1029/2009JE003564
- 1518 Běhouňková M, Tobie G, Choblet G, Čadek O (2012) Tidally-induced melting  
1519 events as the origin of south-pole activity on Enceladus. *Icarus* 219:655–664,  
1520 DOI 10.1016/j.icarus.2012.03.024
- 1521 Běhouňková M, Tobie G, Čadek O, Choblet G, Porco C, Nimmo F (2015) Timing  
1522 of water plume eruptions on Enceladus explained by interior viscosity structure.  
1523 *Nature Geosci* 8:601–604, DOI 10.1038/ngeo2475
- 1524 Běhouňková M, Souček O, Hron J, Čadek O (2017) Plume Activity and Tidal De-  
1525 formation on Enceladus Influenced by Faults and Variable Ice Shell Thickness.  
1526 *Astrobiology* 17(9):941–954, DOI 10.1089/ast.2016.1629
- 1527 Belton MJS, Head JW, Ingersoll AP, Greeley R, McEwen AS, Klaasen KP, Senske  
1528 D, Pappalardo R, Collins G, Vasavada AR, Sullivan R, Simonelli D, Geissler P,  
1529 Carr MH, Davies ME, Veverka J, Gierasch PJ, Banfield D, Bell M, Chapman  
1530 CR, Anger C, Greenberg R, Neukum G, Pilcher CB, Beebe RF, Burns JA,  
1531 Fanale F, Ip W, Johnson TV, Morrison D, Moore J, Orton GS, Thomas P, West  
1532 RA (1996) Galileo’s First Images of Jupiter and the Galilean Satellites. *Science*  
1533 274(5286):377–385, DOI 10.1126/science.274.5286.377
- 1534 Berisford DF, Leichty J, Klesh A, Hand KP (2013) Remote under-ice roving in  
1535 Alaska with the buoyant rover for under-ice exploration. In: *AGU Fall Meeting*  
1536 *Abstracts*
- 1537 Beuthe M (2013) Spatial patterns of tidal heating. *Icarus* 223:308–329
- 1538 Beuthe M (2016) Crustal control of dissipative ocean tides in Enceladus and other  
1539 icy moons. *Icarus* 280:278–299
- 1540 Beuthe M (2018) Enceladus’s crust as a non-uniform thin shell: I tidal deforma-  
1541 tions. *Icarus* 302:145 – 174, DOI 10.1016/j.icarus.2017.11.009
- 1542 Beuthe M, Rivoldini A, Trinh A (2016) Enceladus’s and Dione’s floating ice shells  
1543 supported by minimum stress isostasy. *Geophys Res Lett* 43(19)
- 1544 Bézard B, Yelle RV, Nixon CA (2014) The composition of Titan’s atmosphere.  
1545 In: Müller-Wodarg I, Griffith CA, Lellouch E, Cravens TE (eds) *Titan: Interior,*  
1546 *Surface, Atmosphere, and Space Environment*, Cambridge University Press, p  
1547 158
- 1548 Bierhaus EB, Zahnle K, Chapman CR, Pappalardo RT, McKinnon WB, Khurana  
1549 KK (2009) Europa’s crater distributions and surface ages. In: *Europa*, University  
1550 of Arizona Press Tucson, p 161
- 1551 Billings SE, Kattenhorn SA (2003) Comparison between terrestrial explosion  
1552 crater morphology in floating ice and European chaos. In: *Lunar and Planetary*  
1553 *Institute Science Conference Abstracts*, vol 34, p 1955
- 1554 Billings SE, Kattenhorn SA (2005) The great thickness debate: Ice shell thickness  
1555 models for Europa and comparisons with estimates based on flexure at ridges.  
1556 *Icarus* 177(2):397–412
- 1557 Bland MT, Showman AP, Tobie G (2009) The orbital–thermal evolution and global  
1558 expansion of Ganymede. *Icarus* 200(1):207–221
- 1559 Bouffard M, Labrosse S, Choblet G, Fournier A, Aubert J, Tackley PJ (2017)  
1560 A particle-in-cell method for studying double-diffusive convection in the liquid  
1561 layers of planetary interiors. *J Comput Phys* 346:552–571
- 1562 Bouquet A, Glein CR, Waite Jr JH (2019) How adsorption affects the gas–ice  
1563 partitioning of organics erupted from Enceladus. *Astrophys J* 873(1):28

- 1564 Brown ME, Hand KP (2013) Salts and radiation products on the surface of Europa.  
1565 *Astrophys J* 145:110
- 1566 Buffington B, Lam T, Campagnola S, Ludwinski J, Ferguson E, Bradley B, Scott  
1567 C, Ozimek M, Haapala Chalk A, Siddique F (2017) Evolution of Trajectory  
1568 Design Requirements on NASA's Planned Europa Clipper Mission. In: 68th  
1569 International Astronautical Congress (IAC), IAC-17-C1.7.8
- 1570 Buffo JJ (2019) Multiphase reactive transport in planetary ices. PhD thesis, Geor-  
1571 gia Institute of Technology
- 1572 Buffo JJ, Schmidt BE, Huber C (2018) Multiphase reactive transport and platelet  
1573 ice accretion in the sea ice of McMurdo sound, Antarctica. *J Geophys Res Oceans*  
1574 123(1):324–345
- 1575 Buffo JJ, Schmidt BE, Huber C, Walker CC (2019) Entrainment and Dynamics  
1576 of Ocean Derived Impurities Within Europa's Ice Shell. *Science Advances* In  
1577 review
- 1578 Čadek O, Tobie G, Van Hoolst T, Massé M, Choblet G, Lefèvre A, Mitri G, Baland  
1579 RM, Běhouňková M, Bourgeois O, et al (2016) Enceladus's internal ocean and  
1580 ice shell constrained from Cassini gravity, shape, and libration data. *Geophys*  
1581 *Res Lett* 43(11):5653–5660
- 1582 Čadek O, Běhouňková M, Tobie G, Choblet G (2017) Viscoelastic relaxation of  
1583 Enceladus's ice shell. *Icarus* 291:31 – 35, DOI 10.1016/j.icarus.2017.03.011
- 1584 Čadek O, Souček O, Běhouňková M, Choblet G, Tobie G, Hron J (2019) Long-term  
1585 stability of Enceladus' uneven ice shell. *Icarus* 319:476–484
- 1586 Carlson RW, Calvin WM, Dalton JB, Hansen GB, Hudson RL, Johnson RE, Mc-  
1587 Cord TB, Moore MH (2009) Europa's surface composition. *Europa* pp 283–327
- 1588 Carr MH, Belton MJS, Chapman CR, Davies ME, Geissler P, Greenberg R,  
1589 McEwen AS, Tufts BR, Greeley R, Sullivan R, Head JW, Pappalardo RT,  
1590 Klaasen KP, Johnson TV, Kaufman J, Senske D, Moore J, Neukum G, Schubert  
1591 G, Burns JA, Thomas P, Veverka J (1998) Evidence for a subsurface ocean on  
1592 Europa. *Nature* 391:363–365
- 1593 Casacchia R, Strom RG (1984) Geologic evolution of Galileo Regio, Ganymede. *J*  
1594 *Geophys Res Solid Earth* 89(S02):B419–B428
- 1595 Castillo-Rogez JC, Lunine JI (2010) Evolution of Titan's rocky core constrained  
1596 by Cassini observations. *Geophys Res Lett* 37(20), DOI 10.1029/2010GL044398
- 1597 Chen EMA, Nimmo F (2011) Obliquity tides do not significantly heat Enceladus.  
1598 *Icarus* 214(2):779–781
- 1599 Chen EMA, Nimmo F, Glatzmaier GA (2014) Tidal heating in icy satellite oceans.  
1600 *Icarus* 229:11–30
- 1601 Cheng JS, Aurnou JM, Julien K, Kunnen RPJ (2018) A heuristic framework for  
1602 next-generation models of geostrophic convective turbulence. *Geophys Astro-*  
1603 *phys Fluid Dyn* 112(4):277–300
- 1604 Choblet G, Tobie G, Sotin C, Běhouňková M, Čadek O, Postberg F, Souček O  
1605 (2017a) Powering prolonged hydrothermal activity inside Enceladus. *Nature As-*  
1606 *tron* 1(12):841
- 1607 Choblet G, Tobie G, Sotin C, Kalousová K, Grasset O (2017b) Heat transport  
1608 in the high-pressure ice mantle of large icy moons. *Icarus* 285:252–262, DOI  
1609 10.1016/j.icarus.2016.12.002
- 1610 Choukroun M, Grasset O (2010) Thermodynamic data and modeling of the water  
1611 and ammonia-water phase diagrams up to 2.2 GPa for planetary geophysics. *J*  
1612 *Chem Phys* 133:144502

- 1613 Choukroun M, Sotin C (2012) Is Titan's shape caused by its meteorology and  
1614 carbon cycle? *Geophys Res Lett* 39(4)
- 1615 Christner BC, Priscu JC, Achberger AM, Barbante C, Carter SP, Christianson K,  
1616 Michaud AB, Mikucki JA, Mitchell AC, Skidmore ML, et al (2014) A microbial  
1617 ecosystem beneath the West Antarctic ice sheet. *Nature* 512(7514):310
- 1618 Chyba CF (2000) Energy for microbial life on Europa. *Nature* 403(6768):381
- 1619 Chyba CF, Phillips CB (2001) Possible ecosystems and the search for life on Eu-  
1620 ropa. *Proc Natl Acad Sci* 98(3):801–804
- 1621 Chyba CF, Phillips CB (2002) Europa as an abode of life. *Origins of life and*  
1622 *evolution of the biosphere* 32(1):47–67, DOI 10.1023/A:1013958519734
- 1623 Collins G, Nimmo F (2009) Chaotic terrain on Europa. In: Pappalardo RT, McK-  
1624 innon WB, Khurana KK (eds) *Europa*, Tucson: University of Arizona Press, pp  
1625 259–281
- 1626 Collins GC, Goodman JC (2007) Enceladus' south polar sea. *Icarus* 189(1):72–82
- 1627 Collins GC, Head JW, Pappalardo RT, Spaun NA (2000) Evaluation of models  
1628 for the formation of chaotic terrain on Europa. *J Geophys Res* 105:1709–1716
- 1629 Connolly JAD (2009) The geodynamic equation of state: what and how. *Geochem*  
1630 *Geophys Geosys* 10(10)
- 1631 Consolmagno GJ, Lewis JS (1978) The evolution of icy satellite interiors and  
1632 surfaces. *Icarus* 34(2):280 – 293, DOI 10.1016/0019-1035(78)90168-9
- 1633 Corlies P, Hayes AG, Birch SPD, Lorenz R, Stiles BW, Kirk R, Poggiali V, Ze-  
1634 bker H, Iess L (2017) Titan's Topography and Shape at the End of the Cassini  
1635 Mission. *Geophys Res Lett* 44(23):11–754
- 1636 Cox R, Bauer AW (2015) Impact breaching of Europa's ice: Constraints from  
1637 numerical modeling. *Journal of Geophysical Research: Planets* 120(10):1708–  
1638 1719, DOI 10.1002/2015JE004877
- 1639 Cox R, Ong LCF, Arakawa M, Scheider KC (2008) Impact penetration of Europa's  
1640 ice crust as a mechanism for formation of chaos terrain. *Meteoritics & Planetary*  
1641 *Science* 43(12):2027–2048, DOI 10.1111/j.1945-5100.2008.tb00659.x
- 1642 Craft KL, Patterson GW, Lowell RP, Germanovich L (2016) Fracturing and flow:  
1643 Investigations on the formation of shallow water sills on Europa. *Icarus* 274:297  
1644 – 313, DOI 10.1016/j.icarus.2016.01.023
- 1645 Craven M, Carsey F, Behar A, Matthews J, Brand R, Elcheikh A, Hall S, Trever-  
1646 row A (2005) Borehole imagery of meteoric and marine ice layers in the Amery  
1647 Ice Shelf, East Antarctica. *J Glaciol* 51(172):75–84
- 1648 Craven M, Allison I, Fricker HA, Warner RC (2009) Properties of a marine ice  
1649 layer under the amery ice shelf, east antarctica. *J Glaciol* 55(192):717–728
- 1650 Crawford GD, Stevenson DJ (1988) Gas-driven water volcanism and the resurfac-  
1651 ing of Europa. *Icarus* 73(1):66 – 79, DOI 10.1016/0019-1035(88)90085-1
- 1652 Croft SK, Casacchia R, Strom RG, (US) GS (1994) Geologic map of the tiamat  
1653 sulcus quadrangle (jg-9) of ganymede. *U S Geol Surv Map* I-1548
- 1654 Čuk M, Dones L, Nesvorný D (2016) Dynamical evidence for a late formation of  
1655 Saturn's moons. *Astrophys J* 820(2):97
- 1656 Davaille A, Jaupart C (1993) Transient high-Rayleigh-number thermal con-  
1657 vection with large viscosity variations. *J Fluid Mech* 253:141–166, DOI  
1658 10.1017/S0022112093001740
- 1659 De La Chapelle S, Milsch H, Castelnau O, Duval P (1999) Compressive creep of ice  
1660 containing a liquid intergranular phase: Rate-controlling processes in the disloca-  
1661 tion creep regime. *Geophys Res Lett* 26(2):251–254, DOI 10.1029/1998GL900289

- 1662 Deming JW, Eicken H (2007) Life in ice. *Planets and life: The emerging science*  
1663 *of astrobiology* pp 292–312
- 1664 Dempsey DE, Langhorne PJ (2012) Geometric properties of platelet ice crystals.  
1665 *Cold Regions Science and Technology* 78:1–13
- 1666 Dempsey DE, Langhorne PJ, Robinson NJ, Williams MJM, Haskell TG, Frew  
1667 RD (2010) Observation and modeling of platelet ice fabric in McMurdo Sound,  
1668 Antarctica. *J Geophys Res Oceans* 115(C1)
- 1669 Des Marais DJ, Nuth III JA, Allamandola LJ, Boss AP, Farmer JD, Hoehler TM,  
1670 Jakosky BM, Meadows VS, Pohorille A, Runnegar B, et al (2008) The NASA  
1671 astrobiology roadmap. *Astrobiology* 8(4):715–730
- 1672 Deschamps F, Sotin C (2000) Inversion of two-dimensional numerical convection  
1673 experiments for a fluid with a strongly temperature-dependent viscosity. *Geo-*  
1674 *phys J Int* 143(1):204–218, DOI 10.1046/j.1365-246x.2000.00228.x
- 1675 Deschamps F, Sotin C (2001) Thermal convection in the outer shell of large icy  
1676 satellites. *J Geophys Res Planets* 106(E3):5107–5121
- 1677 Dhingra D, Hedman MM, Clark RN, Nicholson PD (2017) Spatially resolved near  
1678 infrared observations of enceladus tiger stripe eruptions from cassini vims. *Icarus*  
1679 292:1 – 12, DOI <https://doi.org/10.1016/j.icarus.2017.03.002>
- 1680 Dombard AJ, Patterson GW, Lederer AP, Prockter LM (2013) Flanking fractures  
1681 and the formation of double ridges on Europa. *Icarus* 223(1):74 – 81, DOI  
1682 10.1016/j.icarus.2012.11.021
- 1683 Dougherty MK, Khurana KK, Neubauer FM, Russell CT, Saur J, Leisner J, Bur-  
1684 ton ME (2006) Identification of a dynamic atmosphere at Enceladus with the  
1685 Cassini magnetometer. *Science* 311(5766):1406–1409
- 1686 Durand G, Weiss J, Lipenkov V, Barnola JM, Krinner G, Parrenin F, Delmonte  
1687 B, Ritz C, Duval P, Röthlisberger R, Bigler M (2006) Effect of impurities on  
1688 grain growth in cold ice sheets. *J Geophys Res Earth Surface* 111(F1), DOI  
1689 10.1029/2005JF000320
- 1690 Durante D, Hemingway DJ, Racioppa P, Iess L, Stevenson DJ (2019) Titan’s  
1691 gravity field and interior structure after Cassini. *Icarus* 326:123–132
- 1692 Durham WB, Stern LA (2001) Rheological Properties of Water Ice—Applications  
1693 to Satellites of the Outer Planets. *Annu Rev Earth Planet Sci* 29(1):295–330,  
1694 DOI 10.1146/annurev.earth.29.1.295
- 1695 Dutrieux P, De Rydt J, Jenkins A, Holland PR, Ha HK, Lee SH, Steig EJ, Ding Q,  
1696 Abrahamsen EP, Schröder M (2014) Strong sensitivity of Pine Island ice-shelf  
1697 melting to climatic variability. *Science* 343(6167):174–178
- 1698 Egbert GD, Ray RD (2000) Significant dissipation of tidal energy in the deep ocean  
1699 inferred from satellite altimeter data. *Nature* 405:775, DOI 10.1038/35015531
- 1700 Fagents SA (2003) Considerations for effusive cryovolcanism on Europa:  
1701 The post-Galileo perspective. *J Geophys Res Planets* 108(E12), DOI  
1702 10.1029/2003JE002128
- 1703 Fagents SA, Greeley R, Sullivan RJ, Pappalardo RT, Prockter LM, Galileo  
1704 SSI Team T (2000) Cryomagmatic mechanisms for the formation of Rhadaman-  
1705 thys Linea, triple band margins, and other low-albedo features on Europa. *Icarus*  
1706 144(1):54 – 88, DOI 10.1006/icar.1999.6254
- 1707 Fanale FP, Li YH, De Carlo E, Farley C, Sharma SK, Horton K, Granahan JC  
1708 (2001) An experimental estimate of Europa’s “ocean” composition indepen-  
1709 dent of Galileo orbital remote sensing. *Journal of Geophysical Research: Planets*  
1710 106(E7):14595–14600

- 1711 Farber R, Goodman JC (2014) How quickly does drifting material traverse through  
1712 Europa's ocean? *LPI Contributions* 1774:4059
- 1713 Feistel R, Hagen E (1995) On the GIBBS thermodynamic potential of seawater.  
1714 *Prog Oceanogr* 36(4):249–327
- 1715 Fernando HJS, Chen R, Ayotte BA (1998) Development of a point plume in the  
1716 presence of background rotation. *Phys Fluids* 10(9):2369–2383
- 1717 Figueredo PH, Greeley R (2000) Geologic mapping of the northern leading  
1718 hemisphere of Europa from Galileo solid-state imaging data. *J Geophys Res*  
1719 105:22629–22646
- 1720 Figueredo PH, Greeley R (2004) Resurfacing history of Europa from pole-to-pole  
1721 geological mapping. *Icarus* 167:287–312
- 1722 Figueredo PH, Chuang FC, Rathbun JA, Kirk RL, Greeley R (2002) Geology and  
1723 origin of Europa's mitten feature (murius chaos). *J Geophys Res* 107:5026
- 1724 Fischer PD, Brown ME, Hand KP (2015) Spatially resolved spectroscopy of Eu-  
1725 ropa: The distinct spectrum of large-scale chaos. *Astron J* 150(5):164
- 1726 Fortes A, Grindrod P, Trickett S, Vočadlo L (2007) Ammonium sulfate on Ti-  
1727 tan: Possible origin and role in cryovolcanism. *Icarus* 188(1):139–153, DOI  
1728 10.1016/j.icarus.2006.11.002
- 1729 Fricker HA, Popov S, Allison I, Young N (2001) Distribution of marine ice beneath  
1730 the Amery Ice Shelf. *Geophys Res Lett* 28:2241–2244
- 1731 Gaidos E, Lanoil B, Thorsteinsson T, Graham A, Skidmore ML, Han SK, Rust  
1732 T, Popp B (2004) A viable microbial community in a subglacial volcanic crater  
1733 lake, Iceland. *Astrobiology* 4(3):327–344
- 1734 Gaidos EJ, Nimmo F (2000) Tectonics and water on Europa. *Nature* 405:637,  
1735 DOI 10.1038/35015170
- 1736 Galton-Fenzi B, Hunter JR, Coleman R, Marsland SJ, Warner RC (2012) Modeling  
1737 the basal melting and marine ice accretion of the Amery Ice Shelf. *J Geophys*  
1738 *Res* 117:C09031, doi:10.1029/2012JC008214
- 1739 Gao P, Stevenson DJ (2013) Nonhydrostatic effects and the determination of icy  
1740 satellites' moment of inertia. *Icarus* 226(2):1185–1191
- 1741 Gastine T, Wicht J, Aurnou JM (2013) Zonal flow regimes in rotating anelastic  
1742 spherical shells: An application to giant planets. *Icarus* 225:156–172
- 1743 Gastine T, Wicht J, Aubert J (2016) Scaling regimes in spherical shell rotating  
1744 convection. *J Fluid Mech* 808:690–732
- 1745 Geissler P, Greenberg R, Hoppa G, McEwen A, Tufts R, Phillips C, Clark B,  
1746 Ockert-Bell M, Helfenstein P, Burns J, Veverka J, Sullivan R, Greeley R, Pap-  
1747 palaro R, Head J, Belton M, Denk T (1998) Evolution of Lineaments on Eu-  
1748 ropa: Clues from Galileo Multispectral Imaging Observations. *Icarus* 135(1):107  
1749 – 126, DOI <https://doi.org/10.1006/icar.1998.5980>
- 1750 German CR, Boetius A (2019) Robotics-based scientific investigations at an ice-  
1751 ocean interface: First results from nereid under ice in the Arctic. *LPI Contribu-*  
1752 *tions* 2168
- 1753 Gissinger C, Petitdemange L (2019) A magnetically driven equatorial jet in Eu-  
1754 ropa's ocean. *Nature Astron* 1
- 1755 Gleeson DF, Williamson C, Grasby SE, Pappalardo RT, Spear JR, Templeton AS  
1756 (2011) Low temperature S0 biomineralization at a supraglacial spring system in  
1757 the Canadian High Arctic. *Geobiology* 9(4):360–375
- 1758 Gleeson DF, Pappalardo RT, Anderson MS, Grasby SE, Mielke RE, Wright KE,  
1759 Templeton AS (2012) Biosignature detection at an Arctic analog to Europa.

- 1760 Astrobiology 12(2):135–150
- 1761 Glein CR, Postberg F, Vance SD (2018) The geochemistry of Enceladus: Compo-  
1762 sition and controls. In: Enceladus and the Icy Moons of Saturn, University of  
1763 Arizona Press, pp 39–56
- 1764 Goguen JD, Buratti BJ, Brown RH, Clark RN, Nicholson PD, Hedman MM,  
1765 Howell RR, Sotin C, Cruikshank DP, Baines KH, Lawrence KJ, Spencer JR,  
1766 Blackburn DG (2013) The temperature and width of an active fissure on ence-  
1767 ladus measured with cassini vims during the 14 april 2012 south pole flyover.  
1768 Icarus 226(1):1128 – 1137, DOI <https://doi.org/10.1016/j.icarus.2013.07.012>
- 1769 Golden KM, Ackley SF, Lytle VI (1998) The percolation phase transition in sea  
1770 ice. Science 282(5397):2238–2241
- 1771 Golden KM, Eicken H, Heaton AL, Miner J, Pringle DJ, Zhu J (2007) Thermal  
1772 evolution of permeability and microstructure in sea ice. Geophys Res Lett 34(16)
- 1773 Goldsby DL, Kohlstedt DL (2001) Superplastic deformation of ice: Experi-  
1774 mental observations. J Geophys Res Solid Earth 106(B6):11017–11030, DOI  
1775 10.1029/2000JB900336
- 1776 Goldstein DB, Hedman M, Manga M, Perry M, Spitale J, Teolis B (2018) Eceladus  
1777 plume dynamics: From surface to space. In: Enceladus and the Icy Moons of  
1778 Saturn, University of Arizona Press, pp 175–194
- 1779 Golombek MP (1982) Constraints on the expansion of Ganymede and the thickness  
1780 of the lithosphere. J Geophys Res Solid Earth 87(S01):A77–A83
- 1781 Golombek MP, Allison ML (1981) Sequential development of grooved terrain and  
1782 polygons on Ganymede. Geophys Res Lett 8(11):1139–1142
- 1783 Goodman JC, Lenferink E (2012) Numerical simulations of marine hydrothermal  
1784 plumes for Europa and other icy worlds. Icarus 221:970–983
- 1785 Goodman JC, Pierrehumbert RT (2003) Glacial flow of floating marine ice in  
1786 ”Snowball Earth”. J Geophys Res Oceans 108(C10):3308
- 1787 Goodman JC, Collins GC, Marshall J, Pierrehumbert RT (2004) Hydrothermal  
1788 plume dynamics on Europa: Implications for chaos formation. J Geophys Res  
1789 109:E03008
- 1790 Grannan AM, Le Bars M, Cebon D, Aurnou JM (2014) Experimental study of  
1791 global-scale turbulence in a librating ellipsoid. Phys Fluids 26(12):126601, DOI  
1792 10.1063/1.4903003
- 1793 Grannan AM, Favier B, Le Bars M, Aurnou JM (2017) Tidally forced turbulence  
1794 in planetary interiors. Geophys J Int 208:1690–1703
- 1795 Grasset O, Dougherty MK, Coustenis A, Bunce EJ, Erd C, Titov D, Blanc M,  
1796 Coates A, Drossart P, Fletcher LN, et al (2013) JUpiter ICy moons Explorer  
1797 (JUICE): An ESA mission to orbit Ganymede and to characterise the Jupiter  
1798 system. Planet Space Sci 78:1–21
- 1799 Greeley R, Sullivan R, Coon MD, Geissler PE, Tufts B, Head JW, Pappalardo RT,  
1800 Moore JM (1998) Terrestrial Sea Ice Morphology: Considerations for Europa.  
1801 Icarus 135(1):25 – 40, DOI <https://doi.org/10.1006/icar.1998.5977>
- 1802 Greenberg R, Geissler P, Hoppa GV, Tufts BR, Durda DD, Pappalardo RT, Head  
1803 JW, Greeley R, Sullivan R, Carr MH (1998) Tectonic processes on europa: Tidal  
1804 stresses, mechanical response, and visible features. Icarus 135:64–78
- 1805 Greenberg R, Hoppa GV, Tufts BR, Geissler P, Riley J (1999) Chaos on Europa.  
1806 Icarus 141:263–286
- 1807 Gulati S, Richmond K, Flesher C, Hogan BP, Murarka A, Kuhlmann G, Sridha-  
1808 ran M, Stone WC, Doran PT (2010) Toward autonomous scientific exploration

- 1809 of ice-covered lakes—Field experiments with the ENDURANCE AUV in an  
1810 Antarctic Dry Valley. In: 2010 IEEE International Conference on Robotics and  
1811 Automation, IEEE, pp 308–315
- 1812 Hammond NP, Parmentier EM, Barr AC (2018) Compaction and melt transport  
1813 in ammonia-rich ice shells: Implications for the evolution of Triton. *J Geophys*  
1814 *Res Planets* 123(12):3105–3118
- 1815 Han L, Showman AP (2005) Thermo-compositional convection in Europa’s icy  
1816 shell with salinity. *Geophys Res Lett* 32:L20201, DOI 10.1029/2005GL023979
- 1817 Han L, Showman AP (2008) Implications of shear heating and fracture zones  
1818 for ridge formation on Europa. *Geophysical Research Letters* 35(3), DOI  
1819 10.1029/2007GL031957
- 1820 Han L, Showman AP (2010) Coupled convection and tidal dissipation in Europa’s  
1821 ice shell. *Icarus* 207:834–844
- 1822 Hand KP, Carlson RW (2015) Europa’s surface color suggests an ocean rich with  
1823 sodium chloride. *Geophys Res Lett* 42(9):3174–3178
- 1824 Hand KP, Carlson RW, Chyba CF (2007) Energy, chemical disequilibrium,  
1825 and geological constraints on Europa. *Astrobiology* 7(6):1006–1022, DOI  
1826 10.1089/ast.2007.0156
- 1827 Hand KP, Chyba CF, Priscu JC, Carlson RW, Nealson KH (2009) Astrobiology  
1828 and the potential for life on Europa. In: *Europa*, University of Arizona Press  
1829 Tucson, pp 589–629
- 1830 Hand KP, Murray AE, Garvin JB, Brinckerhoff WB, Christner BC, Edgett KS,  
1831 Ehlmann BL, German C, Hayes AG, Hoehler TM, Horst SM, Lunine JI, Nealson  
1832 KH, Paranicas C, Schmidt BE, Smith DE, Rhoden AR, Russell MJ, Templeton  
1833 AS, Willis PA, Yingst RA, Phillips CB, Cable ML, Craft KL, Hofmann  
1834 AE, Nordheim TA, Pappalardo RT, the Project Engineering Team (2017) Report  
1835 of the Europa Lander Science Definition Team. Tech. rep., Jet Propulsion  
1836 Laboratory, California Institute of Technology
- 1837 Hanley J, Dalton III JB, Chevrier VF, Jamieson CS, Barrows RS (2014) Re-  
1838 flectance spectra of hydrated chlorine salts: The effect of temperature with im-  
1839 plications for Europa. *J Geophys Res Planets* 119(11):2370–2377
- 1840 Hansen CJ, Esposito LW, Stewart AIF, Meinke B, Wallis B, Colwell JE, Hendrix  
1841 AR, Larsen K, Pryor W, Tian F (2008) Water vapour jets inside the plume of  
1842 gas leaving Enceladus. *Nature* 456:477–479, DOI 10.1038/nature07542
- 1843 Hansen CJ, Shemansky DE, Esposito LW, Stewart AIF, Lewis BR, Colwell JE,  
1844 Hendrix AR, West RA, Waite Jr JH, Teolis B, Magee BA (2011) The com-  
1845 position and structure of the Enceladus plume. *Geophysical Research Letters*  
1846 38(11), DOI 10.1029/2011GL047415
- 1847 Hansen CJ, Esposito LW, Aye KM, Colwell JE, Hendrix AR, Portyankina G, She-  
1848 mansky D (2017) Investigation of diurnal variability of water vapor in Enceladus’  
1849 plume by the Cassini ultraviolet imaging spectrograph. *Geophysical Research*  
1850 *Letters* 44(2):672–677, DOI 10.1002/2016GL071853
- 1851 Hartkorn O, Saur J (2017) Induction signals from Callisto’s ionosphere and their  
1852 implications on a possible subsurface ocean. *J Geophys Res* 122(11)
- 1853 Hay HCFC, Matsuyama I (2017) Numerically modelling tidal dissipation with  
1854 bottom drag in the oceans of Titan and Enceladus. *Icarus* 281:342–356
- 1855 Hay HCFC, Matsuyama I (2019) Nonlinear tidal dissipation in the subsurface  
1856 oceans of Enceladus and other icy satellites. *Icarus* 319:68–85

- 1857 Hays L, Archenbach L, Bailey J, Barnes R, Barros J, Bertka C, Boston P, Boyd  
1858 E, Cable M, Chen I, et al (2015) NASA Astrobiology strategy. National Aero-  
1859 nautics and Space Administration Washington, DC: NASA
- 1860 Head JW, Pappalardo RT (1999) Brine mobilization during lithospheric heat-  
1861 ing on Europa: Implications for formation of chaos terrain, lenticula texture,  
1862 and color variations. *Journal of Geophysical Research: Planets* 104(E11):27143–  
1863 27155, DOI 10.1029/1999JE001062
- 1864 Head JW, Pappalardo RT, Sullivan R (1999) Europa: Morphological character-  
1865 istics of ridges and triple bands from Galileo data (E4 and E6) and assess-  
1866 ment of a linear diapirism model. *Journal of Geophysical Research: Planets*  
1867 104(E10):24223–24236, DOI 10.1029/1998JE001011
- 1868 Hedman M, Dhingra D, Nicholson P, Hansen C, Portyankina G, Ye S, Dong Y  
1869 (2018) Spatial variations in the dust-to-gas ratio of enceladus plume. *Icarus*  
1870 305:123 – 138, DOI <https://doi.org/10.1016/j.icarus.2018.01.006>
- 1871 Hedman MM, Gosmeyer CM, Nicholson PD, Sotin C, Brown RH, Clark RN,  
1872 Baines KH, Buratti BJ, Showalter MR (2013) An observed correlation be-  
1873 tween plume activity and tidal stresses on Enceladus. *Nature* 500:182–184, DOI  
1874 10.1038/nature12371
- 1875 Heimpel MH, Gastine T, Wicht J (2015) Simulation of deep-seated zonal jets and  
1876 shallow vortices in gas giant atmospheres. *Nature Geosci* 9(1):19
- 1877 Helfenstein P (2014) Y-Shaped Discontinuity, Springer New York, New York, NY,  
1878 pp 1–5
- 1879 Helfenstein P, Parmentier EM (1985) Patterns of fracture and tidal stresses  
1880 due to nonsynchronous rotation: Implications for fracturing on Europa. *Icarus*  
1881 61(2):175–184
- 1882 Hemingway D, Nimmo F, Zebker H, Iess L (2013) A rigid and weathered ice shell  
1883 on Titan. *Nature* 500:550–552, DOI 10.1038/nature12400
- 1884 Hemingway DJ, Mittal T (2019) Enceladus’s ice shell structure as a window on  
1885 internal heat production. *Icarus* <https://doi.org/10.1016/j.icarus.2019.03.011>
- 1886 Hendershott MC (1981) Long waves and ocean tides. In: Warren BA, Wunsch C  
1887 (eds) *Evolution of Physical Oceanography*, MIT Press, Cambridge, Mass., pp  
1888 292–341
- 1889 Hibbitts CA, McCord TB, Hansen GB (2000) Distributions of CO<sub>2</sub> and SO<sub>2</sub> on  
1890 the surface of Callisto. *J Geophys Res Planets* 105(E9):22541–22557
- 1891 Hibbitts CA, Pappalardo RT, Hansen GB, McCord TB (2003) Carbon dioxide on  
1892 Ganymede. *J Geophys Res Planets* 108(E5)
- 1893 Hoffman PF, Schrag DP (2002) The snowball Earth hypothesis: testing the limits  
1894 of global change. *Terra Nova* 14(3):129–155
- 1895 Hogenboom DL (1995) Magnesium sulfate-water to 400 MPa using a novel  
1896 piezometer: Densities, phase equilibria, and planetological implications. *Icarus*  
1897 115(2):258–277, DOI 10.1006/icar.1995.1096
- 1898 Hogenboom DL, Kargel JS, Consolmagno GJ, Holden TC, Lee L, Buyyounouski  
1899 M (1997) The ammonia-water system and the chemical differentiation of icy  
1900 satellites. *Icarus* 128(1):171–180
- 1901 Howell SM, Pappalardo RT (2018) Band formation and ocean-surface interac-  
1902 tion on Europa and Ganymede. *Geophys Res Lett* 45(10):4701–4709, DOI  
1903 10.1029/2018GL077594
- 1904 Hsu HW, Postberg F, Sekine Y, Shibuya T, Kempf SD, Horányi M, Juhász A,  
1905 Altobelli N, Suzuki K, Masaki Y, et al (2015) Ongoing hydrothermal activities

- 1906 within Enceladus. *Nature* 519(7542):207
- 1907 Hudleston PJ (2015) Structures and fabrics in glacial ice: A review. *J Struc Geol*
- 1908 81:1–27, DOI 10.1016/j.jsg.2015.09.003
- 1909 Hussmann H, Spohn T, Wiczerkowski K (2002) Thermal equilibrium states of
- 1910 Europa’s ice shell: Implications for internal ocean thickness and surface heat
- 1911 flow. *Icarus* 156:143–151
- 1912 Hussmann H, Sohl F, Spohn T (2006) Subsurface oceans and deep interiors of
- 1913 medium-sized outer planet satellites and large trans-neptunian objects. *Icarus*
- 1914 185:258–273
- 1915 Hussmann H, Sotin C, Lunine JI (2015) Interiors and evolution of icy satellites.
- 1916 In: Schubert G (ed) *Treatise on Geophysics: Second Edition*, vol 10, Elsevier,
- 1917 pp 605–635
- 1918 Iess L, Rappaport NJ, Jacobson RA, Racioppa P, Stevenson DJ, Tortora P, Arm-
- 1919 strong JW, Asmar SW (2010) Gravity field, shape, and moment of inertia of
- 1920 Titan. *Science* 327:1367–1369
- 1921 Iess L, Jacobson RA, Ducci M, Stevenson DJ, Lunine JI, Armstrong JW, Asmar
- 1922 SW, Racioppa P, Rappaport NJ, Tortora P (2012) The tides of Titan. *Science*
- 1923 337:457–459
- 1924 Iess L, Stevenson DJ, Parisi M, Hemingway D, Jacobson RA, Lunine JI, Nimmo F,
- 1925 Armstrong JW, Asmar SW, Ducci M, et al (2014) The gravity field and interior
- 1926 structure of Enceladus. *Science* 344(6179):78–80
- 1927 Ingersoll AP, Ewald SP (2017) Decadal timescale variability of the ence-
- 1928 ladus plumes inferred from cassini images. *Icarus* 282:260 – 275, DOI
- 1929 <https://doi.org/10.1016/j.icarus.2016.09.018>
- 1930 Ingersoll AP, Pankine AA (2010) Subsurface heat transfer on enceladus:
- 1931 Conditions under which melting occurs. *Icarus* 206(2):594 – 607, DOI
- 1932 <https://doi.org/10.1016/j.icarus.2009.09.015>, cassini at Saturn
- 1933 Jacobson RA, Antreasian PG, Bordi JJ, Criddle KE, Ionasescu R, Jones JB,
- 1934 Mackenzie RA, Meek MC, Parcher D, Pelletier FJ, et al (2006) The gravity
- 1935 field of the Saturnian system from satellite observations and spacecraft tracking
- 1936 data. *Astron J* 132(6):2520
- 1937 Jansen MF (2016) The turbulent circulation of a Snowball Earth ocean. *J Phys*
- 1938 *Oceanogr* 46(6):1917–1933
- 1939 Jaumann R, Kirk RL, Lorenz RD, Lopes RMC, Stofan E, Turtle EP, Keller HW,
- 1940 Wood CA, Sotin C, Soderblom LA, et al (2009) Geology and surface processes
- 1941 on Titan. In: *Titan from Cassini-Huygens*, Springer, pp 75–140
- 1942 Jenkins A (2010) The role of meltwater advection in the formulation of conservative
- 1943 boundary conditions at an ice-ocean interface. *J Phys Ocean* 31:285–296
- 1944 Jia X, Kivelson MG, Khurana KK, Kurth WS (2018) Evidence of a plume on Eu-
- 1945 ropa from Galileo magnetic and plasma wave signatures. *Nature Astron* 2:459–
- 1946 464, DOI 10.1038/s41550-018-0450-z
- 1947 Johnson BC, Sheppard RY, Pascuzzo AC, Fisher EA, Wiggins SE (2017) Porosity
- 1948 and salt content determine if subduction can occur in Europa’s ice shell. *J*
- 1949 *Geophys Res Planets* 122(12):2765–2778
- 1950 Johnston SA, Montési LGJ (2014) Formation of ridges on Europa above crys-
- 1951 tallizing water bodies inside the ice shell. *Icarus* 237:190 – 201, DOI
- 1952 10.1016/j.icarus.2014.04.026
- 1953 Journaux B, et al (2019) High-pressure ices in large ocean worlds. *Space Sci Rev*

- 1954 Kadel S, Fagents SA, Greeley R, Team GS (1998) Trough-bounding ridge pairs  
1955 on Europa: Considerations for an endogenic model of formation. In: Lunar and  
1956 Planetary Institute Science Conference Abstracts, vol 29, p 1078
- 1957 Kadel SD, Chuang FC, Greeley R, Moore JM (2000) Geological history of the  
1958 Tyre region of Europa: A regional perspective on European surface features and  
1959 ice thickness. *Journal of Geophysical Research: Planets* 105(E9):22657–22669,  
1960 DOI 10.1029/1999JE001203
- 1961 Kalousová K, Sotin C (2018) Melting in high-pressure ice layers of large ocean  
1962 worlds – implications for volatiles transport. *Geophys Res Lett* 45(16):8096–  
1963 8103, DOI 10.1029/2018GL078889
- 1964 Kalousová K, Sotin C (2019) Dynamics of Titan’s high-pressure ice layer. *Earth  
1965 Planet Sci Lett* submitted
- 1966 Kalousová K, Souček O, Tobie G, Choblet G, Čadek O (2014) Ice melting and  
1967 downward transport of meltwater by two-phase flow in Europa’s ice shell. *J  
1968 Geophys Res Planets* 119:532–549, DOI 10.1002/2013JE004563
- 1969 Kalousová K, Souček O, Tobie G, Choblet G, Čadek O (2016) Water genera-  
1970 tion and transport below Europa’s strike-slip faults. *J Geophys Res Planets*  
1971 121:2444–2462, DOI 10.1002/2016JE005188
- 1972 Kalousová K, Sotin C, Choblet G, Tobie G, Grasset O (2018) Two-phase con-  
1973 vection in Ganymede’s high-pressure ice layer – implications for its geological  
1974 evolution. *Icarus* 299:133–147, DOI 10.1016/j.icarus.2017.07.018
- 1975 Kargel JS (1991) Brine volcanism and the interior structures of asteroids and icy  
1976 satellites. *Icarus* 94(2):368–390
- 1977 Kargel JS, Kaye JZ, Head III JW, Marion GM, Sassen R, Crowley JK, Prieto-  
1978 Ballesteros O, Grant SA, Hogenboom DL (2000) Europa’s crust and ocean:  
1979 origin, composition, and the prospects for life. *Icarus* 148(1):226–265
- 1980 Kattenhorn SA, Prockter LM (2014) Evidence for subduction in the ice shell of  
1981 Europa. *Nature Geosci* 7(10):762
- 1982 Kempf S, Horányi M, Hsu HW, Hill TW, Juhász A, Smith HT (2018) Saturn’s  
1983 diffuse E ring and its connection with Enceladus. In: *Enceladus and the Icy  
1984 Moons of Saturn*, University of Arizona Press, pp 195–210
- 1985 Kerswell RR (2002) Elliptical instability. *Annu Rev Fluid Mech* 34(1):83–113,  
1986 DOI 10.1146/annurev.fluid.34.081701.171829
- 1987 Kerswell RR, Malkus WVR (1998) Tidal instability as the source for Io’s magnetic  
1988 signature. *Geophys Res Lett* 25(5):603–606
- 1989 Khawaja N, Postberg F, Hillier J, Klenner F, Kempf S, Nölle L, Reviol R, Srama R  
1990 (2019) Low mass organic compounds in Enceladean ice grains. *Monthly Notices  
1991 of the Royal Astronomical Society* in review
- 1992 Khurana KK, Kivelson MG, Stevenson DJ, Schubert G, Russell CT, Walker RJ,  
1993 Polanskey C (1998) Induced magnetic fields as evidence for subsurface oceans  
1994 in Europa and Callisto. *Nature* 395:777–780
- 1995 Khurana KK, Kivelson MG, Russell CT (2002) Searching for liquid water in Eu-  
1996 ropa by using surface observatories. *Astrobiology* 2(1):93–103
- 1997 Kimball PW, Clark EB, Scully M, Richmond K, Flesher C, Lindzey LE, Harman  
1998 J, Huffstutler K, Lawrence J, Lelievre S, et al (2018) The ARTEMIS under-ice  
1999 AUV docking system. *J Field Robotics* 35(2):299–308
- 2000 Kinnon WBM, Melosh H (1980) Evolution of planetary lithospheres: Evidence  
2001 from multiringed structures on Ganymede and Callisto. *Icarus* 44(2):454–471,  
2002 DOI 10.1016/0019-1035(80)90037-8

- 2003 Kite ES, Rubin AM (2016) Sustained eruptions on Enceladus explained by turbulent  
2004 dissipation in tiger stripes. *Proceedings of the National Academy of Sciences*  
2005 113(15):3972–3975, DOI 10.1073/pnas.1520507113
- 2006 Kivelson MG, Khurana KK, Volwerk M (2002) The permanent and inductive  
2007 magnetic moments of Ganymede. *Icarus* 157:507–522
- 2008 Klaser MW, Gross J, Tindall S, Schlichte RW, Potter CJ (2019) Europa’s ice  
2009 tectonics: New insights from physical wax experiments with implications for  
2010 subduction initiation and global resurfacing processes. *Icarus* 321:593–607
- 2011 Kovacs A, Gow AJ (1975) Brine infiltration in the McMurdo Ice Shelf, McMurdo  
2012 Sound, Antarctica. *J Geophys Res* 80(15):1957–1661
- 2013 Kraus RG, Senft LE, Stewart ST (2011) Impacts onto H<sub>2</sub>O ice: Scaling laws  
2014 for melting, vaporization, excavation, and final crater size. *Icarus* 214:724–738,  
2015 DOI 10.1016/j.icarus.2011.05.016
- 2016 Kuskov OL, Kronrod VA (2001) Core sizes and internal structure of Earth’s and  
2017 Jupiter’s satellites. *Icarus* 151(2):204–227
- 2018 Kvorka J, Cadek C, Tobie G, Choblet G (2018) Does Titan’s long-wavelength  
2019 topography contain information about subsurface ocean dynamics? *Icarus*  
2020 310:149–164
- 2021 Le Bars M, Cebon D, Le Gal P (2015) Flows driven by libration, precession, and  
2022 tides. *Annu Rev Fluid Mech* 47:163–193
- 2023 Lee CM, Rudnick DL (2018) Underwater gliders. In: *Observing the Oceans in Real*  
2024 *Time*, Springer, pp 123–139
- 2025 Lefevre A, Tobie G, Choblet G, Čadek O (2014) Structure and dynamics of Ti-  
2026 tan’s outer icy shell constrained from Cassini data. *Icarus* 237:16 – 28, DOI  
2027 10.1016/j.icarus.2014.04.006
- 2028 Lemasquerier D, Grannan AM, Vidal J, Cébron D, Favier B, Le Bars M, Aurnou  
2029 JM (2017) Libration-driven flows in ellipsoidal shells. *J Geophys Res Planets*  
2030 122(9):1926–1950
- 2031 Lemmon EW, Huber ML, McLinden MO (2007) NIST Standard Reference  
2032 Database 23: Reference Fluid Thermodynamic and Transport Properties-  
2033 REFPROP, Version 8.0. National Institute of Standards and Technology, Stan-  
2034 dard Reference Data Program. Standard Reference Data Program, Gaithersburg
- 2035 Lewis EL, Perkin RG (1986) Ice pumps and their rates. *J Geophys Res* 91:11756–  
2036 11762
- 2037 Ligier N, Poulet F, Carter J, Brunetto R, Gourgeot F (2016) VLT/SINFONI  
2038 observations of Europa: new insights into the surface composition. *Astron J*  
2039 151(6):163, DOI 10.3847/0004-6256/151/6/163
- 2040 Liu Y, Peltier WR (2010) A carbon cycle coupled climate model of Neoproterozoic  
2041 glaciation: Influence of continental configuration on the formation of a “soft  
2042 snowball”. *J Geophys Res Atmospheres* 115(D17), DOI 10.1029/2009JD013082
- 2043 Longuet-Higgins MS (1968) The Eigenfunctions of Laplace’s Tidal Equations over  
2044 a Sphere. *Phil Trans R Soc A* 262(1132):511–607, DOI 10.1098/rsta.1968.0003
- 2045 Lowell RP, DuBose M (2005) Hydrothermal systems on Europa. *Geophys Res Lett*  
2046 32:L05202
- 2047 Luan J (2019) Titan’s dynamic love number implies stably-stratified ocean. arXiv  
2048 preprint arXiv:190503802
- 2049 Lucchitta BK (1980) Grooved terrain on Ganymede. *Icarus* 44(2):481–501
- 2050 Lucchitta BK, Soderblom LA (1982) The geology of Europa. In: Morrison D (ed)  
2051 *Satellites of Jupiter*, University of Arizona Press, Tucson, pp 521–555

- 2052 Lunine JI, Artemieva N, Tobie G (2010) Impact Cratering on Titan: Hydrocarbons  
2053 Versus Water. In: Lunar and Planetary Science Conference, Lunar and Planetary  
2054 Science Conference, vol 41, p 1537
- 2055 Lunine JI, Coustenis A, Mitri G, Tobie G, Tosi F (2018) Future exploration of  
2056 Enceladus and other saturnian moons. In: Enceladus and the Icy Moons of Sat-  
2057 urn, University of Arizona Press Tucson, pp 453–468
- 2058 Lunine JI, Cable ML, Hörst SM, Rahm M (2019) The Astrobiology of Titan. In:  
2059 Meadows VS, Arney G, DesMarais D, Schmidt BE (eds) Planetary Astrobiology,  
2060 University of Arizona Press Tucson (in production)
- 2061 Maas LRM (2005) Wave attractors: linear yet nonlinear. *Int J Bifurc Chaos*  
2062 15(09):2757–2782
- 2063 Magee BA, Waite JH (2017) Neutral gas composition of Enceladus’ plume – Model  
2064 parameter insights from Cassini-INMS. In: Lunar and Planetary Institute Sci-  
2065 ence Conference Abstracts, vol 48, p 2974
- 2066 Malkus WVR (1994) Energy sources for planetary dynamos. In: Proctor, M R E  
2067 and Gilbert, AD (ed) Lectures on Solar and Planetary Dynamos, Cambridge:  
2068 Cambridge University Press
- 2069 Manga M, Michaut C (2017) Formation of lenticulae on Europa by saucer-shaped  
2070 sills. *Icarus* 286:261 – 269, DOI 10.1016/j.icarus.2016.10.009
- 2071 Manga M, Sinton A (2004) Formation of bands and ridges on europa by cyclic  
2072 deformation: Insights from analogue wax experiments. *Journal of Geophysical*  
2073 *Research: Planets* 109(E9), DOI 10.1029/2004JE002249
- 2074 Manga M, Wang CY (2007) Pressurized oceans and the eruption of liquid water on  
2075 Europa and Enceladus. *Geophys Res Lett* 34(7), DOI 10.1029/2007GL029297
- 2076 Matsuyama I (2014) Tidal dissipation in the oceans of icy satellites. *Icarus* 242:11–  
2077 18
- 2078 Matsuyama I, Beuthe M, Hay HCFC, Nimmo F, Kamata S (2018) Ocean tidal  
2079 heating in icy satellites with solid shells. *Icarus* 312:208–230
- 2080 McCord TB, Teeter G, Hansen GB, Sieger MT, Orlando TM (2002) Brines ex-  
2081 posed to Europa surface conditions. *J Geophys Res Planets* 107(E1), DOI  
2082 10.1029/2000JE001453
- 2083 McDougall TJ, Barker PM (2011) Getting started with TEOS-10 and the Gibbs  
2084 Seawater (GSW) oceanographic toolbox. *SCOR/IAPSO WG* 127:1–28
- 2085 McKinnon WB (1999) Convective instability in Europa’s floating ice shell. *Geo-*  
2086 *phys Res Lett* 26:951–954
- 2087 McKinnon WB (2006) On convection in ice I shells of outer solar system bod-  
2088 ies, with detailed application to Callisto. *Icarus* 183(2):435 – 450, DOI  
2089 10.1016/j.icarus.2006.03.004
- 2090 McKinnon WB (2015) Effect of Enceladus’s rapid synchronous spin on interpre-  
2091 tation of Cassini gravity. *Geophys Res Lett* 42(7):2137–2143
- 2092 McKinnon WB, Zolensky ME (2003) Sulfate content of Europa’s ocean and shell:  
2093 Evolutionary considerations and some geological and astrobiological implica-  
2094 tions. *Astrobiology* 3(4):879–897
- 2095 Meister M, Dichek D, Spears A, Hurwitz B, Ramey C, Lawrence J, Philleo K,  
2096 Lutz J, Lawrence J, Schmidt BE (2018) Icefin: Redesign and 2017 Antarctic  
2097 Field Deployment. In: OCEANS 2018 MTS/IEEE Charleston, IEEE, pp 1–5
- 2098 Melosh HJ (1989) Impact cratering : a geologic process. New York : Oxford Uni-  
2099 versity Press ; Oxford : Clarendon Press

- 2100 Melosh HJ, Ekholm AG, Showman AP, Lorenz RD (2004) The temperature of  
2101 Europa's subsurface water ocean. *Icarus* 168:498–502
- 2102 Mével L, Mercier E (2007) Large-scale doming on Europa: A model of forma-  
2103 tion of thera macula. *Planetary and Space Science* 55(7):915 – 927, DOI  
2104 <https://doi.org/10.1016/j.pss.2006.12.001>
- 2105 Michaut C, Manga M (2014) Domes, pits, and small chaos on Europa produced by  
2106 water sills. *J Geophys Res Planets* 119(3):550–573, DOI 10.1002/2013JE004558
- 2107 Mikucki JA, Lee PA, Ghosh D, Purcell AM, Mitchell AC, Mankoff KD, Fisher  
2108 AT, Tulaczyk S, Carter SP, Siegfried MR, et al (2016) Subglacial Lake Whillans  
2109 microbial biogeochemistry: a synthesis of current knowledge. *Phil Trans R Soc*  
2110 *A* 374(2059):20140290
- 2111 Miles JW (1974) On Laplace's tidal equations. *J Fluid Mech* 66(2):241–260, DOI  
2112 10.1017/S0022112074000176
- 2113 Miller KE, Glein CR, Waite JH, Bolton SJ (2019) Using D/H ratio of water and  
2114 volatile organics to constrain thermogenic processes inside ice-rock bodies. *Lunar*  
2115 *and Planetary Science Conference* 50
- 2116 Mitri G, Showman AP (2005) Convective-conductive transitions and sensitivity of  
2117 a convecting ice shell to perturbations in heat flux and tidal-heating rate: Impli-  
2118 cations for Europa. *Icarus* 177(2):447 – 460, DOI 10.1016/j.icarus.2005.03.019
- 2119 Mitri G, Bland MT, Showman AP, Radebaugh J, Stiles B, Lopes R, Lunine JI,  
2120 Pappalardo RT (2010) Mountains on Titan: Modeling and observations. *J Geo-*  
2121 *phys Res Planets* 115(E10)
- 2122 Mitri G, Meriggiola R, Hayes A, Lefevre A, Tobie G, Genova A, Lunine JI, Zebker  
2123 H (2014) Shape, topography, gravity anomalies and tidal deformation of Titan.  
2124 *Icarus* 236:169–177
- 2125 Monteux J, Collins GS, Tobie G, Choblet G (2016) Consequences of large impacts  
2126 on Enceladus' core shape. *Icarus* 264:300–310, DOI 10.1016/j.icarus.2015.09.034
- 2127 Moore JM, Schenk PM, Bruesch LS, Asphaug E, McKinnon WB (2004) Large  
2128 impact features on middle-sized icy satellites. *Icarus* 171(2):421 – 443, DOI  
2129 <https://doi.org/10.1016/j.icarus.2004.05.009>
- 2130 Moresi LN, Solomatov VS (1995) Numerical investigation of 2D convection  
2131 with extremely large viscosity variations. *Phys Fluids* 7(9):2154–2162, DOI  
2132 10.1063/1.868465
- 2133 Munk WH (1997) Once again: once again tidal friction. *Prog Oceanogr* 40(1):7 –  
2134 35, DOI 10.1016/S0079-6611(97)00021-9, tidal Science In Honour of David E.  
2135 Cartwright
- 2136 Murchie SL, Head JW (1989) Geologic map of the Philus Sulcus (Jg-4) quadrangle  
2137 of Ganymede. *U S Geol Surv Map I-1966*
- 2138 Murchie SL, Head JW, Plescia JB (1990) Tectonic and volcanic evolution of  
2139 dark terrain and its implications for the internal structure and evolution of  
2140 Ganymede. *J Geophys Res Solid Earth* 95(B7):10743–10768
- 2141 Murray AE, Kenig F, Fritsen CH, McKay CP, Cawley KM, Edwards R, Kuhn E,  
2142 McKnight DM, Ostrom NE, Peng V, et al (2012) Microbial life at- 13 C in the  
2143 brine of an ice-sealed Antarctic lake. *Proc Natl Acad Sci* 109(50):20626–20631
- 2144 Nagel K, Breuer D, Spohn T (2004) A model for the interior structure, evolution,  
2145 and differentiation of Callisto. *Icarus* 169(2):402–412
- 2146 Nakajima M, Ingersoll AP (2016) Controlled boiling on Enceladus:  
2147 1. Model of the vapor-driven jets. *Icarus* 272:309 – 318, DOI  
2148 <https://doi.org/10.1016/j.icarus.2016.02.027>

- 2149 Neubauer FM (1998) The sub-Alfvenic interaction of the Galilean satellites with  
2150 the Jovian magnetosphere. *J Geophys Res* 103(E9):19843–19866
- 2151 Niemann HB, Atreya SK, Bauer SJ, Carignan GR, Demick JE, Frost RL, Gautier  
2152 D, Haberman JA, Harpold DN, Hunten DM, Israel G, Lunine JI, Kasprzak WT,  
2153 Owen TC, Paulkovich M, Raulin F, Raaen E, Way SH (2005) The abundances of  
2154 constituents of Titan’s atmosphere from the GCMS instrument on the Huygens  
2155 probe. *Nature* 438:779–784, DOI 10.1038/nature04122
- 2156 Niemann HB, Atreya SK, Demick JE, Gautier D, Haberman JA, Harpold DN,  
2157 Kasprzak WT, Lunine JI, Owen TC, Raulin F (2010) Composition of Titan’s  
2158 lower atmosphere and simple surface volatiles as measured by the Cassini-  
2159 Huygens probe gas chromatograph mass spectrometer experiment. *J Geophys*  
2160 *Res Planets* 115(E12), DOI 10.1029/2010JE003659
- 2161 Nimmo F, Bills BG (2010) Shell thickness variations and the long-wavelength  
2162 topography of Titan. *Icarus* 208(2):896–904
- 2163 Nimmo F, Gaidos E (2002) Strike-slip motion and double ridge formation on Eu-  
2164 ropa. *J Geophys Res Planets* 107(E4)
- 2165 Nimmo F, Thomas PC, Pappalardo RT, Moore WB (2007) The global shape of  
2166 Europa: Constraints on lateral shell thickness variations. *Icarus* 191:183–192
- 2167 Nimmo F, Bills BG, Thomas PC (2011) Geophysical implications of the long-  
2168 wavelength topography of the saturnian satellites. *J Geophys Res Planets*  
2169 116(E11)
- 2170 Nimmo F, Porco C, Mitchell C (2014) Tidally modulated eruptions on enceladus:  
2171 Cassini iss observations and models. *The Astronomical Journal* 148(3):46
- 2172 Nimmo F, Barr AC, Běhouňková M, McKinnon WB (2018) The thermal and  
2173 orbital evolution of Enceladus: observational constraints and models. In: et al  
2174 PMS (ed) *Enceladus and the Icy Moons of Saturn*, University of Arizona Press,  
2175 pp 79–94
- 2176 Ogawa M (2014) Two-stage evolution of the Earth’s mantle inferred from  
2177 numerical simulation of coupled magmatism-mantle convection system with  
2178 tectonic plates. *J Geophys Res Solid Earth* 119(3):2462–2486, DOI  
2179 10.1002/2013JB010315
- 2180 Pappalardo RT, Sullivan RJ (1996) Evidence for Separation across a Gray Band on  
2181 Europa. *Icarus* 123(2):557 – 567, DOI <https://doi.org/10.1006/icar.1996.0178>
- 2182 Pappalardo RT, Head JW, Greeley R, Sullivan RJ, Pilcher C, Schubert G, Moore  
2183 WB, Carr MH, Moore JM, Belton MJS, Goldsby DL (1998) Geological evidence  
2184 for solid-state convection in Europa’s ice shell. *Nature* 391:365–368
- 2185 Pappalardo RT, Belton MJS, Breneman HH, Carr MH, Chapman CR, Collins  
2186 GC, Denk T, Fagents S, Geissler PE, Giese B, et al (1999) Does europa  
2187 have a subsurface ocean? evaluation of the geological evidence. *J Geophys Res*  
2188 104(E10):24015–24055
- 2189 Pappalardo RT, Collins GC, Head JW, Helfenstein P, McCord TB, Moore JM,  
2190 Prockter LM, Schenk PM, Spencer JR (2004) Geology of Ganymede. In: Bagenal  
2191 FD, Dowling TE, McKinnon WB (eds) *Jupiter*, Cambridge University Press.,  
2192 pp 363–396
- 2193 Pappalardo RT, Vance SD, Bagenal F, Bills BG, Blaney DL, Blankenship DD,  
2194 Brinckerhoff WB, Connerney JEP, Hand KP, Hoehler TM, et al (2013) Science  
2195 potential from a Europa lander. *Astrobiology* 13(8):740–773
- 2196 Paranicas C, Cooper JF, Garrett HB, Johnson RE, Sturmer SJ (2009) Europa’s  
2197 radiation environment and its effects on the surface. In: *Europa*, University of

- 2198 Arizona Press Tucson, pp 529–544
- 2199 Pasek MA, Greenberg R (2012) Acidification of Europa’s subsurface ocean as a  
2200 consequence of oxidant delivery. *Astrobiology* 12(2):151–159
- 2201 Patterson GW, Collins GC, Head JW, Pappalardo RT, Prockter LM, Lucchitta  
2202 BK, Kay JP (2010) Global geological mapping of Ganymede. *Icarus* 207(2):845–  
2203 867
- 2204 Patterson GW, Kattenhorn SA, Helfenstein P, Collins GC, Pappalardo RT (2018)  
2205 The geology of Enceladus. In: *Enceladus and the Icy Moons of Saturn*, University  
2206 of Arizona Press, pp 95–126
- 2207 Pauer M, Musiol S, Breuer D (2010) Gravity signals on Europa from silicate shell  
2208 density variations. *J Geophys Res Planets* 115(E12)
- 2209 Pedlosky J (1987) *Geophysical Fluid Dynamics*. Springer-Verlag, New York
- 2210 Porco C, DiNino D, Nimmo F (2014) How the geyzers, tidal stresses, and thermal  
2211 emission across the south polar terrain of Enceladus are related. *Astronomical*  
2212 *journal* 148, DOI 10.1088/0004-6256/148/3/45
- 2213 Porco CC, Helfenstein P, Thomas PC, Ingersoll AP, Wisdom J, West RA, Neukum  
2214 G, Denk T, Wagner R, Roatsch T, et al (2006) Cassini observes the active south  
2215 pole of Enceladus. *Science* 311(5766):1393–1401
- 2216 Postberg F, Kempf S, Schmidt J, Brilliantov N, Beinsen A, Abel B, Buck U, Srama  
2217 R (2009) Sodium salts in E-ring ice grains from an ocean below the surface of  
2218 Enceladus. *Nature* 459:1098–1101, DOI 10.1038/nature08046
- 2219 Postberg F, Schmidt J, Hillier J, Kempf SD, Srama R (2011) A salt-water reser-  
2220 voir as the source of a compositionally stratified plume on Enceladus. *Nature*  
2221 474(7353):620
- 2222 Postberg F, Clark RN, Hansen CJ, Coates AJ, Ore CMD, Scipioni F, Hedman MM,  
2223 Waite JH (2018a) Plume and surface composition of Enceladus. In: *Enceladus*  
2224 *and the Icy Moons of Saturn*, University of Arizona Press, pp 129–162
- 2225 Postberg F, Khawaja N, Abel B, Choblet G, Glein CR, Gudipati MS, Henderson  
2226 BL, Hsu HW, Kempf S, Klenner F, Moragas-Klostermeyer G, Magee B, Nölle  
2227 L, Perry M, Reviol R, Schmidt J, Srama R, Stolz F, Tobie G, Trieloff M, Waite  
2228 JH (2018b) Macromolecular organic compounds from the depths of Enceladus.  
2229 *Nature* 558:564–568, DOI 10.1038/s41586-018-0246-4
- 2230 Priscu JC, Christner BC (2004) Earth’s icy biosphere. In: *Microbial diversity and*  
2231 *bioprospecting*, American Society of Microbiology, pp 130–145
- 2232 Priscu JC, Fritsen CH, Adams EE, Giovannoni SJ, Paerl HW, McKay CP, Doran  
2233 PT, Gordon DA, Lanoil BD, Pinckney JL (1998) Perennial Antarctic lake ice:  
2234 an oasis for life in a polar desert. *Science* 280(5372):2095–2098
- 2235 Prockter LM, Patterson GW (2009) Morphology and evolution of Europa’s ridges  
2236 and bands. In: Pappalardo RT, McKinnon WB, Khurana KK (eds) *Europa*,  
2237 Univ. Ariz. Press, pp 237–258
- 2238 Prockter LM, Head JW, Pappalardo RT, Senske DA, Neukum G, Wagner R, Wolf  
2239 U, Oberst J, Giese B, Moore JM, et al (1998) Dark terrain on Ganymede:  
2240 Geological mapping and interpretation of Galileo Regio at high resolution. *Icarus*  
2241 135(1):317–344
- 2242 Prockter LM, Figueredo PH, Pappalardo RT, Head JW, Collins GC (2000) Ge-  
2243 ology and mapping of dark terrain on Ganymede and implications for grooved  
2244 terrain formation. *J Geophys Res Planets* 105(E9):22519–22540
- 2245 Prockter LM, Head III JW, Pappalardo RT, Sullivan RJ, Clifton AE, Giese B,  
2246 Wagner R, Neukum G (2002) Morphology of European bands at high resolu-

- 2247 tion: A mid-ocean ridge-type rift mechanism. *Journal of Geophysical Research:*  
2248 *Planets* 107(E5):4-1-4-26, DOI 10.1029/2000JE001458
- 2249 Quick LC, Marsh BD (2016) Heat transfer of ascending cryomagma on Europa. *J*  
2250 *Volcanol Geoth Res* 319:66 – 77, DOI 10.1016/j.jvolgeores.2016.03.018
- 2251 Quick LC, Glaze L, Baloga SM (2017) Cryovolcanic emplacement of domes on  
2252 Europa. *Icarus* 284:477 – 488, DOI 10.1016/j.icarus.2016.06.029
- 2253 Rathbun JA, Musser GSJ, Squyres SW (1998) Ice diapirs on Europa: Implications  
2254 for liquid water. *Geophys Res Lett* 25:4157–4160
- 2255 Requier J, Trinh A, Triana SA, Dehant V (2019) Internal energy dissipation in  
2256 Enceladus’s ocean from tides and libration and the role of inertial waves. arXiv  
2257 e-prints arXiv:1904.02487, 1904.02487
- 2258 Reynolds RT, Squyres SW, Colburn DS, McKay CP (1983) On the habitability of  
2259 Europa. *Icarus* 56(2):246–254
- 2260 Reynolds RT, McKay CP, Kasting JF (1987) Europa, tidally heated oceans, and  
2261 habitable zones around giant planets. *Adv Space Res* 7(5):125–132
- 2262 Rieutord M (2004) Evolution of rotation in binaries: physical processes. In:  
2263 *Symposium-International Astronomical Union, Cambridge University Press, vol*  
2264 *215, pp 394–403*
- 2265 Rieutord M, Georgeot B, Valdettaro L (2011) Inertial waves in a rotating spherical  
2266 shell: attractors and asymptotic spectrum. *J Fluid Mech* 435:103–144
- 2267 Roatsch T, Jaumann R, Stephan K, Thomas PC (2009) Cartographic mapping of  
2268 the icy satellites using ISS and VIMS data. In: *Saturn from Cassini-Huygens,*  
2269 *Springer, pp 763–781*
- 2270 Roberts JH (2015) The fluffy core of Enceladus. *Icarus* 258:54–66
- 2271 Roberts JH, Nimmo F (2008) Tidal heating and the long-term stability of a sub-  
2272 surface ocean on Enceladus. *Icarus* 194(2):675–689
- 2273 Roth L, Saur J, Retherford KD, Strobel DF, Feldman PD, McGrath MA, Nimmo  
2274 F (2014) Transient water vapor at Europa’s south pole. *Science* 343(6167):171–  
2275 174, DOI 10.1126/science.1247051
- 2276 Rovira-Navarro M, Rieutord M, Gerkema T, Maas LR, van der Wal W, Vermeersen  
2277 B (2019) Do tidally-generated inertial waves heat the subsurface oceans of Eu-  
2278 ropa and Enceladus? *Icarus* 321:126–140
- 2279 Rückriemen T, Breuer D, Spohn T (2018) Top-down freezing in a Fe–FeS core and  
2280 Ganymede’s present-day magnetic field. *Icarus* 307:172–196
- 2281 Russell MJ, Murray AE, Hand KP (2017) The possible emergence of life and  
2282 differentiation of a shallow biosphere on irradiated icy worlds: the example of  
2283 Europa. *Astrobiology* 17(12):1265–1273
- 2284 Saur J, Duling S, Roth L, Jia X, Strobel DF, Feldman PD, Christensen UR,  
2285 Retherford KD, McGrath MA, Musacchio F, et al (2015) The search for a sub-  
2286 surface ocean in Ganymede with Hubble Space Telescope observations of its  
2287 auroral ovals. *J Geophys Res* 120(3):1715–1737
- 2288 Schenk PM, McKinnon WB (1989) Fault offsets and lateral crustal movement  
2289 on Europa: Evidence for a mobile ice shell. *Icarus* 79(1):75 – 100, DOI  
2290 [https://doi.org/10.1016/0019-1035\(89\)90109-7](https://doi.org/10.1016/0019-1035(89)90109-7)
- 2291 Schenk PM, Moore JM (1995) Volcanic constructs on Ganymede and Enceladus:  
2292 Topographic evidence from stereo images and photogrammetry. *J Geophys Res*  
2293 *Planets* 100(E9):19009–19022
- 2294 Schenk PM, Turtle EP (2009) Europa’s Impact Craters: Probes of the Icy Shell.  
2295 In: Pappalardo RT, McKinnon WB, Khurana KK (eds) *Europa, University of*

- 2296 Arizona Press, Tucson, pp 181–198
- 2297 Schenk PM, McKinnon WB, Gwynn D, Moore JM (2001) Flooding of Ganymede’s  
2298 bright terrains by low-viscosity water-ice lavas. *Nature* 410(6824):57
- 2299 Schenk PM, Chapman CR, Zahnle K, Moore JM (2004) Ages and interiors: The  
2300 cratering record of the Galilean satellites. In: *Jupiter: The planet, satellites and  
2301 magnetosphere*, vol 2, Cambridge University Press Cambridge, UK, p 427
- 2302 Schilling N, Neubauer FM, Saur J (2007) Time-varying interaction of Europa  
2303 with the Jovian magnetosphere: Constraints on the conductivity of Europa’s  
2304 subsurface ocean. *Icarus* 192:41–55
- 2305 Schmidt BE (2019) The Astrobiology of Europa and the Jovian Moons. In: Mead-  
2306 ows VS, Arney G, DesMarais D, Schmidt BE (eds) *Planetary Astrobiology*,  
2307 University of Arizona Press Tucson (in production)
- 2308 Schmidt BE, Blankenship DD, Patterson GW, Schenk PM (2011) Active formation  
2309 of chaos terrain over shallow subsurface water on Europa. *Nature* 479:502–505
- 2310 Schmidt J, Brilliantov N, Spahn F, Kempf S (2008) Slow dust in enceladus’ plume  
2311 from condensation and wall collisions in tiger stripe fractures. *Nature* 451:685–  
2312 688, DOI 10.1038/nature06491
- 2313 Schmitt RW (1994) Double diffusion in oceanography. *Annu Rev Fluid Mech*  
2314 26(1):255–285
- 2315 Schubert G, Anderson JD, Spohn T, McKinnon WB (2004) Interior composition,  
2316 structure and dynamics of the Galilean satellites. *Jupiter: The Planet, Satellites  
2317 and Magnetosphere* pp 281–306
- 2318 Scipioni F, Schenk P, Tosi F, D’Aversa E, Clark R, Combe JP, Ore CD (2017)  
2319 Deciphering sub-micron ice particles on Enceladus surface. *Icarus* 290:183 – 200,  
2320 DOI <https://doi.org/10.1016/j.icarus.2017.02.012>
- 2321 Senft LE, Stewart ST (2011) Modeling the morphological diversity of impact  
2322 craters on icy satellites. *Icarus* 214:67–81, DOI 10.1016/j.icarus.2011.04.015
- 2323 Seufert M, Saur J, Neubauer FM (2011) Multi-frequency electromagnetic sounding  
2324 of the Galilean moons. *Icarus* 214(2):477–494
- 2325 Shoemaker EM, Lucchitta BK, Wilhelms DE, Plescia JB, Squyres SW (1982) The  
2326 geology of Ganymede. In: Morrison D (ed) *Satellites of Jupiter*, University of  
2327 Arizona Press Tucson, pp 435–520
- 2328 Showman AP, Malhotra R (1997) Tidal Evolution into the Laplace Reso-  
2329 nance and the Resurfacing of Ganymede. *Icarus* 127(1):93 – 111, DOI  
2330 <https://doi.org/10.1006/icar.1996.5669>
- 2331 Smrekar SE, Lognonné P, Spohn T, Banerdt WB, Breuer D, Christensen U, Dehant  
2332 V, Drilleau M, Folkner W, Fuji N, et al (2018) Pre-mission InSights on the  
2333 interior of Mars. *Space Sci Rev* 215(1), DOI 10.1007/s11214-018-0563-9
- 2334 Soderlund KM (2019) Ocean dynamics of outer solar system satellites. arXiv p  
2335 <http://arxiv.org/abs/1901.04093>
- 2336 Soderlund KM, Heimpel MH, King EM, Aurnou JM (2013) Turbulent models of  
2337 ice giant internal dynamics: Dynamos, heat transfer, and zonal flows. *Icarus*  
2338 224:97–113
- 2339 Soderlund KM, Schmidt BE, Wicht J, Blankenship DD (2014) Ocean-driven heat-  
2340 ing of Europa’s icy shell at low latitudes. *Nature Geosci* 7:16–19
- 2341 Sohl F, Spohn T, Breuer D, Nagel K (2002) Implications from galileo observations  
2342 on the interior structure and chemistry of the galilean satellites. *Icarus* 157:104–  
2343 119

- 2344 Sohl F, Hussmann H, Schwentker B, Spohn T, Lorenz RD (2003) Interior structure  
2345 models and tidal Love numbers of Titan. *J Geophys Res Planets* 108(E12)
- 2346 Sotin C, Head JW, Tobie G (2002) Tidal heating of upwelling thermal plumes  
2347 and the origin of lenticulae and chaos melting. *Geophys Res Lett* 29(8):1233,  
2348 doi:10.1029/2001GL013884
- 2349 Sotin C, Tobie G, Wahr J, McKinnon WB (2009) Tides and tidal heating on  
2350 Europa. In: Pappalardo RT, McKinnon WB, Khurana KK (eds) *Europa*, Tucson:  
2351 University of Arizona Press
- 2352 Souček O, Hron J, Běhouňková M, Čadek O (2016) Effect of the tiger stripes  
2353 on the deformation of Saturn's moon Enceladus. *Geophysical Research Letters*  
2354 43(14):7417–7423, DOI 10.1002/2016GL069415
- 2355 Souček O, Běhouňková M, Čadek O, Hron J, Tobie G, Choblet G (2019) Tidal  
2356 dissipation in Enceladus' uneven, fractured ice shell. *Icarus* 328:218 – 231, DOI  
2357 <https://doi.org/10.1016/j.icarus.2019.02.012>
- 2358 Southworth BS, Kempf S, Schmidt J (2015) Modeling Europa's dust plumes. *Geo-*  
2359 *phys Res Lett* 42(24):10,541–10,548, DOI 10.1002/2015GL066502
- 2360 Southworth BS, Kempf S, Spitale J (2019) Surface deposition of the Ence-  
2361 ladus plume and the zenith angle of emissions. *Icarus* 319:33 – 42, DOI  
2362 <https://doi.org/10.1016/j.icarus.2018.08.024>
- 2363 Spahn F, Schmidt J, Albers N, Hörning M, Makuch M, Seiß M, Kempf S, Srama  
2364 R, Dikarev V, Helfert S, Moragas-Klostermeyer G, Krivov AV, Sremčević M,  
2365 Tuzzolino AJ, Economou T, Grün E (2006) Cassini Dust Measurements at Ence-  
2366 ladus and Implications for the Origin of the E Ring. *Science* 311(5766):1416–  
2367 1418, DOI 10.1126/science.1121375
- 2368 Sparks WB, Hand KP, McGrath MA, Bergeron E, Cracraft M, Deustua SE  
2369 (2016) Probing for evidence of plumes on Europa with HST/STIS. *Astrophys J*  
2370 829(2):121
- 2371 Sparks WB, Schmidt BE, McGrath MA, Hand KP, Spencer JR, Cracraft  
2372 M, Deustua SE (2017) Active cryovolcanism on Europa? *Astrophys J Lett*  
2373 839(2):L18
- 2374 Spaun NA, Head JW, Collins GC, Prockter LM, Pappalardo RT (1998) Conamara  
2375 Chaos Region, Europa: Reconstruction of mobile polygonal ice blocks. *Geophys*  
2376 *Res Lett* 25(23):4277–4280
- 2377 Spaun NA, Head JW, Pappalardo RT, Team GS, et al (2001) Scalloped depressions  
2378 on Ganymede from Galileo (G28) very high resolution imaging. In: *Lunar and*  
2379 *Planetary Science Conference*, vol 32
- 2380 Spencer JR, Nimmo F, Ingersoll AP, Hurford TA, Kite ES, Rhoden AR, Schmidt  
2381 J, Howett CJA (2018) Plume origins and plumbing: From ocean to surface. In:  
2382 *Enceladus and the Icy Moons of Saturn*, University of Arizona Press, pp 163–174
- 2383 Spitale JN, Hurford TA, Rhoden AR, Berkson EE, Platts SS (2015) Cur-  
2384 tain eruptions from Enceladus south-polar terrain. *Nature* 521:57–60, DOI  
2385 10.1038/nature14368
- 2386 Spohn T, Schubert G (2003) Oceans in the icy Galilean satellites of Jupiter? *Icarus*  
2387 161(2):456–467
- 2388 Steinbrügge G, Schroeder DM, Haynes MS, Hussmann H, Grima C, Blankenship  
2389 DD (2018) Assessing the potential for measuring Europa's tidal Love number  
2390 h2 using radar sounder and topographic imager data. *Earth Planet Sci Lett*  
2391 482:334–341

- 2392 Sullivan R, Greeley R, Homan K, Klemaszewski J, Belton MJS, Carr MH, Chap-  
2393 man CR, Tufts R, Head JW, Pappalardo R, Moore J, Thomas P, the Galileo  
2394 Imaging Team (1998) Episodic plate separation and fracture infill on the surface  
2395 of Europa. *Nature* 391:371–373, DOI 10.1038/34874
- 2396 Tajeddine R, Soderlund KM, Thomas PC, Helfenstein P, Hedman MM, Burns  
2397 JA, Schenk PM (2017) True polar wander of Enceladus from topographic data.  
2398 *Icarus* 295:46–60
- 2399 Taubner RS, et al (2019) Experimental and simulation efforts in the astrobiological  
2400 exploration of exooceans. *Space Sci Rev*
- 2401 Teolis BD, Perry ME, Hansen CJ, Waite JH, Porco CC, Spencer JR, Howett CJA  
2402 (2017) Enceladus plume structure and time variability: Comparison of cassini  
2403 observations. *Astrobiology* 17(9):926–940, DOI 10.1089/ast.2017.1647
- 2404 Thomas PC, Burns JA, Helfenstein P, Squyres S, Veverka J, Porco C, Turtle EP,  
2405 McEwen A, Denk T, Giese B, et al (2007) Shapes of the saturnian icy satellites  
2406 and their significance. *Icarus* 190(2):573–584
- 2407 Thomas PC, Tajeddine R, Tiscareno MS, Burns JA, Joseph J, Loredó TJ, Helfen-  
2408 stein P, Porco CC (2016) Enceladus’s measured physical libration requires a  
2409 global subsurface ocean. *Icarus* 264:37–47
- 2410 Thomson RE, Delaney JR (2001) Evidence for a weakly stratified European ocean  
2411 sustained by seafloor heat flux. *J Geophys Res* 106:12355–12365
- 2412 Tobie G, Choblet G, Sotin C (2003) Tidally heated convection: Con-  
2413 straints on Europa’s ice shell thickness. *J Geophys Res* 108(E11):5124,  
2414 doi:10.1029/2003JE002099
- 2415 Tobie G, Grasset O, Lunine JI, Mocquet A, Sotin C (2005) Titan’s internal struc-  
2416 ture inferred from a coupled thermal-orbital model. *Icarus* 175(2):496–502, DOI  
2417 10.1016/j.icarus.2004.12.007
- 2418 Tobie G, Lunine JI, Sotin C (2006) Episodic outgassing as the origin of atmospheric  
2419 methane on Titan. *Nature* 440(7080):61
- 2420 Tobie G, Čadež O, Sotin C (2008) Solid tidal friction above a liquid water reservoir  
2421 as the origin of the south pole hotspot on Enceladus. *Icarus* 196(2):642–652
- 2422 Travis BJ, Palguta J, Schubert G (2012) A whole-moon thermal history model of  
2423 Europa: Impact of hydrothermal circulation and salt transport. *Icarus* 218:1006–  
2424 1019
- 2425 Trumbo SK, Brown M, Hand KP (2019) Sodium chloride on the surface of Europa.  
2426 *Science Advances* 5(6):eaaw7123
- 2427 Tufts B, Greenberg R, Hoppa G, Geissler P (2000) Lithospheric Dilation on Eu-  
2428 ropa. *Icarus* 146(1):75 – 97, DOI <https://doi.org/10.1006/icar.2000.6369>
- 2429 Turtle EP (1998) Finite-element modeling of large impact craters: Implications for  
2430 the size of the Vredefort structure and the formation of multiple ring craters.  
2431 Ph.D. dissertation. Univ. of Arizona, Tucson
- 2432 Turtle EP, Pierazzo E (2001) Thickness of a European ice shell from impact crater  
2433 simulations. *Science* 294:1326–1328, DOI 10.1126/science.1062492
- 2434 Turtle EP, Melosh HJ, Phillips CB (1998) Tectonic modeling of the formation of  
2435 European ridges. In: *EOS Trans. AGU*, vol 79, p F541
- 2436 Turtle EP, Barnes JW, Trainer MG, Lorenz RD, MacKenzie SM, Hibbard KE  
2437 (2017) Exploring Titan’s prebiotic organic chemistry and habitability. *LPI Con-*  
2438 *tributions* p 1958
- 2439 Tyler RH (2008) Strong ocean tidal flow and heating on moons of the outer planets.  
2440 *Nature* 456:770–773

- 2441 Tyler RH (2009) Ocean tides heat Enceladus. *Geophys Res Lett* 36(15), DOI  
2442 10.1029/2009GL038300, L15205
- 2443 Tyler RH (2014) Comparative estimates of the heat generated by ocean tides on  
2444 icy satellites in the outer Solar System. *Icarus* 243(Supplement C):358 – 385,  
2445 DOI 10.1016/j.icarus.2014.08.037
- 2446 Van Hoolst T, Baland RM, Trinh A (2016) The diurnal libration and interior  
2447 structure of Enceladus. *Icarus* 277:311–318
- 2448 Vance S, Brown JM (2005) Layering and double-diffusion style convection in Eu-  
2449 ropa’s ocean. *Icarus* 177:506–514
- 2450 Vance S, Brown JM (2013) Thermodynamic properties of aqueous MgSO<sub>4</sub> to 800  
2451 MPa at temperatures from -20 to 100 °C and concentrations to 2.5 mol kg<sup>-1</sup>  
2452 from sound speeds, with applications to icy world oceans. *Geochem Cosmochim*  
2453 *Acta* 110:176–189
- 2454 Vance S, Goodman JC (2009) Oceanography of an ice-covered moon. In: Pappalardo RT, McKinnon WB, Khurana KK (eds) *Europa*, Tucson: University of  
2455 Arizona Press, pp 459–482
- 2456 Vance S, Bouffard M, Choukroun M, Sotin C (2014) Ganymede’s internal structure  
2457 including thermodynamics of magnesium sulfate oceans in contact with ice.  
2458 *Planet Space Sci* 96:72–70
- 2459 Vance S, Panning MP, Stahler S, Cammarano F, Bills BG, Tobie G, Kamata S,  
2460 Kedar S, Sotin C, Pike WT, Lorenz RD, Huang HH, Jackson JM, Banerdt B  
2461 (2018a) Geophysical investigations of habitability in ice-covered ocean worlds.  
2462 *J Geophys Res* 123:180–205
- 2463 Vance SD, Goodman JC (2013) The structure and evolution of Europa’s ocean  
2464 and ice shell in the presence of aqueous MgSO<sub>4</sub>. *LPI Contributions* 1719:1877
- 2465 Vance SD, Harnmeijer J, Kimura J, Hussmann H, DeMartin B, Brown JM (2007)  
2466 Hydrothermal systems in small ocean planets. *Astrobiology* 7(6):987–1005
- 2467 Vance SD, Hand KP, Pappalardo RT (2016) Geophysical controls of chemical  
2468 disequilibria in Europa. *Geophys Res Lett* 43(10):4871–4879
- 2469 Vance SD, Kedar S, Panning MP, Stähler SC, Bills BG, Lorenz RD, Huang HH,  
2470 Pike WT, Castillo JC, Lognonné P, et al (2018b) Vital signs: Seismology of icy  
2471 ocean worlds. *Astrobiology* 18(1):37–53, DOI 10.1089/ast.2016.1612
- 2472 Vance SD, Barge LM, Cardoso SSS, Cartwright JHE (2019) Self-assembling ice  
2473 membranes on Europa: Brinicle properties, field examples, and possible energetic  
2474 systems in icy ocean worlds. *Astrobiology* 19(5):685–695
- 2475 Verma AK, Margot JL (2018) Expected precision of Europa Clipper gravity mea-  
2476 surements. *Icarus* 314:35–49
- 2477 Vu TH, Hodyss R, Choukroun M, Johnson PV (2016) Chemistry of frozen sodium-  
2478 magnesium-sulfate-chloride brines: implications for surface expression of Eu-  
2479 ropa’s ocean composition. *Astrophys J Lett* 816(2):L26
- 2480 Waite JH, Niemann H, Yelle RV, Kasprzak WT, Cravens TE, Luhmann JG, Mc-  
2481 Nutt RL, Ip WH, Gell D, De La Haye V, Müller-Wodarg I, Magee B, Borggren  
2482 N, Ledvina S, Fletcher G, Walter E, Miller R, Scherer S, Thorpe R, Xu J, Block  
2483 B, Arnett K (2005) Ion neutral mass spectrometer results from the first flyby  
2484 of Titan. *Science* 308(5724):982–986, DOI 10.1126/science.1110652
- 2485 Waite JH, Combi MR, Ip WH, Cravens TE, McNutt RL, Kasprzak WT, Yelle  
2486 RV, Luhmann JG, Niemann HB, Gell D, Magee BA (2006) Cassini ion and  
2487 neutral mass spectrometer: Enceladus plume composition and structure. *Science*  
2488 311(5766):1419–1422
- 2489

- 2490 Waite JH, Lewis WS, Magee BA, Lunine JI, McKinnon WB, Glein CR, Mousis  
2491 O, et al (2009) Liquid water on Enceladus from observations of ammonia and 40  
2492 ar in the plume. *Nature* 460(7254):487
- 2493 Waite JH, Glein CR, Perryman RS, Teolis BD, Magee BA, Miller G, Grimes J,  
2494 Perry ME, Miller KE, Bouquet A, Lunine JI, Brockwell T, Bolton SJ (2017)  
2495 Cassini finds molecular hydrogen in the Enceladus plume: Evidence for hy-  
2496 drothermal processes. *Science* 356(6334):155–159, DOI 10.1126/science.aai8703
- 2497 Walker CC, Schmidt BE (2015) Ice collapse over trapped water bod-  
2498 ies on Enceladus and Europa. *Geophys Res Lett* 42(3):712–719, DOI  
2499 10.1002/2014GL062405
- 2500 Warren SG, Brandt RE, Grenfell TC, McKay CP (2002) Snowball Earth: Ice  
2501 thickness on the tropical ocean. *J Geophys Res* 107(C10):3167
- 2502 Weertman J (1957) On the sliding of glaciers. *J Glaciol* 3(21):33–38
- 2503 Weller MB, Fuchs L, Becker TW, Soderlund KM (2019) Convection in thin shells  
2504 of icy satellites: Effects of latitudinal surface temperature variations. *J Geophys*  
2505 *Res Planets* doi: 10.1029/2018JE005799
- 2506 Wilson A, Kerswell RR (2018) Can libration maintain Enceladus’s ocean? *Earth*  
2507 *Planet Sci Lett* 500:41 – 46, DOI 10.1016/j.epsl.2018.08.012
- 2508 Wilson EH, Atreya SK (2000) Sensitivity studies of methane photolysis and its  
2509 impact on hydrocarbon chemistry in the atmosphere of Titan. *J Geophys Res*  
2510 *Planets* 105(E8):20263–20273, DOI 10.1029/1999JE001221
- 2511 Wilson TW, Ladino LA, Alpert PA, Breckels MN, Brooks IM, Browse J, Burrows  
2512 SM, Carslaw KS, Huffman JA, Judd C, Kilhau WP, Mason RH, McFiggans  
2513 G, Miller LA, Njera JJ, Polishchuk E, Rae S, Schiller CL, Si M, Temprado JV,  
2514 Whale TF, Wong JPS, Wurl O, Yakobi-Hancock JD, Abbatt JPD, Aller JY,  
2515 Bertram AK, Knopf DA, Murray BJ (2015) A marine biogenic source of atmo-  
2516 spheric ice-nucleating particles. *Nature* 525:234–238, DOI 10.1038/nature14986
- 2517 Yeoh SK, Chapman TA, Goldstein DB, Varghese PL, Trafton LM (2015) On un-  
2518 derstanding the physics of the Enceladus south polar plume via numerical sim-  
2519 ulation. *Icarus* 253:205 – 222, DOI <https://doi.org/10.1016/j.icarus.2015.02.020>
- 2520 Zahnle KJ, Korycansky DG, Nixon CA (2014) Transient climate effects of large  
2521 impacts on Titan. *Icarus* 229:378–391, DOI 10.1016/j.icarus.2013.11.006
- 2522 Zhu P, Manucharyan GE, Thompson AF, Goodman JC, Vance SD (2017) The  
2523 influence of meridional ice transport on Europa’s ocean stratification and heat  
2524 content. *Geophys Res Lett* 44:doi:10.1002/2017GL072996
- 2525 Zimmer C, Khurana KK, Kivelson MG (2000) Subsurface oceans on Europa and  
2526 Callisto: Constraints from Galileo magnetometer observations. *Icarus* 147:329–  
2527 347
- 2528 Zolotov M, Shock E (2001) Composition and stability of salts on the surface of  
2529 Europa and their oceanic origin. *J Geophys Res* 106(E12):32815–32827
- 2530 Zolotov MY, Kargel JS (2009) On the chemical composition of Europa’s icy shell,  
2531 ocean, and underlying rocks. In: *Europa*, vol 431, University of Arizona Press  
2532 Tucson, AZ
- 2533 Zolotov MY, Shock EL (2003) Energy for biologic sulfate reduction in a hydrother-  
2534 mally formed ocean on Europa. *J Geophys Res Planets* 108(E4)
- 2535 Zolotov MY, Shock EL (2004) A model for low-temperature biogeochemistry of  
2536 sulfur, carbon, and iron on Europa. *J Geophys Res Planets* 109(E6)
- 2537 Zotikov IA, Zagorodnov VS, Raikovskiy JV (1980) Core drilling through the Ross  
2538 Ice Shelf (Antarctica) confirmed basal freezing. *Science* 207(4438):1463–1465